



**UNIVERSITI TEKNIKAL MALAYSIA MELAKA**

**DESIGN ENHANCEMENT OF PADDLE FIN FOR**

**FISHING KAYAK**

This report is submitted in accordance with the requirement of the Universiti Teknikal Malaysia Melaka (UTeM) for the Bachelor Degree of Manufacturing Engineering with Honours.



**MUHAMMAD FIRDAUS BIN NORIZAN**

FACULTY OF MANUFACTURING ENGINEERING

2021

## DECLARATION

I hereby, declared this report entitled DESIGN ENHANCEMENT OF PADDLE FIN FOR FISHING KAYAK is the results of my own research except as cited in references.



Signature:

.....*firdaus*.....  
اونيزر بن محمد فيرداوس

Author : MUHAMMAD FIRDAUS BIN

NORIZAN

Date:

2 SEPTEMBER 2021


## APPROVAL

This report is submitted to the Faculty of Mechanical and Manufacturing Engineering Technology of Universiti Teknikal Malaysia Melaka (UTeM) as a partial fulfilment of the requirements for the degree of Bachelor Degree of Manufacturing Engineering with Honours. The member of the supervisory is as follow:



Signature: .....

Supervisor: .....

  
**MAHASAN BIN MAT ALI**  
*Lecturer*  
Faculty of Manufacturing Engineering  
Universiti Teknikal Malaysia Melaka

## ABSTRAK

Pengeluaran kayak telah mengubah kayak rekreasi mereka sekarang dalam beberapa tahun terakhir untuk memuaskan orang yang minat memancing dengan kayak rekreasi mereka. Kayak rekreasi sering dirancang untuk memberikan kecekapan maksimum. Jenis pergerakan yang dilakukan oleh pengguna biasanya dibatasi untuk mendayung. Oleh itu, objektif utamanya adalah untuk menyiasat jenis reka bentuk aerofoil lain yang dapat digunakan untuk memaksimumkan prestasinya. Beberapa jenis aerofoil yang ada dipelajari dengan beberapa kriteria aspek yang perlu dipertimbangkan untuk meningkatkan prestasi kayak memancing dengan perbezaan jenis aerofoil. Beberapa kaedah telah digunakan dalam projek ini untuk mencapai objektif projek. Kaedah pengumpulan data telah dilakukan untuk mencari beberapa jenis aerofoil yang sesuai untuk pemacu sirip dayung. Dari hasil pengumpulan data, langkah selanjutnya adalah mempelajari keperluan reka bentuk dan juga reka bentuk dengan menggunakan perisian reka bentuk dan analisis. Objektif ketiga yang telah dikenal pasti adalah untuk mengesahkan jenis aerofoil dengan tujahan ke depan yang optimum untuk memancing kayak. Setelah selesai menghasilkan reka bentuk sirip dengan pelbagai jenis udara dalam perisian Solidwork, reka bentuk sirip diimport ke perisian ANSYS untuk meneruskan analisis dalam projek ini. Berdasarkan hasilnya, reka bentuk pesawat udara yang mempunyai prestasi yang baik adalah NACA 2414 (separa simetri) berbanding dengan dua pesawat udara yang lain. Ini kerana NACA 2414 mempunyai prestasi yang baik dalam Coefficient of lift (CL), Coefficient of drag (CD) dan Lift force.

## ABSTRACT

Kayak manufacturers have changed their current recreational kayaks in recent years to satisfy people who are interested in fishing with their recreational kayaks. Recreational kayaks are often designed to provide maximum efficiency, for example speed and directional stability, for good stability or balance between the two. The type of movement carried out by the user is normally restricted to paddling in a recreational kayak. Hence, the main objectives are to investigate other type of aerofoil design that can be used to maximize its performance. The literature review it was conducted to investigate the several type of aerofoil for paddle fin fishing kayak. A some existed type of aerofoil it was studied with several criteria an aspect was taken to considerate to improve the performance fishing kayak with differences type of aerofoil. Some method has been used in this project to achieve the objectives of project. A collecting data method has been conducted to find several types of aerofoils that suitable for paddle fin drive. From the result collecting data, the next step is to study the design requirements as well as the design by using design and analysis software. The third objective that has been identified is to validate the type of aerofoil with an optimum forward thrust for fishing kayak. After finish generate the fin design with different type of airfoil in Solidwork software, the design of fin was imported to ANSYS software to continue the analysis in this project. According to the result, the airfoil design that have good performance is the NACA 2414 (semi symmetrical) compared with other two airfoil. It is because the NACA 2414 have good performance in Coefficient of lift (CL), Coefficient of drag (CD) and Lift force.

## ACKNOWLEDGEMENTS

The name of Allah, Alhamdulillah, I'm grateful because able to finish the project as one the requirements that want to be complete in the time given.

I want to give my appreciation and gratitude to all those who gave the corporation for finish the report. A special thanks to my supervisor, En Mahasan Bin Mat Ali, whose helped me to coordinate my project.

Next, thank you to my parents for encouraging and supporting me to finish this project. This project it was prepared with the support and cooperation from many people. Then, not to forget beloved friends for give many supports and suggestions to me for finish the project.

Last, I want to thanks those that contributed and involve directly or indirectly for complete this project.

## DEDICATION

Alhamdulillah,

Praise to Allah S.W.T

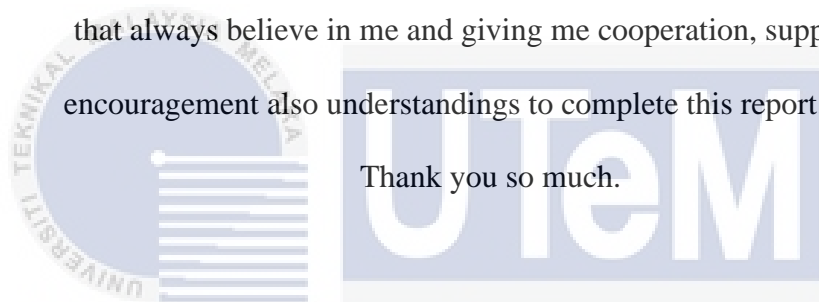
Special appreciation this study to my family,

My supervisor, En Mahasan bin Mat Ali,

My lecturer and my superb friends

that always believe in me and giving me cooperation, support and encouragement also understandings to complete this report.

Thank you so much.



اونيورسيتي تيكنيكل مليسيا ملاك

UNIVERSITI TEKNIKAL MALAYSIA MELAKA

## TABLE OF CONTENTS

	<b>PAGE</b>
<b>DECLARATION</b>	<b>i</b>
<b>APPROVAL</b>	<b>ii</b>
<b>ABSTRAK</b>	<b>iii</b>
<b>ABSTRACT</b>	<b>iv</b>
<b>ACKNOWLEDGEMENTS</b>	<b>v</b>
<b>DEDICATION</b>	<b>vi</b>
<b>TABLE OF CONTENTS</b>	<b>vii</b>
<b>LIST OF TABLES</b>	<b>xiii</b>
<b>LIST OF FIGURES</b>	<b>xiv</b>
<b>LIST OF APPENDICES</b>	<b>xiv</b>
<b>LIST OF SYMBOLS</b>	<b>xx</b>



<b>LIST OF ABBREVIATIONS</b>	<b>xxi</b>
<b>CHAPTER 1</b>	<b>1</b>
INTRODUCTION	1
1.1 Project Background	1
1.2 Problem Statement	3
1.3 Research Objectives	4
1.4 Scope of Research	5
1.5 Significant of Study	6
<b>CHAPTER 2</b>	<b>7</b>
LITERATURE REVIEW	7
2.1 Hobie Mirage Kayak	7
2.2 Mirage Drive Propulsion System	10
2.3 Geometry of Surf Fins	11
2.4 Aerodynamics	12
2.5 Introduction Aerofoil	15
2.6 Theoretical Background	17
2.6.1 Lift Force	18
2.6.2 Drag Force	20
2.7 Parametric construction model Aerofoil / Hydrofoil	21
2.8 Hydrodynamic Modelling for Active Fins	23

2.9	Design of Aeroplane using Principle of Aerofoil Shape	24
2.10	Design of Aerofoil Based on Turtle's Fin	26
2.11	Design of Aerofoil Based on Dolphin's Fin	27
2.12	Naca Airfoil	28
<b>CHAPTER 3</b>		<b>31</b>
METHODOLOGY		31
3.1	Project Flow Chart	32
3.2	Investigate different type of aerofoil design that can be apply to paddle fin drive	33
3.2.1	Collection Data	33
3.2.2	Primary Sources	33
3.2.2.1	Observation	34
3.2.3	Secondary Sources	34
3.2.3.1	Journal/ Articles	34
3.2.3.2	Books	35
3.2.3.3	Internet	36
3.3	Develop viable prototype of paddle fin drive that integrates with different type of aerofoils	36
3.3.1	Design of product using 3D CAD software (SOLIDWORKS)	36
3.3.2	Analyse the type of aerofoil with an optimum forward thrust for fishing kayak	37

3.3.3	Model Analysis Design and Simulation using ANSYS Software	38
3.3.4	Modelling and meshing analysis	38
3.3.5	Pressure and Velocity Analysis	39
<b>CHAPTER 4</b>		<b>41</b>
RESULT AND DISCUSSION		41
4.1	Design of Fin with Different Type of Airfoil Using Solidwork Software	41
4.1.1	Design of fin with NACA 0015 (Symmetrical) Airfoil	42
4.1.2	Design of fin with NACA 2414 (Semi Symmetrical) Airfoil	44
4.1.3	Design of fin with NACA 4415 (Chambered) Airfoil	47
4.2	Analysis of Naca 0015 Airfoil Design	50
4.2.1	Process of Modelling and Meshing generation	51
4.2.2	Static pressure NACA 0015	53
4.2.3	Velocity magnitude NACA 0015	55
4.2.4	Variation of lift and drag coefficient with Angle of attack (AOA)	57
4.3	Analysis of Naca 2414 Airfoil Design	61
4.3.1	Process of Modelling and Meshing generation	61
4.3.2	Static pressure NACA 2414	64
4.3.3	Velocity magnitude NACA 2414	66
4.3.4	Variation of lift and drag coefficient with Angle of attack (AOA)	67
4.4	Analysis of Naca 4415 Airfoil Design	71

4.4.1	Process of Modelling and Meshing generation	71
4.4.2	Static pressure NACA 4415	74
4.4.3	Velocity magnitude NACA 4415	76
4.4.4	Variation of lift and drag coefficient with Angle of attack (AOA)	77
4.5	Comparison Result of NACA 0015, NACA 2414 and NACA 4415	81
4.5.1	Comparison Result of NACA 0015, NACA 2414 and NACA 4415 Based on Coefficient of Lift (CL)	82
4.5.2	Comparison Result of NACA 0015, NACA 2414 and NACA 4415 Based on Coefficient of Drag (CD)	83
4.5.3	Comparison Result of NACA 0015, NACA 2414 and NACA 4415 Based on Lift Force	84
<b>CHAPTER 5</b>		<b>86</b>
<b>CONCLUSION &amp; RECOMMENDATION</b>		<b>86</b>
5.1	Introduction	86
5.2	Conclusion	86
5.3	Recommendation	88
5.4	Sustainable Design and Development	89
5.5	Complexity	89
5.6	Life Long Learning	90
<b>REFERENCE</b>		<b>91</b>



## LIST OF TABLES

TABLE	TITLE	PAGE
Table 4.1.1-1:	Database NACA 0015	42
Table 4.1.2-1:	Database NACA 2414	45
Table 4.1.3-1:	Database NACA 4415	48
Table 4.2.4-1:	Result Coefficient of Lift (CL), Coefficient of Drag (CD) and Lift Force with different angle of attack for NACA 0015	58
Table 4.3.4-1:	Result Coefficient of Lift (CL), Coefficient of Drag (CD) and Lift Force with different angle of attack for NACA 2414	68
Table 4.4.4-1:	Result Coefficient of Lift (CL), Coefficient of Drag (CD) and Lift Force with different angle of attack for NACA 4415	78

اونيورسيتي تيكنيكل مليسيا ملاك

UNIVERSITI TEKNIKAL MALAYSIA MELAKA

## LIST OF FIGURES

FIGURE	TITLE	PAGE
Figure 1.1-1:	Fishing Kayak	2
Figure 1.1-2:	Fin Drive System	3
Figure 1.2-1:	Paddle Fin	4
Figure 2.1-1:	Hobie Mirage Kayak	8
Figure 2.1-2:	Original Concept Sketch Mirage	9
Figure 2.1-3:	Technology of Mirage	9
Figure 2.2-1:	Design and placement of the Gauges Mirage Drive Propulsion System	10
Figure 2.2-2:	Mirage Drive Propulsion System Instrumented kayak equipment	11
Figure 2.3-1:	Diagram of Surf Fin with Key Geometries	12
Figure 2.4-1:	General Section of An Airfoil	14
Figure 2.5-1:	Aerodynamics Characteristics on Bird	17
Figure 2.6-1:	Hydrofoil physics diagram immersed on a free surface	18
Figure 2.6-2:	Hydrofoil Lifting and Drag Vectors	19
Figure 2.6-3:	Breakdown of Drag Components	21
Figure 2.7-1:	Parameters Definition of Foil	23

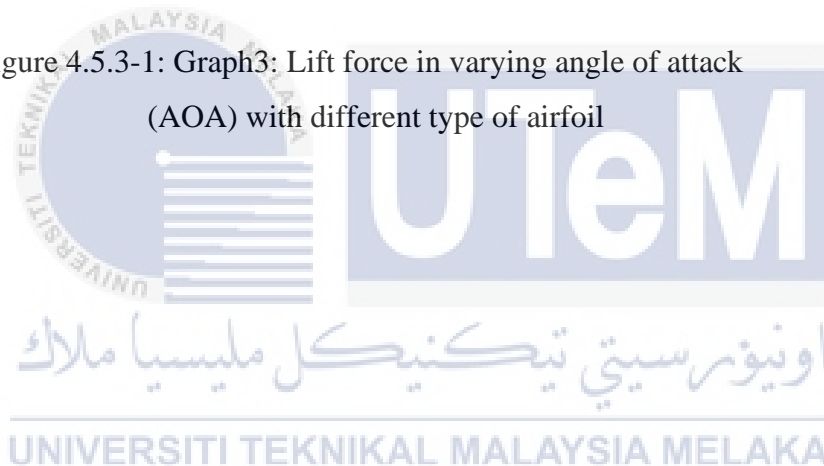
Figure 2.8-1: Concept Model of fin active stabilizer used at 0 Speed	24
Figure 2.9-1: Modern Aeroplane	25
Figure 2.9-2: 10 Types of Airfoil	25
Figure 2.10-1: Diagram Force and Moment Turtle	26
Figure 2.10-2: Hydrofoil Turtle	27
Figure 2.11-1: Original Dolphin Airfoil	28
Figure 2.12-1: NACA 0015	29
Figure 2.12-2: NACA 2414	29
Figure 2.12-3: NACA 4415	30
Figure 3.1-1: Flow Chart Project	32
Figure 3.3.1-1: Drawing Paddle Fin Drive	37
Figure 3.3.3-1: Corresponding analysis model	38
Figure 3.3.4-1: Meshing Analysis Model	39
Figure 3.3.5-1: Static Pressure for 0°	40
Figure 3.3.5-1: Contours velocity magnitude	40
Figure 4.1.1-1: Coordinate airfoil after import Database NACA 0015	43
Figure 4.1.1-2: Generate model NACA 0015	44
Figure 4.1.2-3: Full design fin with airfoil NACA 0015	44
Figure 4.1.2-1: Coordinate airfoil after import Database NACA 2414	46
Figure 4.1.2-2: Generate model NACA 2414	47
Figure 4.1.2-3: Full design fin with airfoil NACA 2414	47



Figure 4.1.3-1: Coordinate airfoil after import Database NACA 4415	49
Figure 4.1.3-2: Generate model NACA 4415	50
Figure 4.1.3-3: Full design fin with airfoil NACA 4415	50
Figure 4.2.1-1: Coordinates of NACA 0015	51
Figure 4.2.1-2: Grid generation of NACA 0015	52
Figure 4.2.1-3: Geometry of the NACA 0015 airfoil section	52
Figure 4.2.1-4: Meshing of air profile around the NACA 0015 airfoil	53
Figure 4.2.2-1: Static pressure contour distribution around the NACA 0015 at 0° Angle of attack (AOA)	54
Figure 4.2.2-2: Streamline of static pressure NACA 0015	55
Figure 4.2.3-1: Contours of velocity magnitude in m/s of NACA 0015 at 0° Angle of attack (AOA)	56
Figure 4.2.3-2: Streamline of velocity magnitude NACA 0015	57
Figure 4.2.4-1: Graph 1: Coefficient of lift (CL) in varying angle of attack (AOA) for NACA 0015	59
Figure 4.2.4-2: Graph 2: Coefficient of drag (CD) in varying angle of attack (AOA) for NACA 0015	60
Figure 4.2.4-3: Graph 3: Lift force in varying angle of attack (AOA) for NACA 0015	61
Figure 4.3.1-1: Coordinates of NACA 2414	62
Figure 4.3.1-2: Grid generation of NACA 2414	63
Figure 4.3.1-3: Geometry of the NACA 2414 airfoil section	63

Figure 4.3.1-4: Meshing of air profile around the NACA 2414 airfoil	64
Figure 4.3.2-1: Static pressure contour distribution around the NACA 2414 at 0° Angle of attack (AOA)	65
Figure 4.3.2-2: Streamline of static pressure NACA 2414	65
Figure 4.3.3-1: Contours of velocity magnitude in m/s of NACA 2414 at 0° Angle of attack (AOA)	66
Figure 4.3.2-2: Streamline of velocity magnitude NACA 2414	67
Figure 4.3.4-1: Graph 1: Coefficient of lift (CL) in varying angle of attack (AOA) for NACA 2414	69
Figure 4.3.4-2: Graph 2: Coefficient of drag (CD) in varying angle of attack (AOA) for NACA 2414	70
Figure 4.3.4-3: Graph 3: Lift force in varying angle of attack (AOA) for NACA 2414	71
Figure 4.4.1-1: Coordinates of NACA 4415	72
Figure 4.4.1-2: Grid generation of NACA 4415	73
Figure 4.4.1-3: Geometry of the NACA 4415 airfoil section	73
Figure 4.4.1-4: Meshing of air profile around the NACA 2414 airfoil	74
Figure 4.4.2-1: Static pressure contour distribution around the NACA 4415 at 0° Angle of attack (AOA)	75
Figure 4.4.2-2: Streamline of static pressure NACA 4415	75
Figure 4.4.3-1: Contours of velocity magnitude in m/s of NACA 4415 at 0° Angle of attack (AOA)	76
Figure 4.4.3-2: Streamline of velocity magnitude NACA 4415	77

Figure 4.4.4-1: Graph 1: Coefficient of lift (CL) in varying angle of attack (AOA) for NACA 4415	79
Figure 4.4.4-2: Graph 2: Coefficient of drag (CD) in varying angle of attack (AOA) for NACA 4415	80
Figure 4.4.4-3: Graph 3: Lift force in varying angle of attack (AOA) for NACA 4415	81
Figure 4.5.1-1: Graph 1: Coefficient of lift (CL) in varying angle of attack (AOA) with different type of airfoil	82
Figure 4.5.2-1: Graph 2: Coefficient of drag (CD) in varying angle of attack (AOA) with different type of airfoil	83
Figure 4.5.3-1: Graph3: Lift force in varying angle of attack (AOA) with different type of airfoil	85



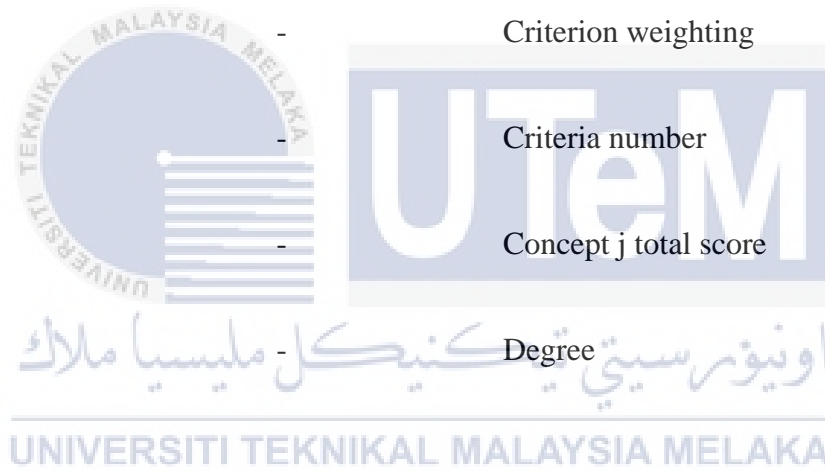
## LIST OF APPENDICES

APPENDIX	TITLE	PAGE
APPENDIX 1:	GANTT CHART PSM 1	95
APPENDIX 2:	GANTT CHART PSM 2	96



## LIST OF SYMBOLS

%	-	Percentage
Kg	-	Kilogram
Mm	-	Millimetre
Cm	-	Centimetre
$r_{ij}$	-	Concept j raw rating for the criterion
$w_i$	-	Criterion weighting
$n$	-	Criteria number
$s_j$	-	Concept j total score
°	-	Degree



## LIST OF ABBREVIATIONS

UTeM	-	Universiti Teknikal Malaysia Melaka
PSM	-	Projek Sarjana Muda
NACA	-	National Advisory Committee for Aeronautics
CAD	-	Computer Aided Design
CAE	-	Computer Aided Engineering
FEA	-	Finite Engineering Analysis
SUP	-	Stand Up Paddle
FCS	-	Fin Control System
F <sub>x</sub>	-	Force x اونيورسي تيكنيكل مليسيا ملاك
F <sub>y</sub>	-	Force y UNIVERSITI TEKNIKAL MALAYSIA MELAKA
CF	-	Coefficient Force
CD	-	Coefficient of Drag
CL	-	Coefficient of Lift
LF	-	Lift Force

# CHAPTER 1

## INTRODUCTION

A brief introduction to the project is given in this chapter. The introduction begins with a research history which describes briefly current knowledge or previous relevant studies on the topic discussed. The problem statement subsequently provides a summary of the current problem in relation to these issues. The aim is to show the objectives that want to achieve. The scope that determines the project border or limitations is then defined. The significance of this analysis is seen at the end of this chapter in terms of project importance.

UNIVERSITI TEKNIKAL MALAYSIA MELAKA

### 1.1 Project Background

Kayak manufacturers have changed their current recreational kayaks in recent years to satisfy people who are interested in fishing with their recreational kayaks. like in Figure 1.1.1. There is always a trade-off between efficiency and stability when making recreational kayaking. Recreational kayaks are often designed to provide maximum efficiency, for example speed and directional stability, for good stability or balance between the two. The type of movement carried out by the user is normally restricted to

paddling in a recreational kayak. None the less, highly stable traditional kayaking recreational kayaks frequently struggle to perform in terms of speed and/or navigational facility.



Figure 2.6.1-1: Fishing Kayak

Source: (Yan et al., 2016)

Conversely, the paddle fin drive system has been used in new fishing kayak to increase the speed performance as well providing good stability. Technically, paddle fin drive system as shown in Figure 1.1.2 involves oscillating fin propulsion assembly attached at watercraft, which travels on or around a water body, in which fins which sweep in general transversely relative to a longitudinal axis of the watercraft may produce a power propulsion force. The fins can be rotated on the longitudinal axis of the ship by the first coplanar axis. Rotating drive members of the second axis can be operatively connected with fins, relatively to the first axis. The fine oscillatory motion can be regulated by torque in the second axis when the drive members are reciprocal. The oscillating fins will act as a propellant for moving the watercraft in both directions longitudinally forward as they sweep back and forth.





Figure 2.6.1-2: Fin Drive System

Source: (Yan et al., 2016)



## 1.2 Problem Statement

With the rapid technology advancement that available nowadays, it is now possible to custom design different type of aerofoil in order to suit a particular application for instance, paddle fin drive. The recent studies have shown that inverse approach is suitable for designing aerofoil with systematic variations in the aerofoil performance characteristics. In addition, it is well known that different type of aerofoil has their own performance characteristics. In a good note, symmetrical aerofoil design with very low drag tends to be more suitable for high-speed performance. Meanwhile, semi-symmetrical type of aerofoil that has high camber able to produce a good lift to drag ratio. Even with all the advance technology in aerofoil design however, there were limited guidance in the literature on how to tailor an aerofoil design on paddle fin drive for fishing kayak.

There two types paddle fishing kayak, which is propeller and fin. The project focus at the second types fishing kayak. The second types of fishing kayak are the paddle fin. There are different lift force generation mechanisms of fin stabilizer employed by zero-low speed working mode and middle-high-speed working mode, which results in the different requirements for fin-type. Currently, the fin used utilize the shape of symmetrical aerofoil design. However, there are different type of aerofoil design that can be apply to the paddle fin in which can produce different characteristics performance. Hence, the main problem statement is to investigate other type of aerofoil design that can be used to maximize its performance.

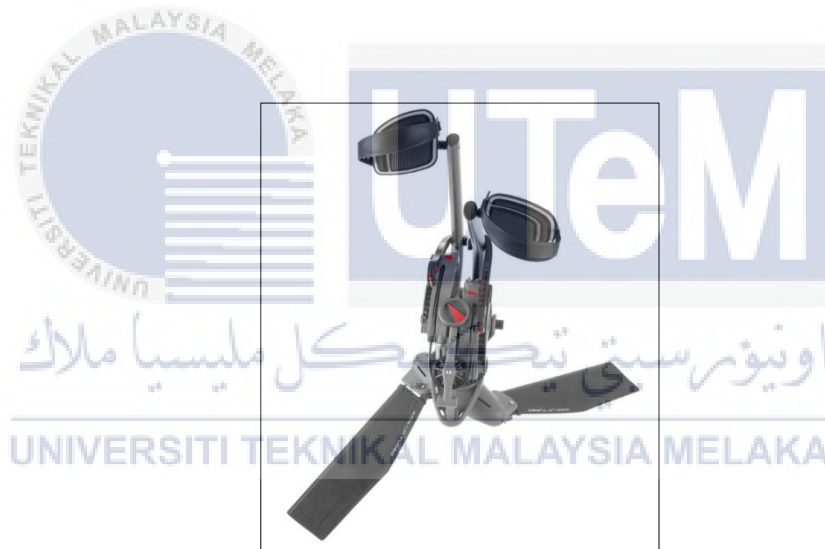


Figure 2.6.1-1: Paddle Fin

Source: (Yan et al., 2016)

### 1.3 Research Objectives

The research objectives are:

1. To investigate different type of airfoil design that can be apply to paddle fin drive.
2. To design the paddle fin drive that integrates with different type of airfoils.
3. To evaluate the performance of airfoil with an optimum forward thrust for fin fishing kayak in term of Static pressure, Velocity magnitude, Angle of Attack (AOA), Coefficient of Lift (CL), Coefficient of Drag (CD) and Lift Force (LF).



#### **1.4 Scope of Research**

1. Identify on different types of airfoil design with the focus on NACA 0015 (Symmetrical), NACA 2414 (Semi Symmetrical) and NACA 4415 (Chambered).
2. Using Solidwork software to design the paddle fin drive with the chosen type of airfoil designs in which focus on NACA 0015 (Symmetrical), NACA 2414 (Semi Symmetrical) and NACA 4415 (Chambered).

- Using ANSYS software to evaluate the performance of NACA 0015 (Symmetrical), NACA 2414 (Semi Symmetrical) and NACA 4415 (Chambered) in which give the forward thrust for fishing kayak in term of Static pressure, Velocity magnitude, Angle of Attack (AOA), Coefficient of Lift (CL), Coefficient of Drag (CD) and Lift Force (LF).

### 1.5 Significant of Study

This research presents the differences type of aerofoil that used for fin in fishing kayak. This study was carried out to improve and maximise the performance for fin fishing kayak. In addition, the increase of fin was achieved in order to improve movement of fishing kayak and better performance.



## **CHAPTER 2**

### **LITERATURE REVIEW**

In first chapter of study, the aims, scope, problem statements, background, study significance and general organization of research will be defined, and a detailed analysis from relevant literature is given in this chapter. The chapter presents literature reviews that provide the information in accordance with the objectives of chapter 1. In this chapter, the theory and research identified by different researchers years ago are described in particular. Reference and discussion were obtained from previous studies based on research on the form of aerofoil/hydrofoil. Info analysis from a review books, journals, related website, and articles collected.

#### **2.1 Hobie Mirage Kayak**

Hobie Mirage Kayak has legs and feet driven which push back and forth a pair of pedals. This movement is moved through an ingenious mechanism into the side-by-side movement of a couple of fins below the kayak which swings in opposite directions. The fins are versatile. They transform and flex and assume the form of a propeller pale when

water pressure strikes them. The mechanism is compared to the way a penguin is propelled by the sea. Figure 2.1.1 shown as an example of Hobie Mirage Kayak (Industrial Designers Society of America, 2003).



Figure 2.6.1-1: Hobie Mirage Kayak

Source: (Selk, 2005)

The Mirage mechanism fins are like a big, slow turning propeller. On approximately 10 cubic feet of water, there is one stroke in the fin or one-half cycle in the Mirage process. A paddle operates on a smaller volume of water and the paddle induces turbulence by contrast. Figure 2.1.2 shown the original design drawing reveals the initial idea of the system building up into a boat's hull so that there was no structure to hold the shafts. The intention was to use cables to move the fins on the drums. (Industrial Designers Society of America, 2003)

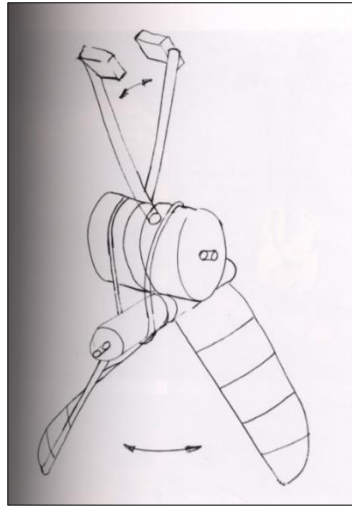


Figure 2.6.1-2: Original Concept Sketch Mirage

Source: (Industrial Designers Society of America, 2003)

The fins act as the wings of an aircraft, build strength or grow in a direction that is perpendicular to the fin. The drives help the boat progress. The figure 2.1.3 shown as Mirage's development technologies. In order to be able to do so more effectively, the design of fins was essential. (Industrial Designers Society of America, 2003).



Figure 2.6.1-3: Technology of Mirage

Source: (Selk, 2005)

## 2.2 Mirage Drive Propulsion System

According to (Yan et al., 2016) The Mirage Drive is a propulsion device that converts a driver's pedal motion into a tandem movement of two underwater foils shown in Figure 2.2.1. The device is mounted by installing it into the cockpit so that the foil protrudes below the cockpit and the drivers can reach the pedals a boat top shown in Figure 2.2.2. Foils are tandem and can be switched at a maximum angle of  $196^\circ$ . The foils pass underwater as the driver pedals. Periodic movement of foil dominated by the main steel shaft rotation on the front edge of the foil.

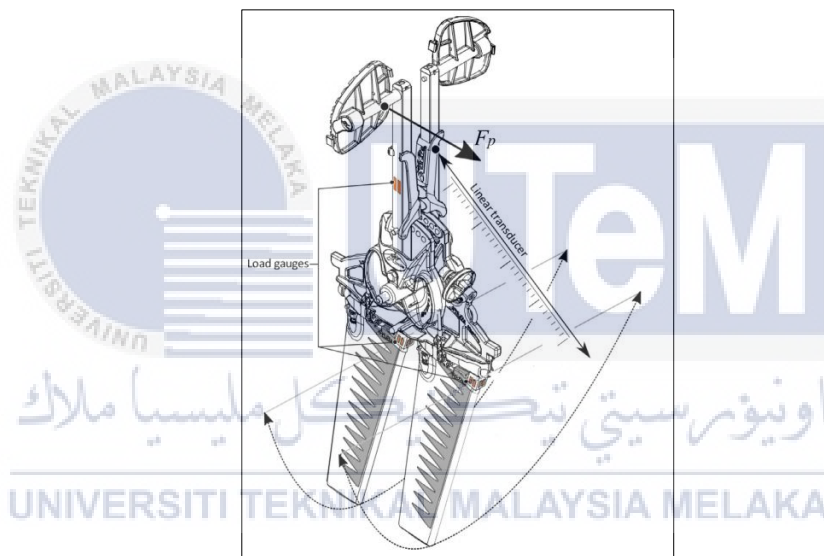


Figure 2.6.1-1: Design and placement of the Gauges Mirage Drive Propulsion System

Source: (Yan et al., 2016)



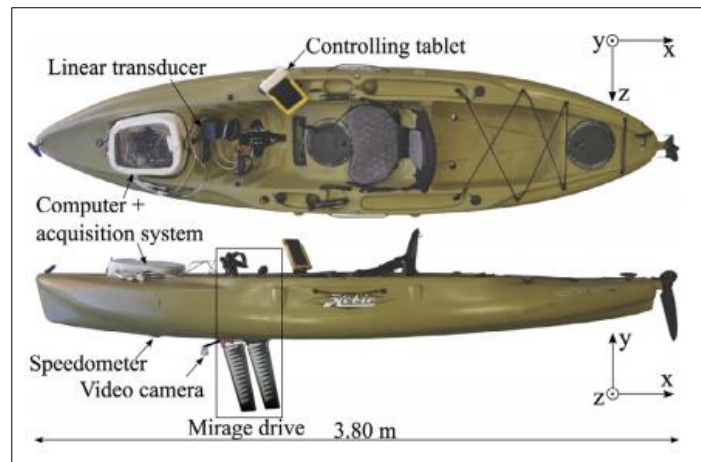


Figure 2.6.1-2: Mirage Drive Propulsion System Instrumented kayak equipment

Source: (Yan et al., 2016)

### 2.3 Geometry of Surf Fins

The geometry of the surfboard fin with several designs of organic forms that are hard to describe with precise parametric CAD tools (Carswell & Lavery, 2006). At the fundamental level, surfers and fin manufacturers also identify several main features shown in Figure 2.3.1. The fine structure is the material block on the base of a fine and slots in a surfboard or SUP board. There are many common systems on the market, two of which are most prominent are 'FCS' and 'Futures' (Gately et al., 2017), whereas longboards and SUP boards also use an adjustable single fin position as shown in Figure 2.3.1. Fin systems are proprietary and switching between systems requires the following market adapters, so many surfers use surf fins developed with their board-fitting fin system. The base of the fine is the length of the fin system and the base of the surfboard is flush. The length of the base is related to speed and ability to transform on a wave (Selk,

2005). The depth of the fin is the vertical length of the base of the end, which is larger and more stable. The sweep/rake is an angle from the back of the base to the tip of the fin with a lower sweeping angle which is believed to allow for tighter turning of the swing, while an extended sweeping angle produces more drawn turns. The foil crosses the fine and is responsible directly for the production of the lift, as is an aerodynamic aircraft wedge, which is of weak hydrodynamic form and draws water (Carswell & Lavery, 2006). A middle fin has a double convex symmetric foil as shown in Figure 2.3.1, a single convex foil on the outside and a flat or concentric foil inside can be present in the outside fins. Similarly, external fins can have an angle of can not to improve rotation, while a center fin will not.

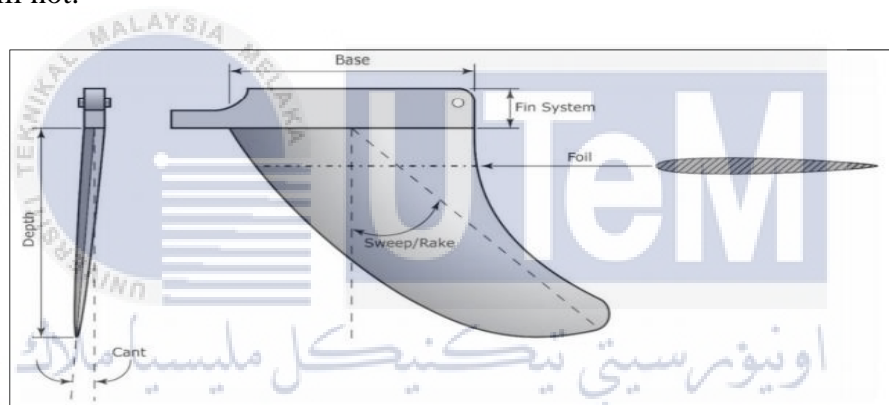


Figure 2.6.1-1: Diagram of Surf Fin with Key Geometries

Source: (Novak, 2020)

## 2.4 Aerodynamics

According to (Kumar, 2014), Aerodynamics is a theoretical extension focusing on air movement particularly when it is connected to object like aerofoil. Aerodynamics is an environment in which progress and gas movement are carried out, and in these areas

some parts of aerodynamics are regular. By way of contrast, 'gas dynamics' was used to analyse the motion of all gases, not just air. Formal aerodynamics think of the latest trends started in the 18th century, even though core ideas have been recorded much earlier in aerodynamic drags. Wilbur and Orville Wright demonstrated in 1903 a vast majority of early aerodynamic work on heavy flights over the air. Aerodynamics have since been used as a basis of investigation, observational calculations, wind-tunnel research and leisure station to further boost heavy-duty flights and several different inventions. Late aerodynamics research based in the future on problems related to compressible streams, turbulences and limits.

The elevator on an airfoil is basically due to its form. The airfoil then transforms the approached air and generates energy in the opposite direction on the airfoil when arranged on an appropriate edge. This power is referred to as aerodynamic motor and can be calculated by lifting and dragging in two parts. The majority of thwart forms need positive lifting approach, but camber airfoils will generate zero lifting. This turn of the air into bended streamlines in the region of the airfoil, creating more weight on the one side and more weight on the other hand. This weight is combined to a speed difference by the Bernoulli standard, so the following stream field over the airfoil is more natural speed at the surface above the surface at the stage above. Specifically, the lifting power can be related to the usual top-base contrast without registering weight using the flow idea (Kumar, 2014).

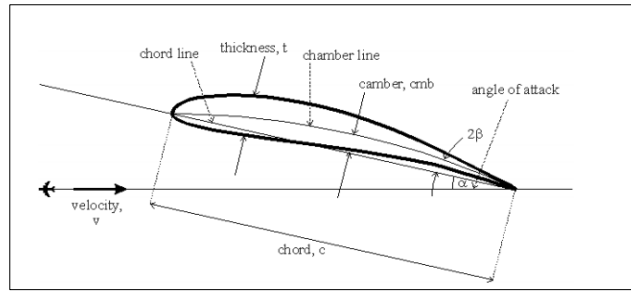


Figure 2.6.1-1: General Section of An Airfoil

Source: (Kumar, 2014)

Some of Airfoil terms are:

1. Edge leading

- The airfoil is on the edge of the line of the aircraft. It is round and disconnects the air to a velocity greater than that at the bottom of the upper surface of the airfoil.

2. Edge trailing

- It is the edge of the airfoil pattern. It's at the rear of the airfoil.

3. Line chord

- It's a straight line between the front edge and the front edge. It separates an airfoil into two parts, but for an asymmetrical airfoil it does not. It specifies an additional significant parameter of Angle Attack.

4. Attack angle

- The movement angle of the plane is the chord line. A significant parameter is the lifting and drag coefficient.

#### 5. Line chamber

- It is a line that connects the front edge with the front edge and divides the flange into two components symmetrical. It may or may not be straight.

#### 6. Lift coefficient

- The lifting force on the body is a dimensional coefficient that is its speed, surface area and fluid density related.

#### 7. Drag coefficient

- The force of drag within the body is connected to its speed, surface area and liquid density.

#### 8. Attack angle stall

- Attack angle is highest lifting factor and after that the lifting factor begins to decrease.

## 2.5 Introduction Aerofoil

Similar to the wing of the bird, the wing of the aircraft is the surface of the selected aerofoil portion, which can differ in shape/geometry in order to achieve improved efficiency. The elevation created by the wing retains the aircraft's weight for aircraft. Once again, the primary source of aircraft drag is related to the wing from perspective an aerodynamic. Around two-thirds of total drag created by the wing of modern cruise aircraft. The effects of aerodynamic properties (drag, lift and lift ratio) which efficiency and performance depend are therefore important for the wing shape and size. The world now continues to focus on the best lifts and the lowest drag capacity for various wing forms/geometries.(Torenbeek, 2013).

Experimental research with and without bird feathers like aerodynamic properties of rectangular wings for different Reynold Numbers. The test results show a decrease of 25~30 per cent in drag coefficient and an improvement of 10~20 per cent in lift coefficient by the use of bird feathers as winglets at an 8-degree angle of attack (Hossain et al., 2011).

A basic methodology was followed for studies Study of static stability aerodynamics of various types of wings. Low-speed wind tunnels have been regulated with different air speeds and link angles with reduced wings in different shapes including with curved tips and tapered. The authors find that the curved tapering wing is stable operating at various speeds and angles (Paudel, 2016).

The three simple, untwisted wings with the same elliptical chord have been inspected and the four chords have different curvatures. The elliptical wing has a low lifting effect, an unweather four-string elliptical one with the unwept end and a crescent-shaped wing has the best lifting performance and efficiency. (Madnia, 2010).

Geobat Flying Saucer Aviation inc. has tested and manufactured a no-spinning circular plane-box with an aviation portion configuration in the Wind Tunnel University of Auburn. A Cessna 172 model has also been evaluated for comparative purposes. The

author found the position of Geobat elevation was lower than Cessna 172, but it had better resistance. (Buscher et al., 2013).

The fundamental findings were analysed and presented for the preparation of the optimisation wing for minimum drag with structural weight and maximum elevation constraints. In addition, aerodynamic characteristics research has been performed for different airfoils in various corners of the world (Wakayama & Kroo, 1995) like (Gordnier, 2009) bicamber surface airfoil's efficacy was evaluated, Fluid flow and aerodynamic forces were tested on airfoils (Kandwal & Singh, 2012). The difference in airfoil pressure distribution with Reynold's number has been studied (Pinkerton, 1936). Analyzed the flow activity across the body of the airfoil (Albrecht et al., 2012).

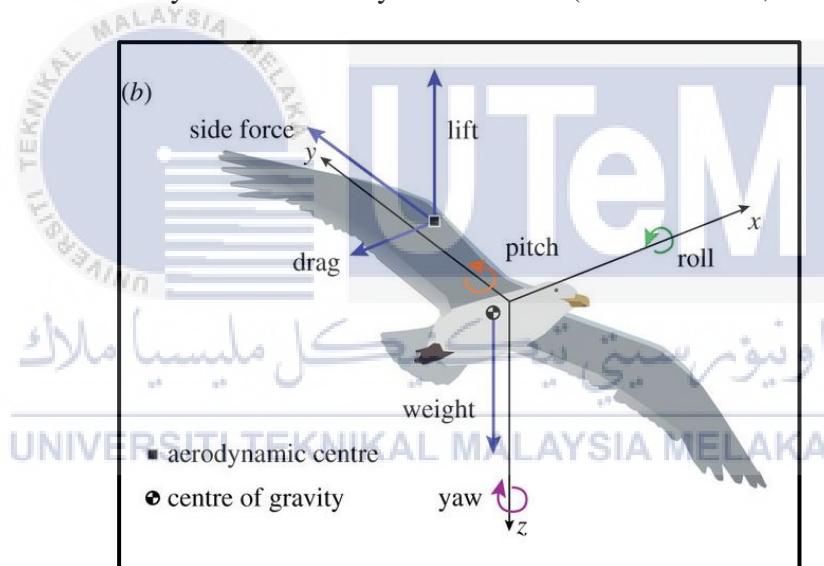


Figure 2.6.1-1: Aerodynamics Characteristics on Bird

Source: (Albrecht et al., 2012)

## 2.6 Theoretical Background

According to (Mohammed et al., 2015) from Figure 2.6.1, Hydrofoil physics schematics immersed in an open surface.  $U$  is the inflow speed,  $c$  is the chord,  $h$  is immersion depth,  $\alpha$  is the attack angle and  $\alpha_0$  is the active zero attack angle. As the water flow flows through the hydrofoil, two resulting forces, Lift ( $L$ ) and Drag ( $D$ ), are re-generated.  $F_x$  as drag force and  $F_y$  as lifting force, coordinate system fits the OpenFOAM axis system. The aim of foils to lift, described before, is to generate a considerable the upward force would increase the performance of the vessel.

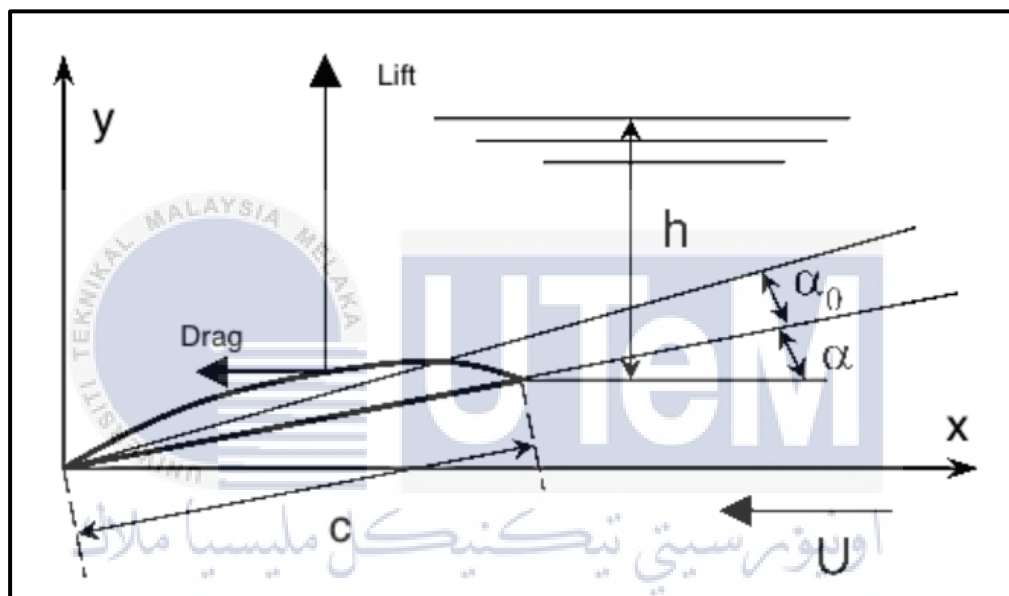


Figure 2.6.1-1: Hydrofoil physics diagram immersed on a free surface

Source: (Mohammed et al., 2015)

### 2.6.1 Lift Force

The lifting force ( $L$ ) acts perpendicularly to the free flow of the film transverse plane. The lift created by a two-dimensional foil free stream is:



$$L = \frac{1}{2} \rho V^2 A C_L$$

In the angle of attack, the  $C_L$  lift coefficient is considered to differ linearly. The following is an approximate formula for the  $C_L$  variance:

$$C_L = 2\pi \alpha_T$$

In terms of the zero lifting angle the  $\alpha_T$  angle is AoA. Formula 1 shows that the speed of the lift varies significantly (V). This shows that the lifts are not particularly appropriate for low-speed handling operations but give distinctive advantages to high-speed handling. In a variety of ways, physical lift can be expressed:

1. Pressure difference: The pressure of the water on the lower part of the film is higher than on the top. Friction differential produces the resulting force upwards. This wording derives from the equation of Bernoulli.
2. The 3rd Law of Newton: The hydrofoil forces water down, producing an upward strain hydrofoil.

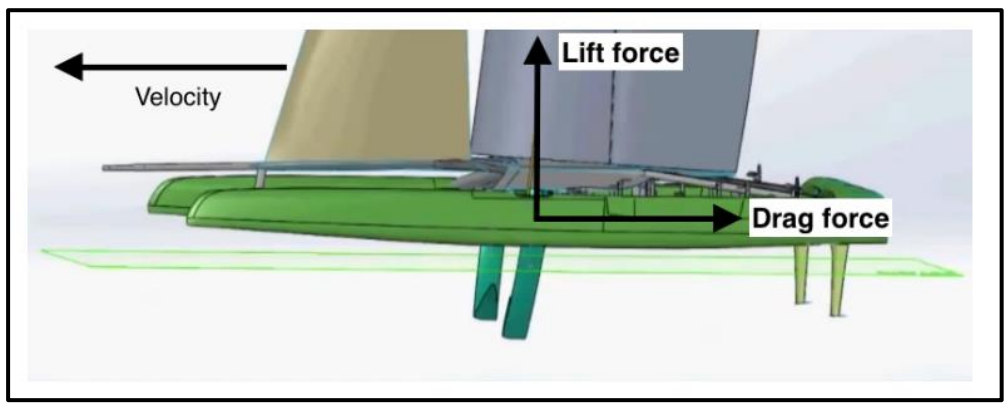


Figure 2.6.1-1: Hydrofoil Lifting and Drag Vectors

Source: (Mohammed et al., 2015)

## 2.6.2 Drag Force

The drag force (D) acts as the free flow instead. The drag power equation in general is:

$$D = \frac{1}{2} \rho V^2 A C_D$$

The established drag force based on several variables can be divided into one of the most important components:

1. Viscous Drag

The interaction of the body and the fluid with viscous characteristics is induced. There is a very small region close to the body, known as an edge layer, which is like the water flows through the body as a viscoso material. The velocity of the body is null and essentially goes well beyond the free flow velocity.

2. Induced Drag

Occurs due to the lifting force produced by the foil.

3. Wave and Spray Drag

This is because a wave pattern is created on the free surface and spray is produced. (apply to hydrofoils for surface piercing).

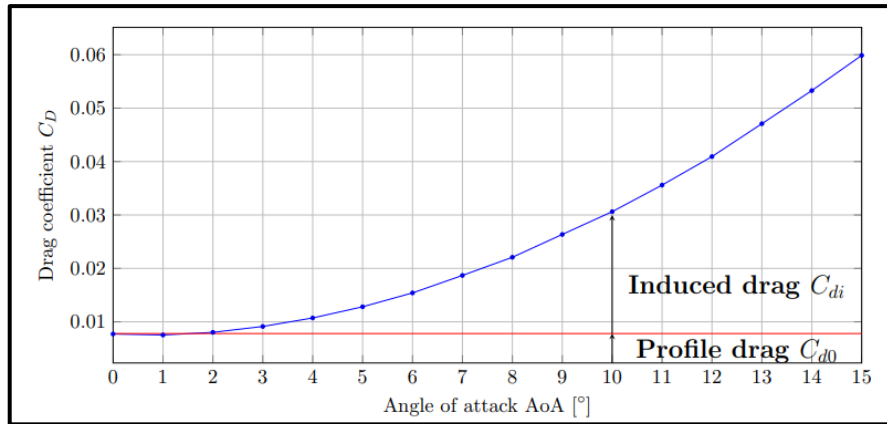


Figure 2.6.2-1: Breakdown of Drag Components

Source: (Mohammed et al., 2015)

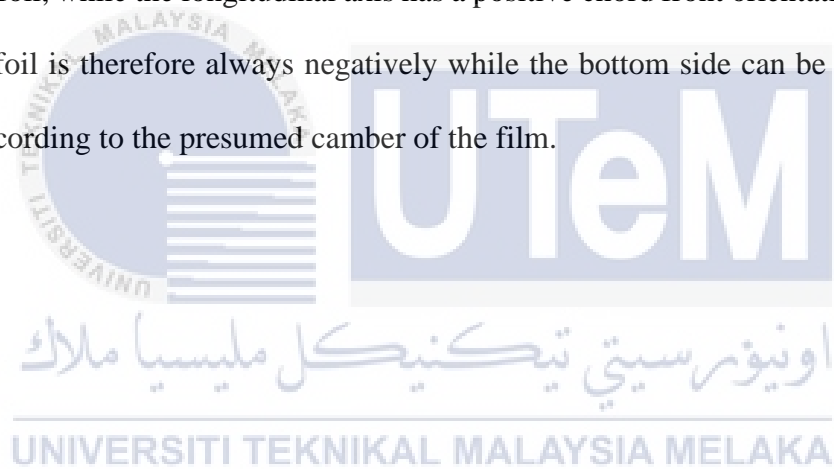
## 2.7 Parametric construction model Aerofoil / Hydrofoil

According to (Kostas et al., 2017), The reference parameter for a hydrofoil and/or airfoil in this work is the model extension parameter. The model shown produces an 8-parameter closed cubic B-Spline curve. In order to remove complex interdependent constraints and increase model robustness, the parameters are used were specified as suitable non-dimensional ratios that lie at (0.1). This paper also takes the same approach as non-dimensional proportion parameters and adds some additional parameters to increase the space of the generated shape.

In addition to the various parameters used in these two parametric models, their key distinction is the manner in which the foil structure is formed. The upper portion of the foil (suction side) and its camber curve were used with a set of parameters. The bottom (pressure side) was then constructed by reflecting the top of the camber curve and

ultimately, the two sides were combined in a single cubic curve B-spline representing the case of the foil. The parameters are used directly during the development of the two foil sides in the current paper and no intermediate stage of camber curve construction is needed. This approach increases the number of parameters needed slightly but has the double benefit of enriching the covered geometrical region of the parametric model and reducing the number of check points required in the final curve.

Figure 2.7.1 presents the parameters used, their significations and their dimensional equivalent ranges in the parametric model. Notice that the chord length of the foil,  $L$ , is not used for sizing. The position of the coordinate is taken in account at the front of the foil, while the longitudinal axis has a positive chord front orientation. The top part of the foil is therefore always negative while the bottom side can be negative or positive, according to the presumed camber of the film.



Nr.	Name	description	symbol	actual range
0	Length	Length of foil's chord	L	free
1	Upper-side max width	Maximum width of suction side w.r.t. Chord	u_max	$[0, 1] \rightarrow \left(\frac{L}{500}, \frac{L}{5}\right)$
2	Upper-side max width position	Longitudinal position of suction side's max width	x_u_max	$[0, 1] \rightarrow \left[\frac{L}{10}, \frac{7L}{10}\right]$
3	Upper-side angle	Suction's side angle at trailing edge w.r.t. Chord	a_b_u	$[0, 1] \rightarrow [0, 90]^\circ$
4	Upper-side tip shape	Leading edge upper part form factor	tip_u	$[0, 1] \rightarrow [0.05, 1]$
5	Upper-side aft-part shape	Inflection point position and/or shape fullness	s_u	$[0, 1] \rightarrow [0.05, 1](L - x_u_{max})$
6	Lower-side max width	Maximum width of lower side w.r.t. Chord	l_max	$[0, 1] \rightarrow \left[\frac{L}{500}, \frac{L}{5}\right]$
7	Lower-side max width position	Longitudinal position of lower side's max width	x_l_max	$[0, 1] \rightarrow \left[\frac{L}{10}, \frac{7L}{10}\right]$
8	Lower-side angle	Suction's side angle at trailing edge w.r.t. Chord	a_b_l	$[0, 1] \rightarrow [-a_b_l, a_b_l]^\circ$
9	Lower-side tip shape	Leading edge upper part form factor	tip_l	$[0, 1] \rightarrow [0.05, 1]$
10	Lower-side aft-part shape	Inflection point position and/or shape fullness	s_l	$[0, 1] \rightarrow [0.05, 1](L - x_l_{max})$
11	Tangent angle at leading edge	The angle between the vertical axis and foil's tangent direction at the leading edge	a	$[0, 1] \rightarrow [-20, 20]^\circ$

UNIVERSITI TEKNIKAL MALAYSIA MELAKA

Figure 2.6.2-1: Parameters Definition of Foil

Source: (Kostas et al., 2017)

## 2.8 Hydrodynamic Modelling for Active Fins

From the point of view of fluid mechanics, the fluid moves under a drag force consisting of a pressing gap and a frictional tension. The fluid flow on the fine surface in the boundary layers often involves a viscous pressure drag called a vortex drag.

Eventually the efforts to solve this force become the kinetic energy of the vortex and then heat energy (“Prandtl’s Essentials Fluid Mech.,” 2004). In addition, a certain amount is accelerated or decelerated as you kick up and down the fluid, giving the end power because of its inertia Some fluid mass is also called an additional mass and the force is an additional mass force. It is the kinetic force of added mass that is overcome.

The pressure difference, the vortex drag and the additional mass power make the frictional stress slightly lower. Therefore, the hydrodynamic force of the active fin represents a combined friction, vortex drag and inertia. Remember, the fluid refers in particular to water in this document.

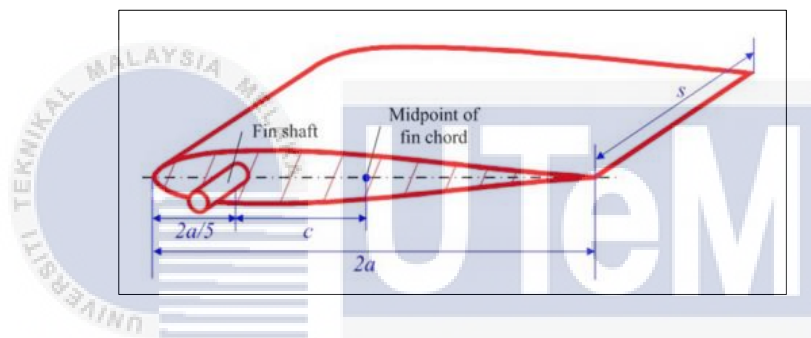


Figure 2.6.2-1: Concept Model of fin active stabilizer used at 0 Speed

Source: (“Prandtl’s Essentials Fluid Mech.,” 2004)

## 2.9 Design of Aeroplane using Principle of Aerofoil Shape

According to (Vishnu Chavan & Suresh Pawar, 2018), The architecture of the aircraft fuselage body is based on the aerofoil concept. The aircraft wings are fully aerofoil, but the main body is not in aerofoil form perfectly. Therefore, reducing traction force is very significant in the aircraft design. Advanced automobiles are strictly aerodynamic in nature and are highly helpful for overcoming drag on automobile. Modern

aeroplane as shown in Figure 2.9.1 typically have a speed of 250 m/s almost equal to the sound speed and thus their aerodynamic form significantly affects the energy requirement of the aircraft. In modern aircraft, the aerofoil types mainly for wings and for fuselage of aircraft are illustrated. As shown in Figure 2.9.2, The design analyses these shapes for the design and development of airplane fuselage for 10 forms of aerofoil form.



Figure 2.6.2-1: Modern Aeroplane

Source: (Vishnu Chavan & Suresh Pawar, 2018)

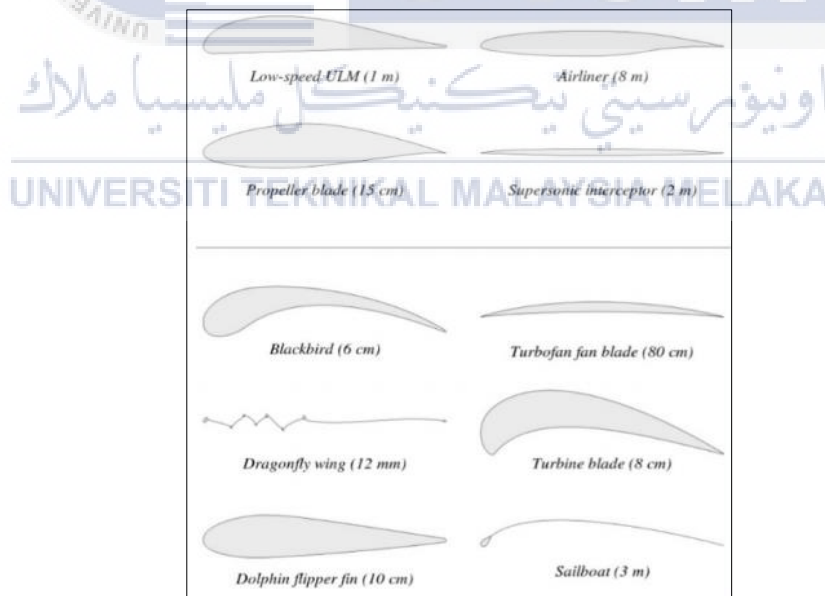


Figure 2.6.2-2: 10 Types of Airfoil

Source: (Vishnu Chavan & Suresh Pawar, 2018)

## 2.10 Design of Aerofoil Based on Turtle's Fin

Turtle is the inspiration of biomimetic. The hydrofoil turtle that is known as a fin or forelimb and its main propulsion source. The skeleton of the fin turtle is distinguished by the very thickness but not too long of the humerus and radius. These properties create an efficient swimming adaptable hydrofoil because it decreases the dynamic resistance of the hydrofoil swirls. Furthermore, the head of the turtle can reduce its forward resistance by adjusting its course to the navigation path (Wyneken, 2001). Figure 2.10.1 is diagram of the strength and momentum that works on sea turtle swimming. The force vectors are in the positive direction with the vector of flow shown relative to the reference structure of the turtle. When the tortoise travels in the still water, the flow rate equals the swimming speed (Watson & Granger, 1998).

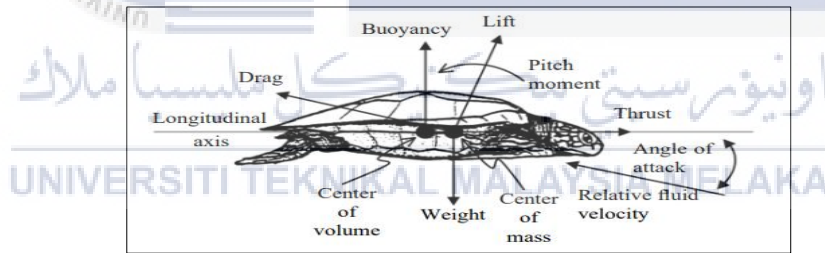


Figure 2.6.2-1: Diagram Force and Moment Turtle

Source: (Watson & Granger, 1998)

The turtle's prediction like Figure 2.10.2 (a) shown the figure as the wing and the lead-edge bone portion is created. The soft part of the trailing edge, in which the main part of a tortoise is guided while the trailing part supports the movement. Figure 2.10.2 (b) shown the hydrofoil's chord directive section shows the hydrofoil is a well structural



streamline in the current direction. This function greatly decreases the resistance of the dynamic swirl hydrofoil. This hydrofoil motion is primarily responsible for the marine turtle movement for force propulsion, close to the flapping wings of flying birds (Chu et al., 2007).

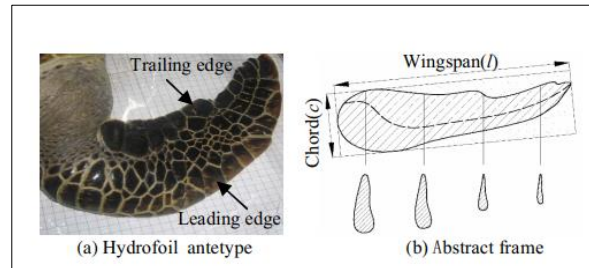


Figure 2.6.2-2: Hydrofoil Turtle

Source: (Chu et al., 2007)

## 2.11 Design of Aerofoil Based on Dolphin's Fin

Dolphins have long been a typical focus of bionic research for eliminating drag and noise, which is one of the quickest sea swimming species. It can achieve a maximum swimming speed in water of about 15m/s (Pavlov et al., 2007). An ordinary crowd of tanned grooves covered the dolphin snout to the back and the mid of the dolphin body, which was nearly perpendicular to the long body axis. (Shoele & Zhu, 2015) proposed that the Separation of laminarly boundary layer and transformation of the delay border layer with a versatile, flexible skin and a maximum rate of drag decrease of the flexible drag reduction content. According to (Zhang et al., 2018) dolphin used using the flexible skin to absorb the pressurized, damped pressurized energy the TS turbulence wave that

formed preserved the stability of the laminar flow and drag reduction. Figure 2.11.1 shown as the design of the original dolphin airfoil.

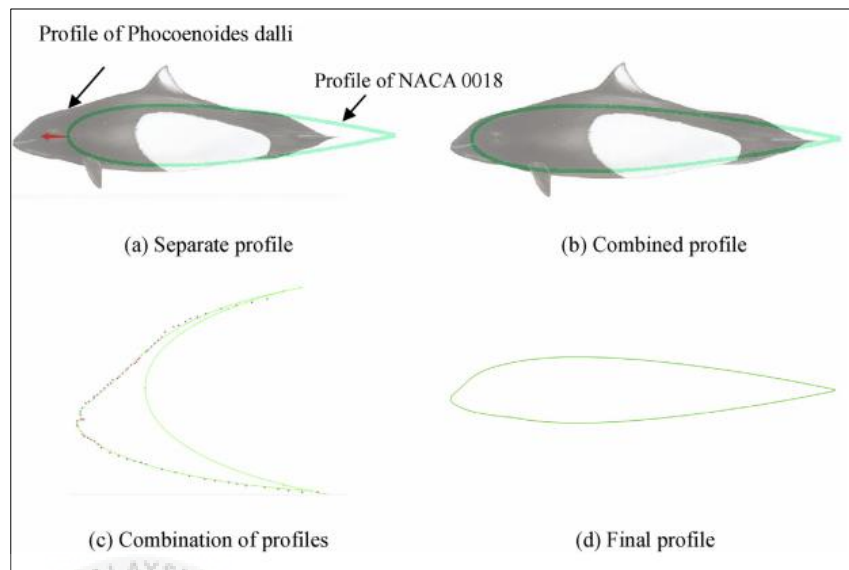


Figure 2.6.2-1: Original Dolphin Airfoil

Source: (Huang et al., 2021)

## 2.12 Naca Airfoil

The National Advisory Committee for Aeronautics (NACA) proposed airfoil aircraft wing numbers. These aircraft profiles are typically four digit code (Tuncay Kamas, 2009). The four-digit code wing profiles of the NACA are described as follows:

- The maximum distance between the top and the bottom (camber) is defined by a digit as a percentage of the chord.
- The distance from the leading edge is defined by a single digit by ten percentage of the chord.
- The airfoil describes two digits as the chord's maximum thickness.

For example, the NACA 0015 is symmetrical, for instance, since the first two digits do not describe a camber, the NACA 2414 is a semi symmetrical avion with a maximum of 2% camber at 40% (0.4 chords) from the leading edge at a maximum chord thickness of 14% and the NACA 4415 is a chambered with a maximum of 15% camber at 40.2% from the leading edge at a maximum chord thickness of 15%. Figure 2.12.1, Figure 2.12.2 and Figure 2.12.3 shown example the NACA 0015, NACA 2414 and NACA 4415.

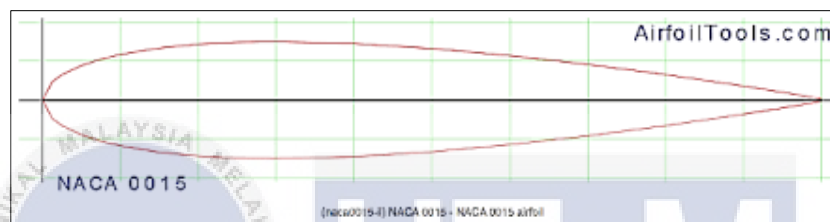


Figure 2.6.2-1: NACA 0015

Source: (Tuncay Kamas, 2009)

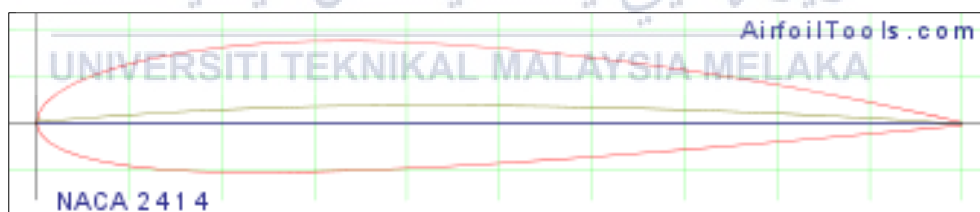


Figure 2.6.2-2: NACA 2414

Source: (Tuncay Kamas, 2009)

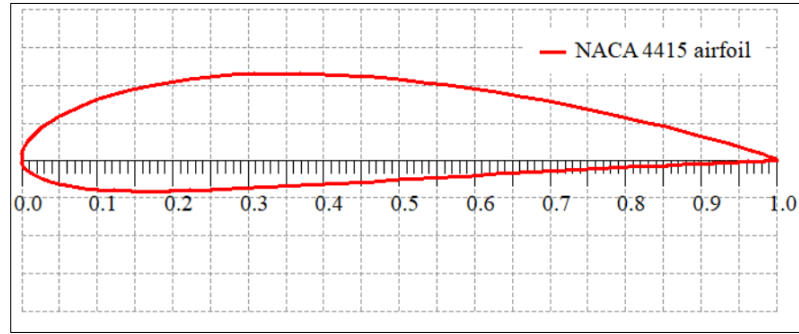


Figure 2.6.2-3: NACA 4415

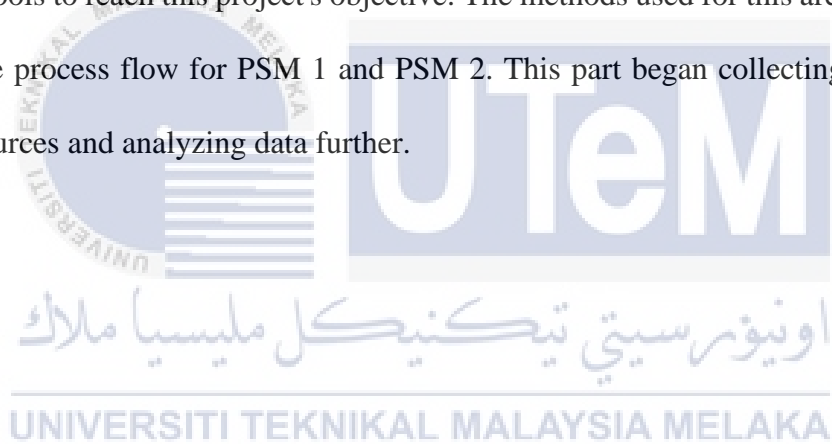
Source: (Tuncay Kamas, 2009)



## CHAPTER 3

### METHODOLOGY

This chapter explains how this research is to be carried out. It will discuss on the method or tools to reach this project's objective. The methods used for this are detailed in terms of the process flow for PSM 1 and PSM 2. This part began collecting data from different sources and analyzing data further.



### 3.1 Project Flow Chart

The following is a method flow chart for the entire activities carried out in PSM 1 and PSM 2. This flow chart was used to show the flow of the project starting from defining the problem statement until making the final result.

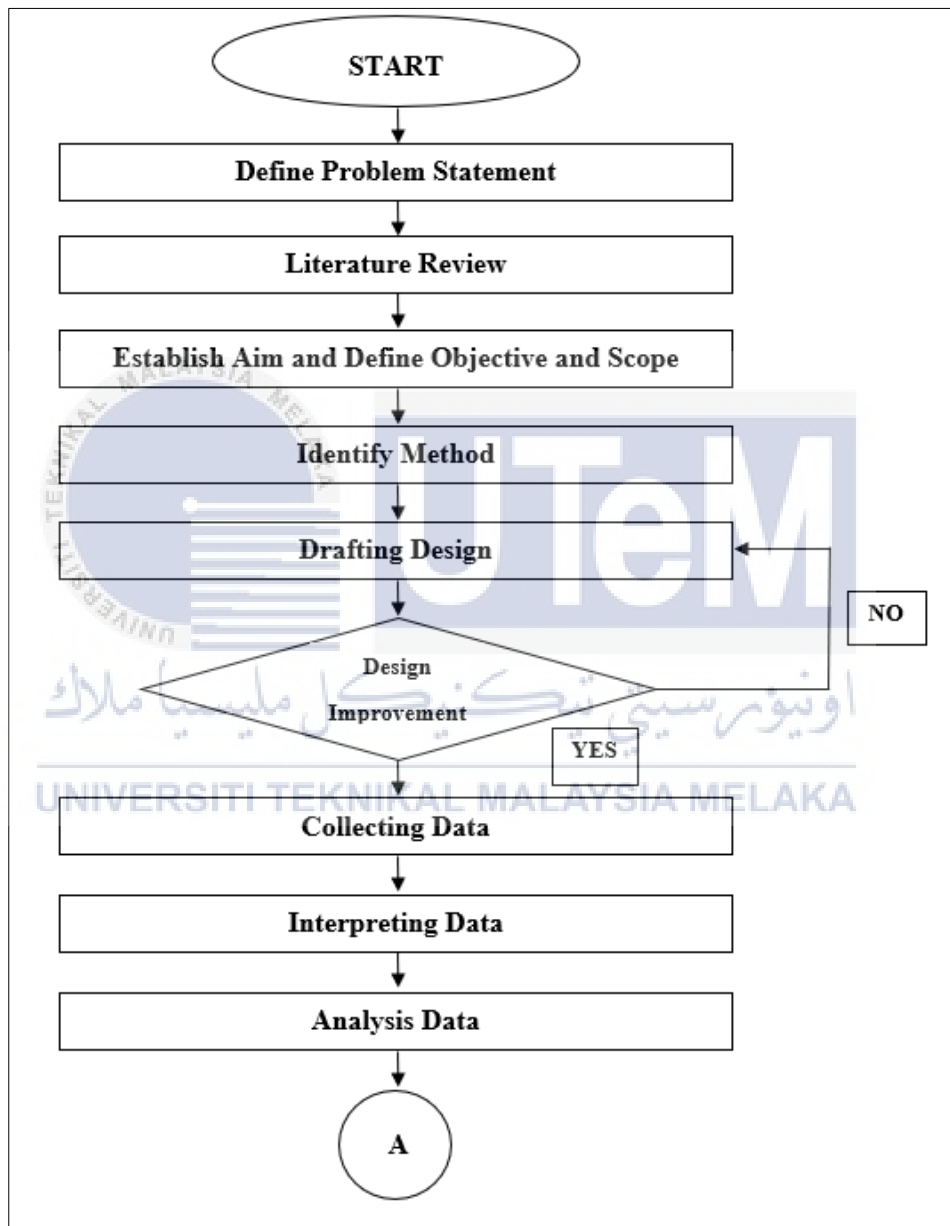


Figure 3.1-1: Flow Chart Project

### **3.2 Investigate different type of aerofoil design that can be apply to paddle fin drive**

In order to complete the first objectives for this project which to investigate different type of aerofoil design that can be apply to paddle fin drive. Some methods will be discussed. The method was used fata collection.

#### **3.2.1 Collection Data**

The details obtained in the processing of data has been decided to update the technique in doing this project. In statistical research, data collection plays a very important role. In this project, there were various methods to collect information. The methods were be classified in two group. First, primary sources and next secondary sources.

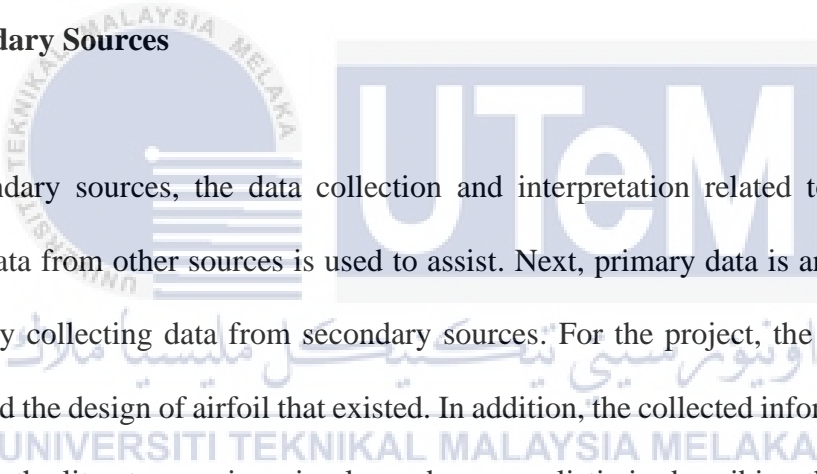
#### **3.2.2 Primary Sources**

Primary sources are initial and factual knowledge details emerging for the first time from the researcher. Primary sources are essential in order to collect and collect information for this project.

### **3.2.2.1 Observation**

Method of observation in advance of knowledge collection by observation, human behavior, or physical characteristics. For the project, observations were performed to evaluate the project problem statement, purpose and scope. The place where paddle fin drive fishing kayak were used has been observed.

### **3.2.3 Secondary Sources**



Secondary sources, the data collection and interpretation related to facts and theoretical data from other sources is used to assist. Next, primary data is analyzed and interpreted by collecting data from secondary sources. For the project, the source was helpful to find the design of airfoil that existed. In addition, the collected information was used to make the literature review simpler and more realistic in describing the problem. The secondary sources for the project were journals and articles and internet.

#### **3.2.3.1 Journal/ Articles**

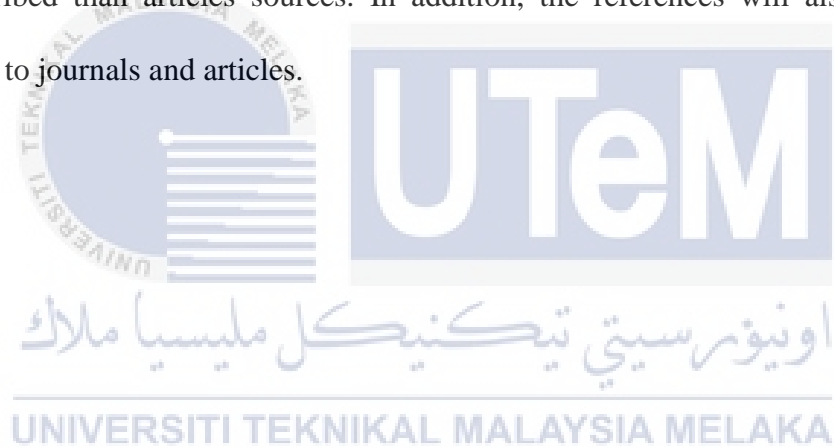
This project uses papers and articles to locate the evidence and collect the information to complete the analysis of the literature. Some newspapers and documents



cannot be read because of their copyright. Some references come from universities in the overseas countries. Because of their information, the data coming from this source are essentially directly linked to the project name.

### 3.2.3.2 Books

The most important data production is the source of books. Most of the writers want to clarify the project themselves extensively. The data also was much longer and better described than articles sources. In addition, the references will also be more comparable to journals and articles.



### **3.2.3.3 Internet**

Internet sources are more widely used to collect literature review data and information. The use of the Internet will contrast with the sources in the best and fastest way. In addition, the data offers understanding and information about the guided project and research.

### **3.3 Develop viable prototype of paddle fin drive that integrates with different type of aerofoils**

In second objectives for this project which to develop viable prototype of paddle fin drive that integrates with different type of aerofoil. Several approaches to obtain design requirements will be discussed in this section as well as the design by using software.

#### **3.3.1 Design of product using 3D CAD software (SOLIDWORKS)**

Detailed design is based on a conceptual design, design and detail, and ultimately results in well-designed solutions when done professionally. This process of refining concept and developing schedules, requirements and estimates. Outputs including 2D and 3D models will be included. Detail design was performed using Solidworks software.

Solidworks Software is a CAD and CAE framework used for the development of solid model models. It helps to draw geometry for 2D drawings and generates 3D models for any piece or assembly with exact dimensions. Figure 3.3.1-1 shown drawing of paddle fin drive using Solidwork software.

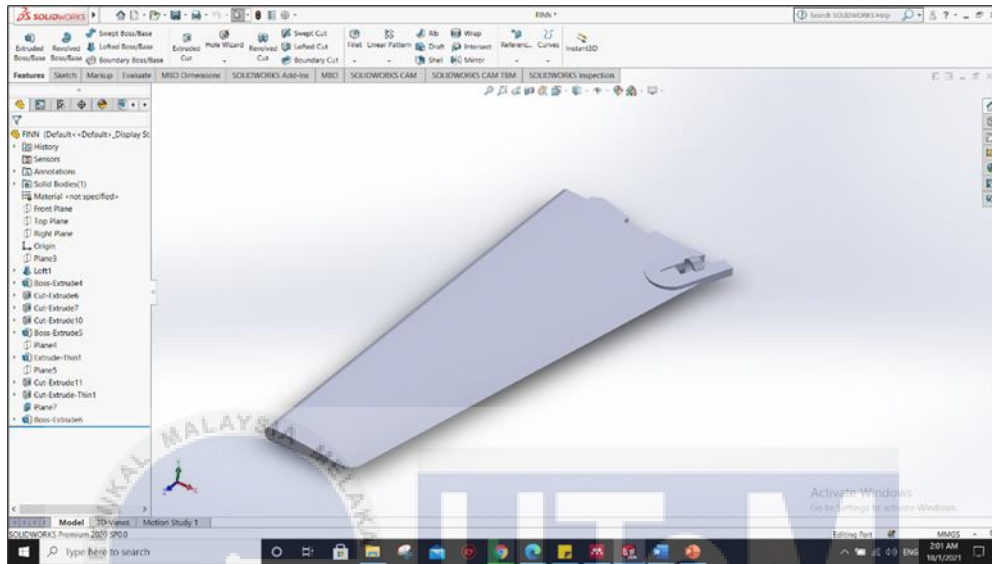


Figure 3.3.1-1: Drawing Paddle Fin Drive

### 3.3.2 Analyse the type of aerofoil with an optimum forward thrust for fishing kayak

In third objectives for this project which to analyse the type of aerofoil with an optimum forward thrust for fishing kayak. This section was conducted to reach the third objective project. The section was slightly longer and detail because this section very critical part to produce the good result for this project.

### 3.3.3 Model Analysis Design and Simulation using ANSYS Software

ANSYS software is for structural analysis allows complex structural engineering issues to be overcome and stronger and more rapid design decisions taken. With Finite Element Analysis (FEA) in the suite, solutions can be personalized, automated and parameterized for the analysis of multiple design scenarios for structural engineering problems. It can also conveniently link to other resources for physics research for greater faithfulness. An analysis modal of an aerofoil will be conducted to detect the natural properties or mode types and frequencies responsible for aerofoil vibration. Figure 3.3.3-1 shown example corresponding modal analysis result.

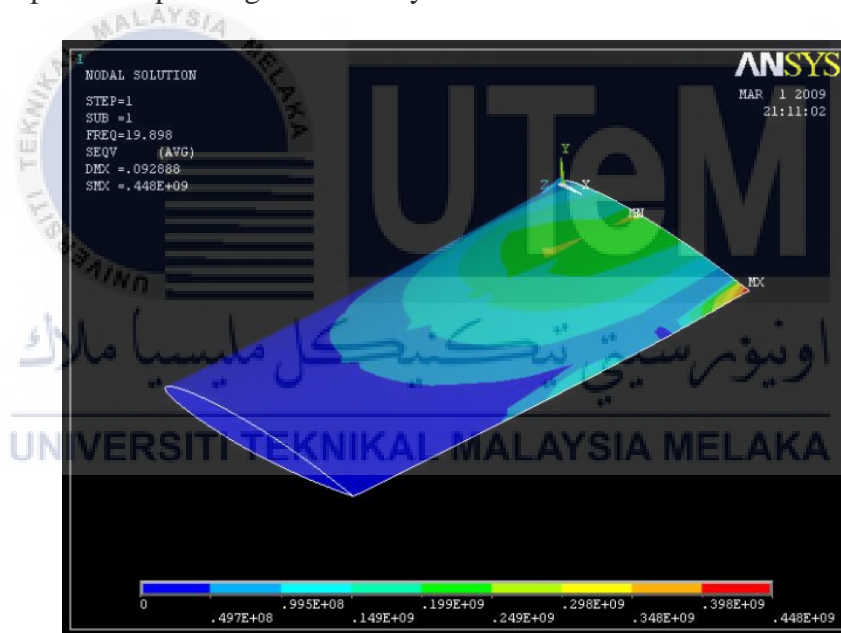


Figure 3.3.3-1: Corresponding analysis model

### 3.3.4 Modelling and meshing analysis

Meshing is part of the engineering field simulation process, where complex geometries are divided into single components, which can be used to provide the broader region with discrete local approximations. The mesh affects the accuracy, convergence and speed of simulation. In addition, since machining normally takes most of the time to generate simulation results, the quicker and more specifically, the more automated and better the machining tools are. Ansys offers the most suitable mesh for reliable, effective, high-performance mesh software. Figure 3.3.4-1 shown example meshing analysis model.

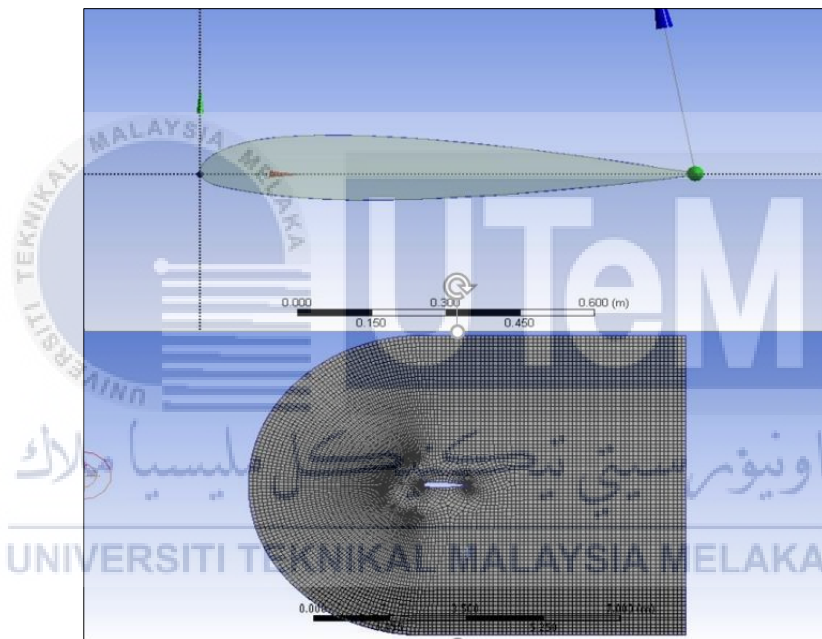


Figure 3.3.4-1: Meshing Analysis Model

### 3.3.5 Pressure and Velocity Analysis

With regard to the structural design, it is especially advisable to estimate the critical number of the Mach if the torque factor of the press distribution through aerofoils is not possible for testing. On top and under surfaces the pressure distribution is equal to zero lift. Static pressure contours illustrate that the static pressure increases with increasing angle of attack on the lower surface of the aerofoil. Figure 3.3.5-1 shown example static pressure for  $0^\circ$ .

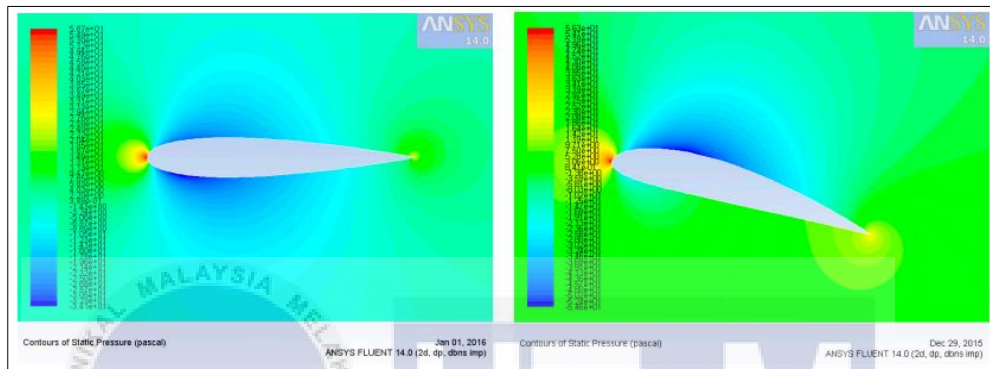


Figure 3.3.5-1: Static Pressure for  $0^\circ$

Static pressure on the lower surface of the aerofoil is increased and the reverse magnitude is increased by velocity contours on the lower surface. Figure 3.3.5-2 shown example of contours of velocity magnitude.

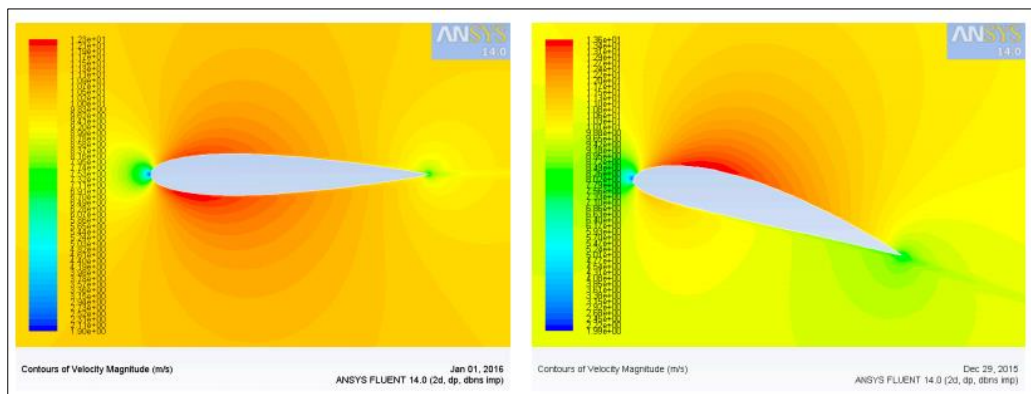


Figure 3.3.5-2: Contours velocity magnitude

## **CHAPTER 4**

### **RESULT AND DISCUSSION**

This chapter explains the substantial finding for the types of airfoil design that can be apply to paddle fin drive. Besides, this chapter will include the findings for viable prototype of paddle fin drive that integrates with three types of aerofoils which by using the Solidwork software. Other than that, this chapter also will explain the investigation process to find the Angle of Attack (AOA), Coefficient of Lift (CL), Coefficient of Drag (CD) and Lift Force (LF) of three (3) different types of airfoils which includes, NACA 0015 (Symmetrical), NACA 2414 (Asymmetrical) and NACA 4415 (Chambered). These 3 types of airfoils will go through the same process which are Mesh generation, Modelling and Meshing, Static pressure, and Velocity magnitude by using ANSYS. After the result obtained, a comparison of three different types of air foils is made.

#### **4.1 Design of Fin with Different Type of Airfoil Using Solidwork Software**

#### 4.1.1 Design of fin with NACA 0015 (Symmetrical) Airfoil

Table 4.1.1-1: Database NACA 0015

NACA 0015			
1.0000	0.00158	0.0125	-0.02367
0.9500	0.01008	0.0250	-0.03268
0.9000	0.01810	0.0500	-0.04443
0.8000	0.03279	0.0750	-0.05250
0.7000	0.04580	0.1000	-0.05853
0.6000	0.05704	0.1500	-0.06682
0.5000	0.06617	0.2000	-0.07172
0.4000	0.07254	0.2500	-0.07427
0.3000	0.07502	0.3000	-0.07502
0.2500	0.07427	0.4000	-0.07254
0.2000	0.07172	0.5000	-0.06617
0.1500	0.06682	0.6000	-0.05704
0.1000	0.05853	0.7000	-0.04580
0.0750	0.05250	0.8000	-0.03279
0.0500	0.04443	0.9000	-0.01810
0.0250	0.03268	0.9500	-0.01008
0.0125	0.02367	1.0000	-0.00158
0.0000	0.00000		

As the first step for creating the airfoil model, the data of airfoil was taken from the NACA database where data regarding various airfoils are stored like a repository. Table 4.1.1-1 shows the NACA database of NACA 0015 was located. Those coordinates of airfoil were saved in Excel file. Then, data of NACA 0015 profile were imported to Solidwork software and the model was generated. Details for NACA 0015, Max thickness 15% at 30% chord and Max chamber 0% at 0% chord.



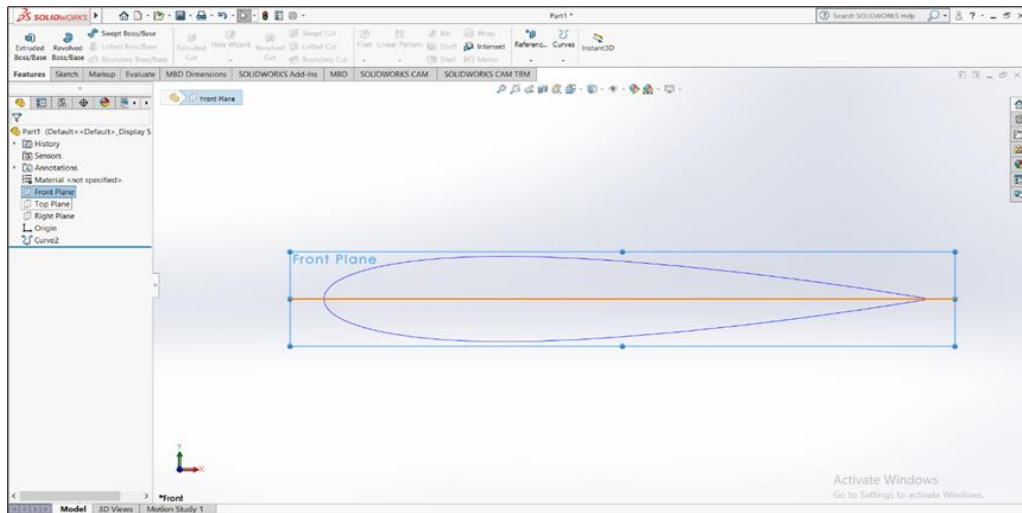
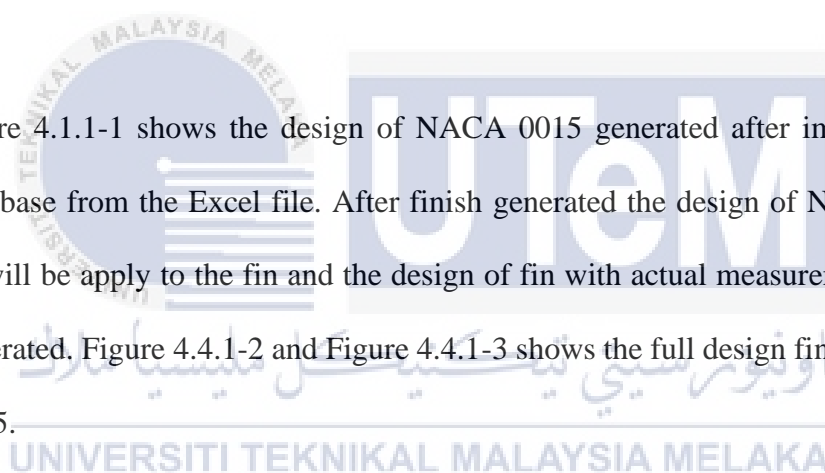


Figure 4.1.1-1: Coordinate airfoil after import Database NACA 0015

Figure 4.1.1-1 shows the design of NACA 0015 generated after importing the NACA database from the Excel file. After finish generated the design of NACA 0015, the airfoil will be apply to the fin and the design of fin with actual measurement design will be generated. Figure 4.4.1-2 and Figure 4.4.1-3 shows the full design fin with airfoil NACA 0015.



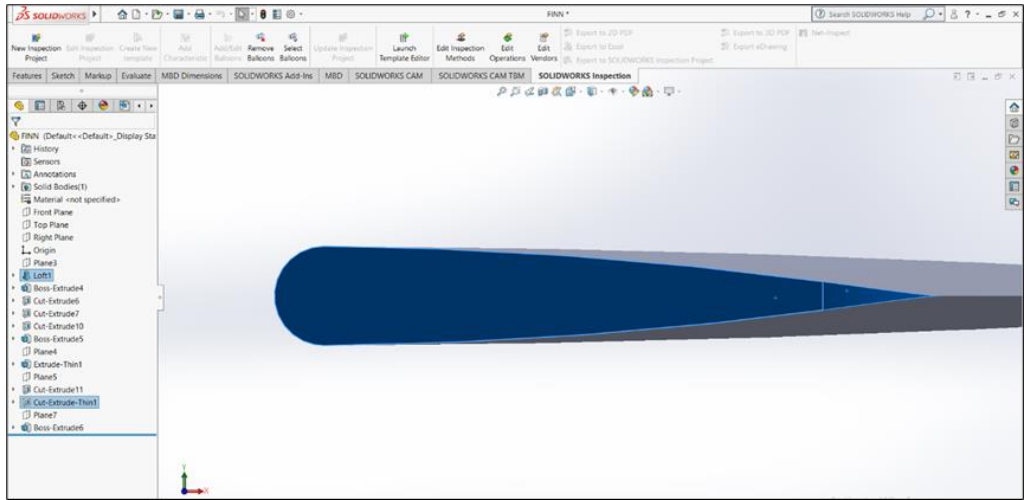


Figure 4.1.1-2: Generate model NACA 0015

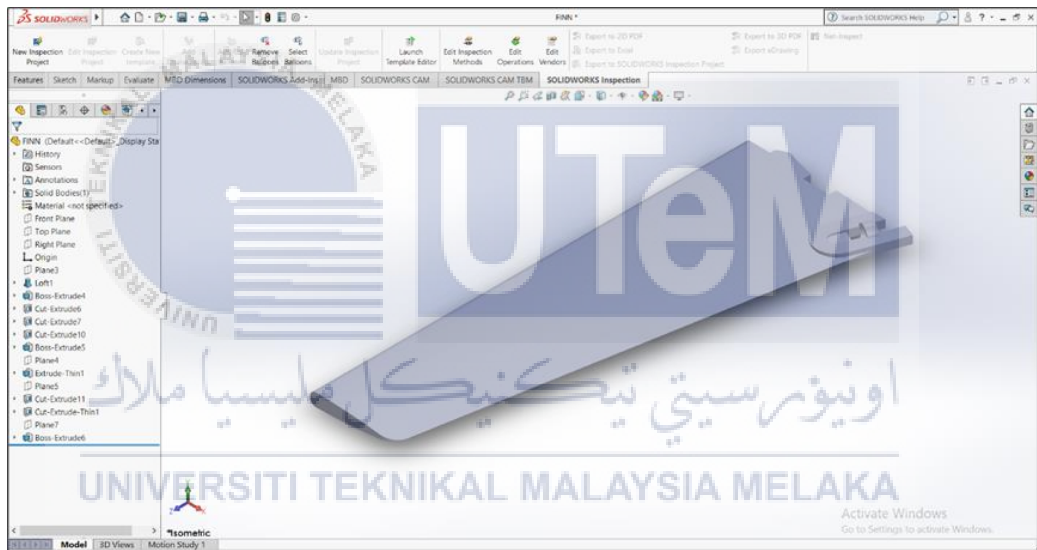


Figure 4.1.1-3: Full design fin with airfoil NACA 0015

#### 4.1.2 Design of fin with NACA 2414 (Semi Symmetrical) Airfoil

Table 4.1.2-1: Database NACA 2414

NACA 2414					
1.00000	0.00147	0.24740	0.08645	0.25260	-0.05208
0.99739	0.00210	0.20285	0.08255	0.29844	-0.05133
0.98929	0.00396	0.16169	0.07707	0.34644	-0.04987
0.97587	0.00700	0.12440	0.07014	0.39611	-0.04787
0.95729	0.01112	0.09141	0.06198	0.44739	-0.04537
0.93372	0.01620	0.06310	0.05281	0.49931	-0.04232
0.90542	0.02207	0.03977	0.04289	0.55129	-0.03886
0.87267	0.02857	0.02165	0.03245	0.60276	-0.03516
0.83582	0.03552	0.00892	0.02171	0.65316	-0.03132
0.79527	0.04274	0.00169	0.01085	0.70194	-0.02745
0.75143	0.05004	0.00000	0.00000	0.74857	-0.02365
0.70480	0.05723	0.00379	-0.01031	0.79252	-0.01998
0.65586	0.06412	0.01293	-0.01956	0.83331	-0.01650
0.60515	0.07053	0.02730	-0.02770	0.87048	-0.01328
0.55324	0.07629	0.04669	-0.03471	0.90360	-0.01035
0.50069	0.08120	0.07087	-0.04054	0.93230	-0.00776
0.44808	0.08512	0.09957	-0.04516	0.95626	-0.00557
0.39598	0.08787	0.13246	-0.04858	0.97518	-0.00381
0.34454	0.08913	0.16918	-0.05082	0.98886	-0.00252
0.29482	0.08866	0.20937	-0.05195	0.99713	-0.00173
				1.00000	-0.00147

Next, this step for creating the NACA 2414 airfoil model, the data of airfoil was taken from the NACA database where data regarding various airfoils are stored like a repository. Table 4.1.2-1 show the NACA database of NACA 2414 was located. Those coordinates of airfoil were saved in Excel file. Then, data of NACA 2414 profile were imported to Solidwork software and the model was generated. Details for NACA 2414, Max thickness 14% at 29.5% chord and Max chamber 2% at 39.6% chord.

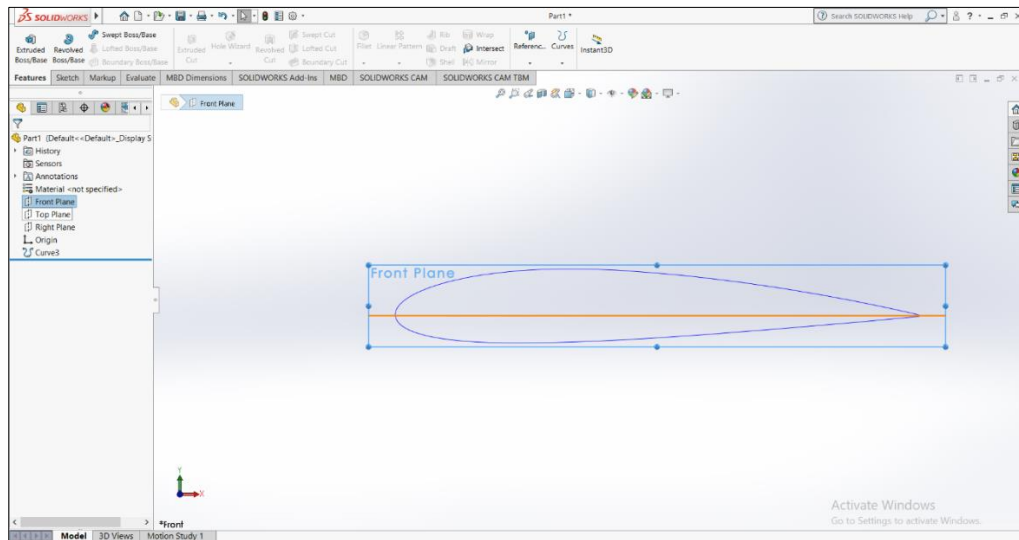


Figure 4.1.2-1: Coordinate airfoil after import Database NACA 2414

Figure 4.1.2-1 shows the design of NACA 2414 generated after importing the NACA database from the Excel file. After finish generated the design of NACA 2414, the airfoil will be apply to the fin and the design of fin with actual measurement design will be generated. Figure 4.1.2-2 and Figure 4.1.2-3 shows the full design fin with airfoil NACA 2414.

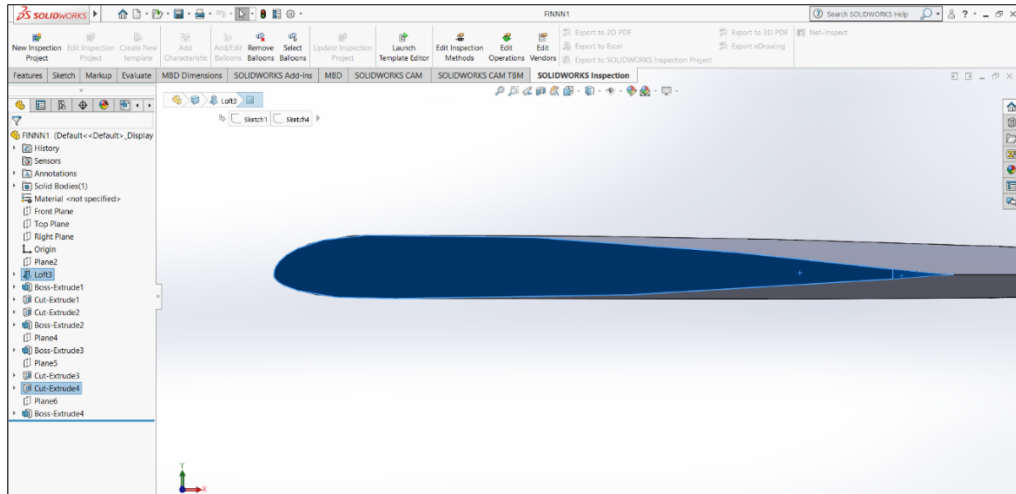


Figure 4.1.2-2: Generate model NACA 2414

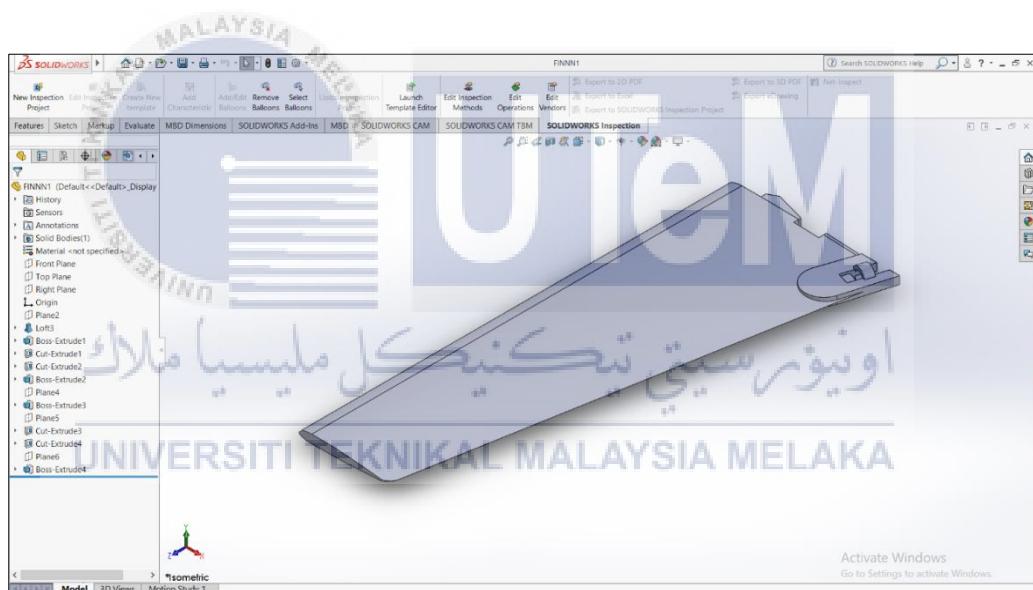


Figure 4.1.2-3: Full design fin with airfoil NACA 2414

### 4.1.3 Design of fin with NACA 4415 (Chambered) Airfoil

Table 4.1.3-1: Database NACA 4415

<b>NACA 4415</b>							
1.00000	0.00000	0.50000	0.10538	0.00000	0.00075	0.50000	-0.02713
0.99893	0.00039	0.46730	0.10837	0.00107	-0.00566	0.53270	-0.02529
0.99572	0.00156	0.43474	0.11076	0.00428	-0.01102	0.56526	-0.02340
0.99039	0.00349	0.40245	0.11248	0.00961	-0.01590	0.59755	-0.02149
0.98296	0.00610	0.37059	0.11345	0.01704	-0.02061	0.62941	-0.01958
0.97347	0.00932	0.33928	0.11361	0.02653	-0.02502	0.66072	-0.01772
0.96194	0.01303	0.30866	0.11294	0.03806	-0.02915	0.69134	-0.01596
0.94844	0.01716	0.27886	0.11141	0.05156	-0.03281	0.72114	-0.01430
0.93301	0.02166	0.25000	0.10903	0.06699	-0.03582	0.75000	-0.01277
0.91573	0.02652	0.22221	0.10584	0.08427	-0.03817	0.77779	-0.01136
0.89668	0.03171	0.19562	0.10190	0.10332	-0.03991	0.80438	-0.01006
0.87592	0.03717	0.17033	0.09726	0.12408	-0.04106	0.82967	-0.00886
0.85355	0.04283	0.14645	0.09195	0.14645	-0.04166	0.85355	-0.00775
0.82967	0.04863	0.12408	0.08607	0.17033	-0.04177	0.87592	-0.00674
0.80438	0.05453	0.10332	0.07970	0.19562	-0.04147	0.89668	-0.00583
0.77779	0.06048	0.08427	0.07283	0.22221	-0.04078	0.91573	-0.00502
0.75000	0.06642	0.06699	0.06541	0.25000	-0.03974	0.93301	-0.00431
0.72114	0.07227	0.05156	0.05753	0.27886	-0.03845	0.94844	-0.00364
0.69134	0.07795	0.03806	0.04937	0.30866	-0.03700	0.96194	-0.00297
0.66072	0.08341	0.02653	0.04118	0.33928	-0.03547	0.97347	-0.00227
0.62941	0.08858	0.01704	0.03303	0.37059	-0.03390	0.98296	-0.00156
0.59755	0.09341	0.00961	0.02489	0.40245	-0.03229	0.99039	-0.00092
0.56526	0.09785	0.00428	0.01654	0.43474	-0.03063	0.99572	-0.00042
0.53270	0.10185	0.00107	0.00825	0.46730	-0.02891	0.99893	-0.00011
						1.00000	0.00000

Furthermore, this step also for creating the NACA 4415 airfoil model, the data of airfoil was taken from the NACA database where data regarding various airfoils are stored like a repository. Table 4.1.3-1 show the NACA database of NACA 4415 was located. Those coordinates of airfoil were saved in Excel file. Then, data of NACA 4415 profile were imported to Solidwork software and the model was generated. Details for NACA 4415, Max thickness 15% at 30.9% chord and Max chamber 4% at 40.2% chord.

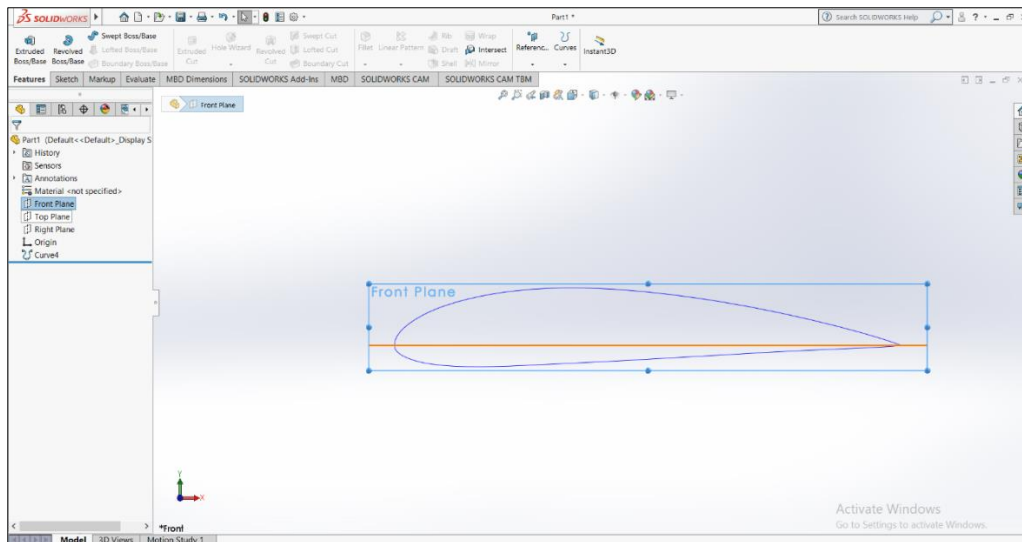
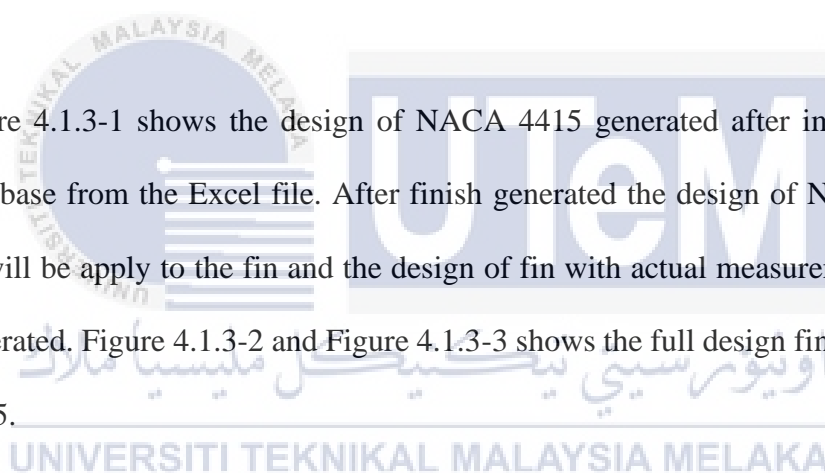


Figure 4.1.3-1: Coordinate airfoil after import Database NACA 4415

Figure 4.1.3-1 shows the design of NACA 4415 generated after importing the NACA database from the Excel file. After finish generated the design of NACA 4415, the airfoil will be apply to the fin and the design of fin with actual measurement design will be generated. Figure 4.1.3-2 and Figure 4.1.3-3 shows the full design fin with airfoil NACA 4415.



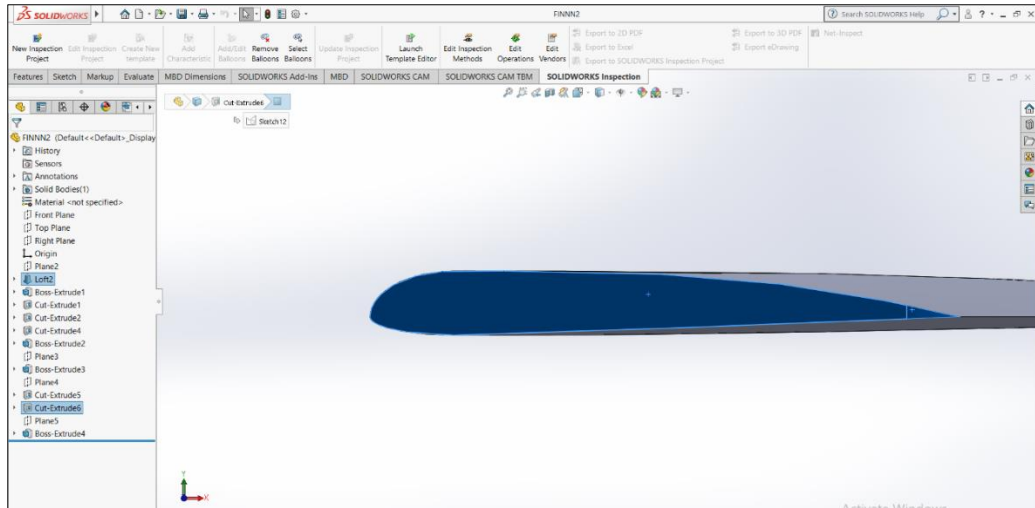


Figure 4.1.3-2: Generate model NACA 4415

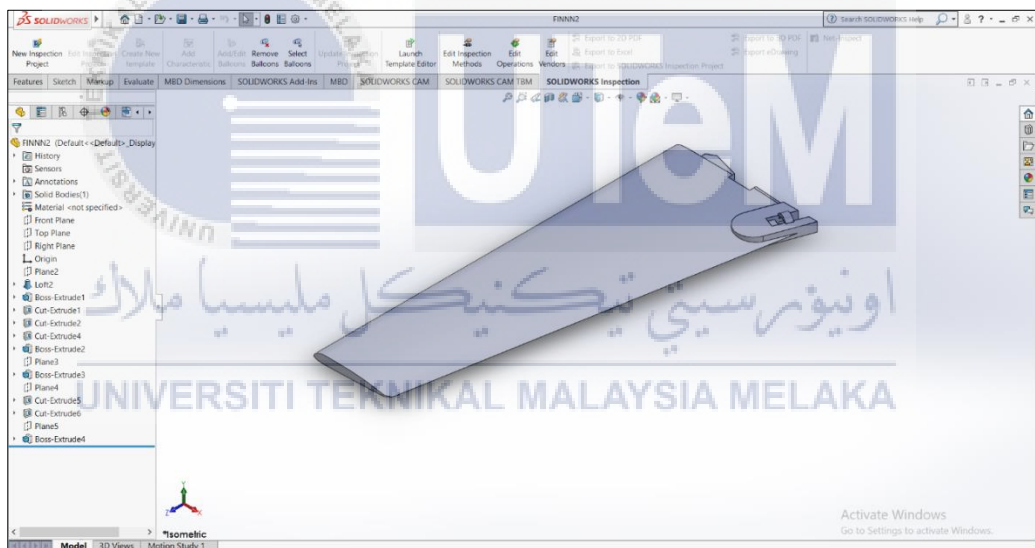


Figure 4.1.3-3: Full design fin with airfoil NACA 4415

## 4.2 Analysis of Naca 0015 Airfoil Design



## 4.2.1 Process of Modelling and Meshing generation

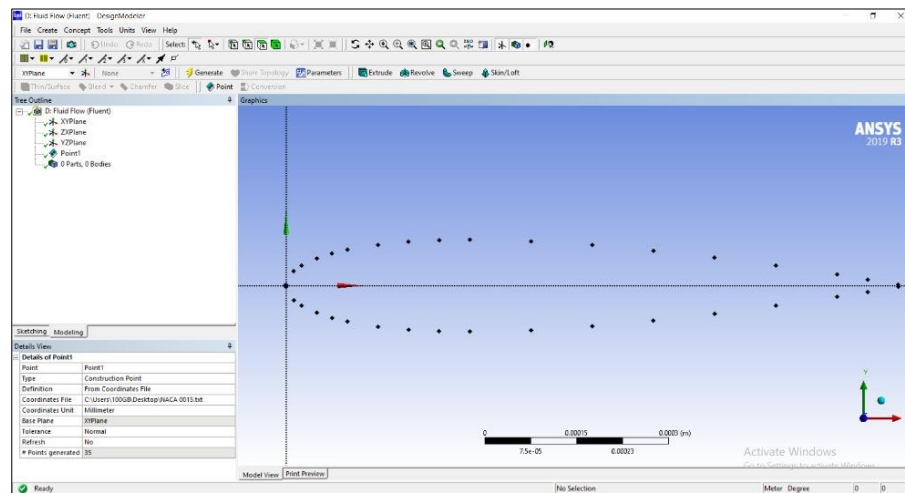


Figure 4.2.1-1: Coordinates of NACA 0015

As an example, this step shows a subsonic tunnel was used to simulate a NACA 0015 airfoil placed at varying angles of attack. Fluent is used to create a simulation environment for this experiment. A table of coordinates is compiled, from which the profile is drawn as in Figure 4.2.1-1 and Figure 4.2.1-2. To build the geometric shape that would be used in the simulation procedure, the NACA 0015 airfoil coordinates were input in this stage and converted. Figure 4.2.1-3 shows the geometry of the NACA 0015 airfoil section.

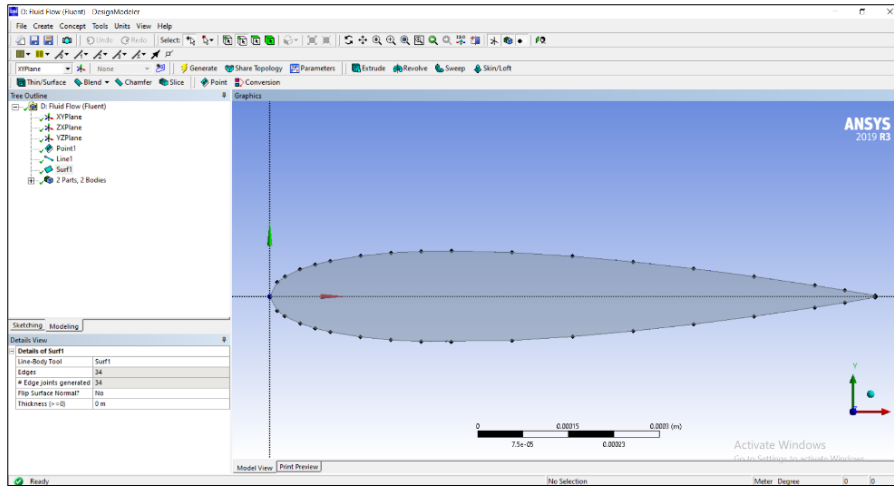


Figure 4.2.1-2: Grid generation of NACA 0015

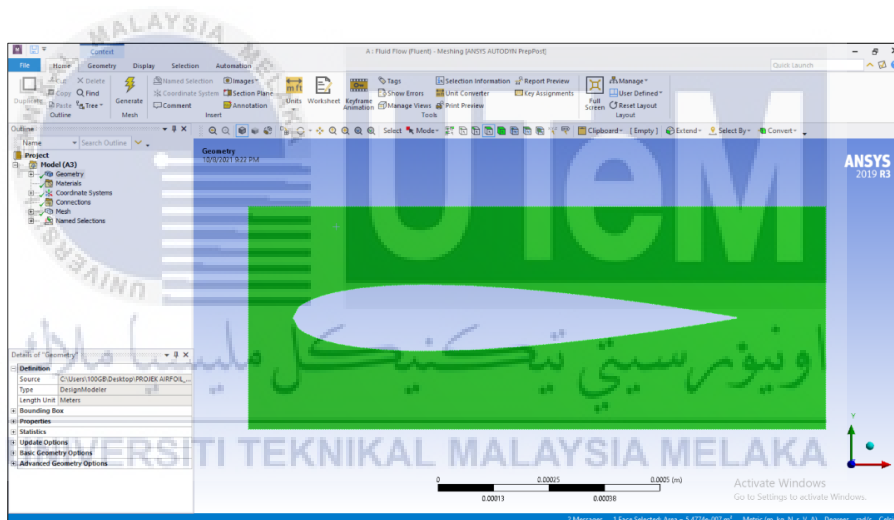


Figure 4.2.1-3: Geometry of the NACA 0015 airfoil section

To specify boundary conditions, the mesh able surface must be created after the airfoil profile has been generated. The meshing procedure begins with the creation of a coordinate system at the tail of the airfoils. The flow domain must be divided into smaller subdomains in order to analyse the fluid flow. Figure 4.2.1-4 shows the meshing of air profile around the NACA 0015 airfoil. These are each mesh elements. As a result of mesh

analysis, it has total nodes are 2564 and total elements is 2360. Analyzed mesh based on the assumption that the relevance centre is fine and smoothing.

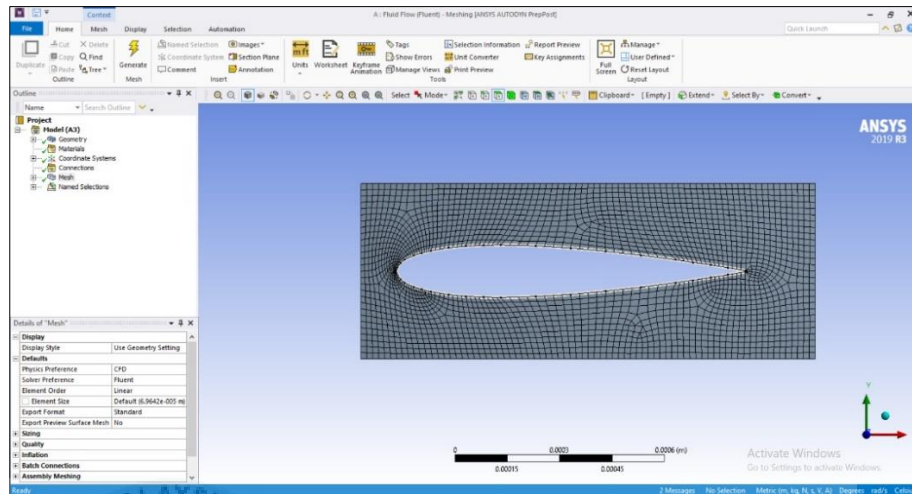


Figure 4.2.1-4: Meshing of air profile around the NACA 0015 airfoil

#### 4.2.2 Static pressure NACA 0015

The figure 4.2.2-1 shows the visualization of static pressure contour distribution around the NACA 0015 at  $0^\circ$  Angle of attack. From the flow visualization at  $0^\circ$  Angle of attack (AOA) particles collide with the airfoil on. At zero angle of attack, both the upper and lower layers of airfoils have a similar static pressure.

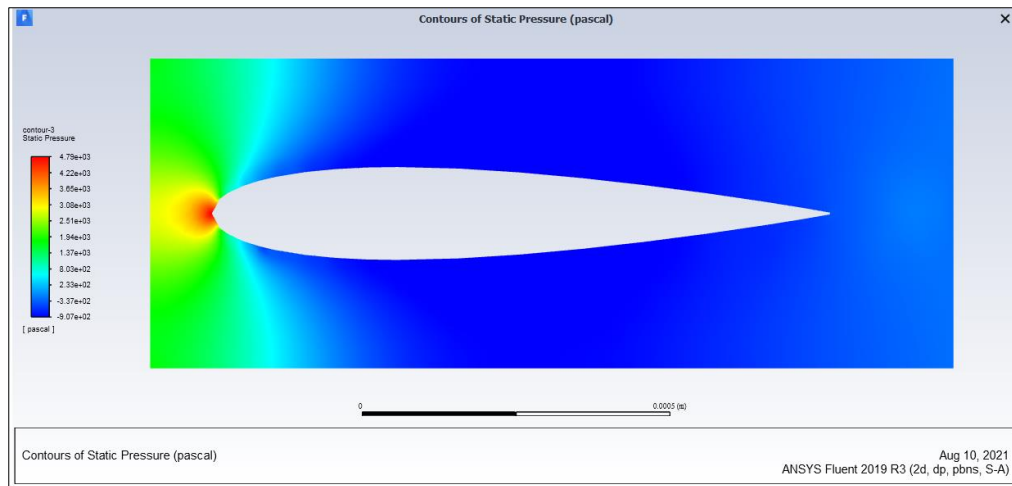


Figure 4.2.2-1: Static pressure contour distribution around the NACA 0015 at 0° Angle of attack (AOA)

Figure 4.2.2-2 shows the streamline of static pressure NACA 0015 at zero angle of attack. At the angles of attack at maximum coefficients of lift, it can see that the low-pressure zone is much more concentrated on the upper layer than lower layer. On the bottom side of the airfoil, a high-pressure zone is generated, causing a force to act on the airfoil. As a result, the vertical component of this force gives us lift and the horizontal component drag.

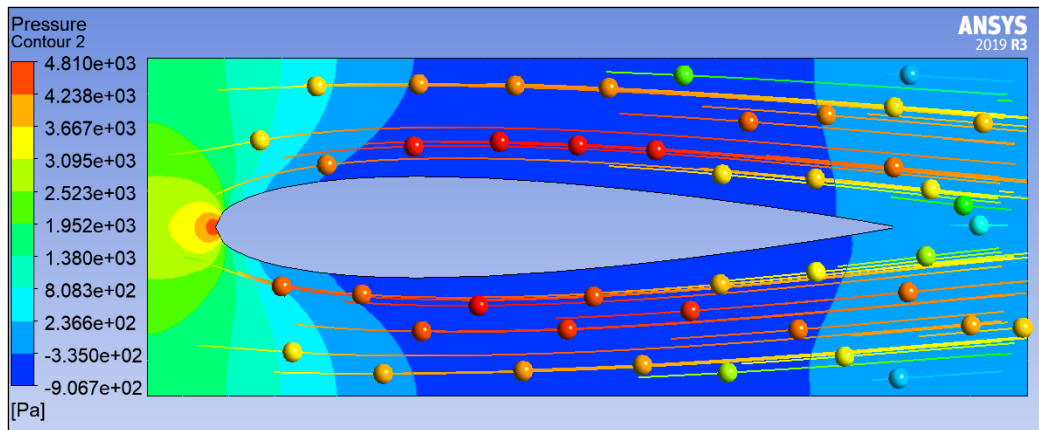


Figure 4.2.2-2: Streamline of static pressure NACA 0015

### 4.2.3 Velocity magnitude NACA 0015

Since it is symmetric in nature. From the Figure 4.2.3-1, At zero angle of attack, both the upper and lower layers of airfoils have a similar velocity magnitude. Due to the same velocity, the pressure on the upper and lower layers will be the same or the difference will be very small.

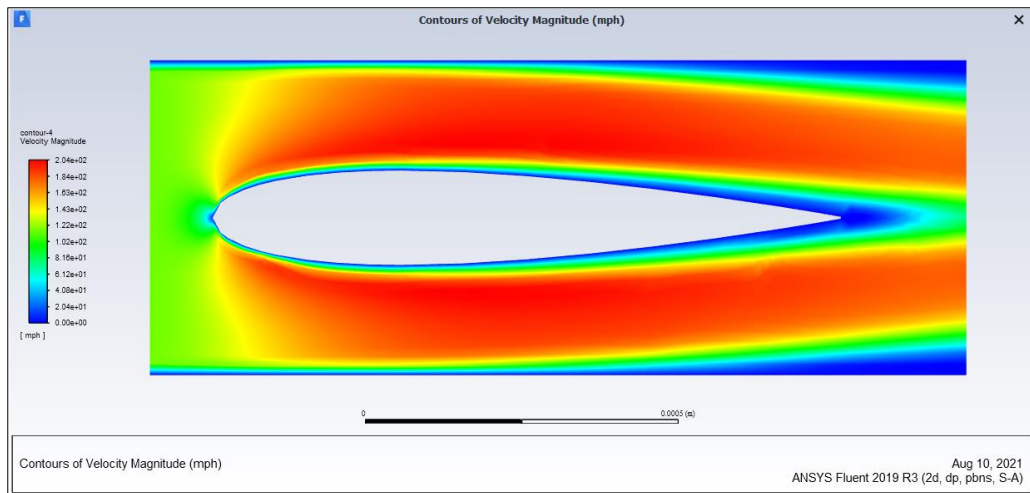


Figure 4.2.3-1: Contours of velocity magnitude in m/s of NACA 0015 at 0° Angle of attack (AOA)

Velocity distribution at zero angle of attack can be seen very as similar on both upper and lower layer of airfoils. Figure 4.2.3-2 shows the streamline of velocity magnitude NACA 0015, it can see which gives rise to same velocity on both the surface of airfoil. At higher angle of attack, the flow separates from upper layer of flow thus leading to increase in velocity in upper layer of flow and decrease in value of lift coefficient.

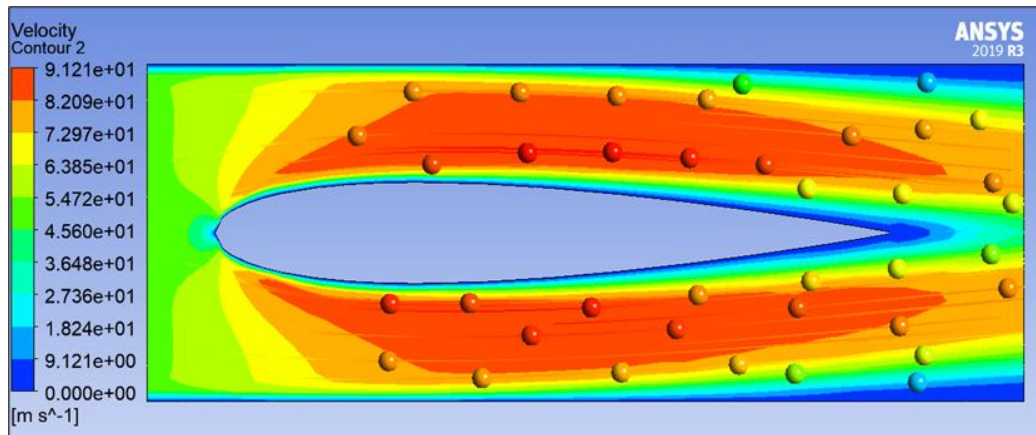


Figure 4.2.3-2: Streamline of velocity magnitude NACA 0015

#### 4.2.4 Variation of lift and drag coefficient with Angle of attack (AOA)

From the simulation of static pressure and magnitude velocity of NACA 0015, the data coefficient of lift (LF), coefficient of drag (LD) and Lift Force (LF) of NACA 0015 were found for different angle of attack. Finally, the ratio of CL to CD was calculated. The Table 4.2.4-1 shown the data CL, CD and LF with different AOA.

Table 4.2.4-1: Result Coefficient of Lift (CL), Coefficient of Drag (CD) and Lift Force with different angle of attack for NACA 0015

Angle of Attack (AOA) *Parameter	Result		
	Coefficient of Lift (CL)	Coefficient of Drag (CD)	Lift Force
0	0.1628	0.0306	607.1
0.5	0.3128	0.0294	1869.5
1	0.4132	0.0282	2186.2
1.5	0.4569	0.0273	2448.4
2	0.4852	0.0276	2693.5
2.5	0.5294	0.0280	2829.1
3	0.5562	0.0289	2998.6
3.5	0.5643	0.0298	3189.3
4	0.5782	0.0309	3393.2
4.5	0.5864	0.0315	3505.3
5	0.5917	0.0326	3621.5
5.5	0.6188	0.0354	3812.6
6	0.6257	0.0381	3998.2
6.5	0.5878	0.0438	4178.6
7	0.5528	0.0517	4256.2
7.5	0.4829	0.0568	4302.4
8	0.4731	0.0824	3401.3
8.5	0.4612	0.0915	3512.4

Coefficient of lift (LF) depends on angle of attack (AOA). The analysis results obtained from the model airfoil NACA 0015 are plotted on graph. The Figure 4.2.4-1 shows that the lift coefficient increases with increasing angle of attack and after a certain angle of attack it is decreased and this angle is called stall angle. It can be observed from the graph that lift coefficient increases and maximum (0.657) at angle of attack 6°, degree after which it begins to decrease (0.4612) at angle of attack 8.5°, degree. Therefore, Stall angle of attack in this graph at angle of attack 6°, degree.



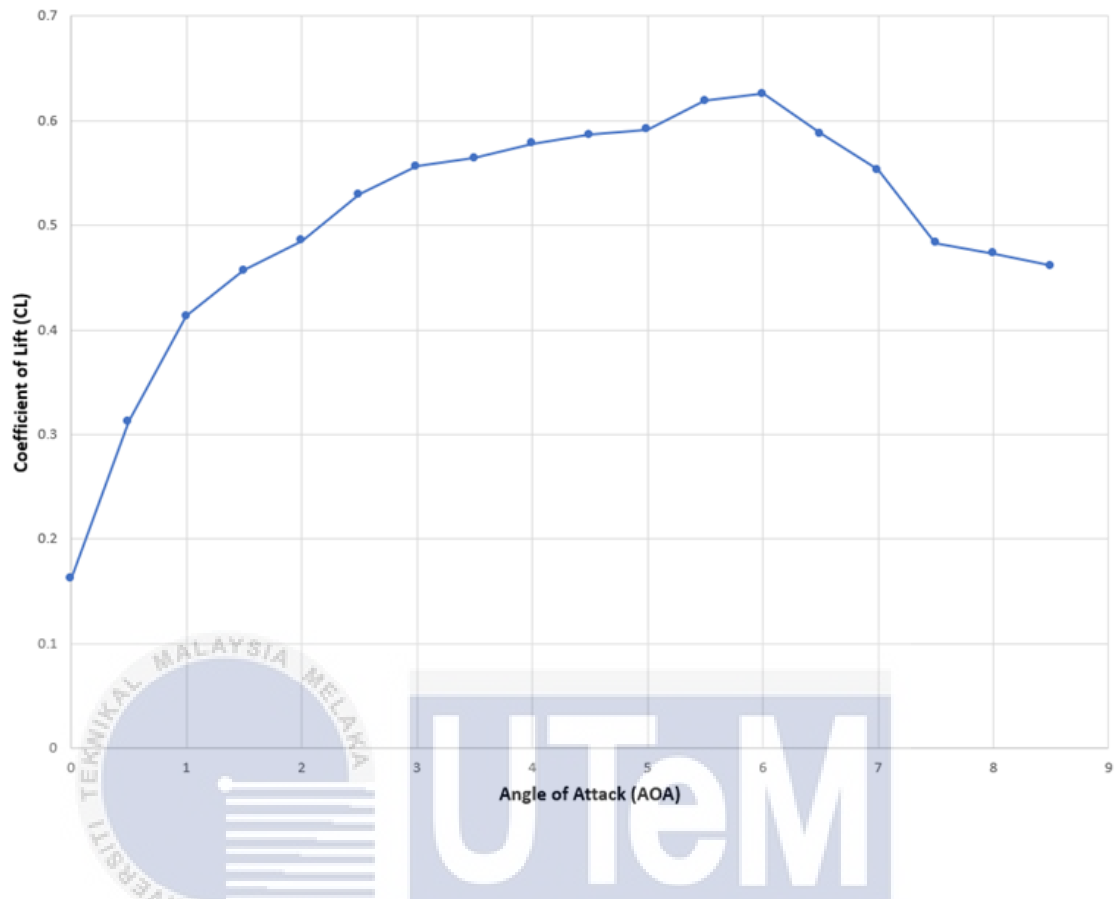


Figure 4.2.4-1: Graph 1: Coefficient of lift (CL) in varying angle of attack (AOA) for

اونیورسیتی تیکنیکل مالیزیا ملاک  
 NACA 0015

UNIVERSITI TEKNIKAL MALAYSIA MELAKA

Coefficient of drag (CD) also depends on angle of attack (AOA). The analysis results obtained from the model airfoil NACA 0015 are plotted on graph. From Figure 4.2.4-2 in the case of drag coefficient it can see that the drag coefficient decreases ever so slightly till angle of attack at 1.5 °, degree at the value 0.0273 but at the angle of attack 2° degree, (0.0276) the value of drag coefficient become increases. The value drag coefficient is increased as angle of attack is increased. Drag coefficient is maximum (0.0915) at angle of attack 8.5°, degree.

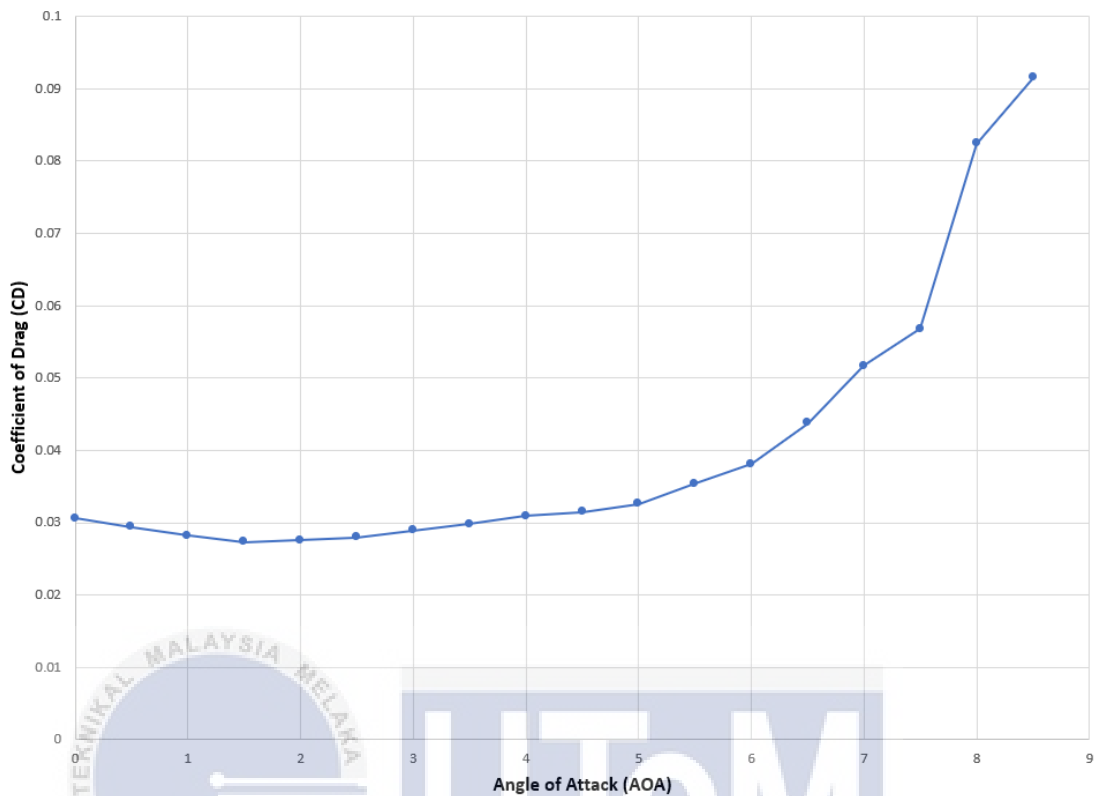


Figure 4.2.4-2: Graph 2: Coefficient of drag (CD) in varying angle of attack (AOA) for

اونیورسیتی تیکنیکل ملیسیا ملاک  
 NACA 0015  
 UNIVERSITI TEKNIKAL MALAYSIA MELAKA

Lift force (LF) was calculated using the lift coefficient and plotted against the angle of attack. The speed was assumed as 10 m/s for the calculation of lift force. The analysis results obtained from the model airfoil NACA 0015 are plotted on graph. From figure 4.2.4-3 shows that the lift force increases from the point 607.1 at angle of attack 0°, degree till the point 4302.4 at angle of attack 7.5 °, degree and at angle of attack 8°, degree it is decreased but the point increases again at angle of attack 8.5°, degree.

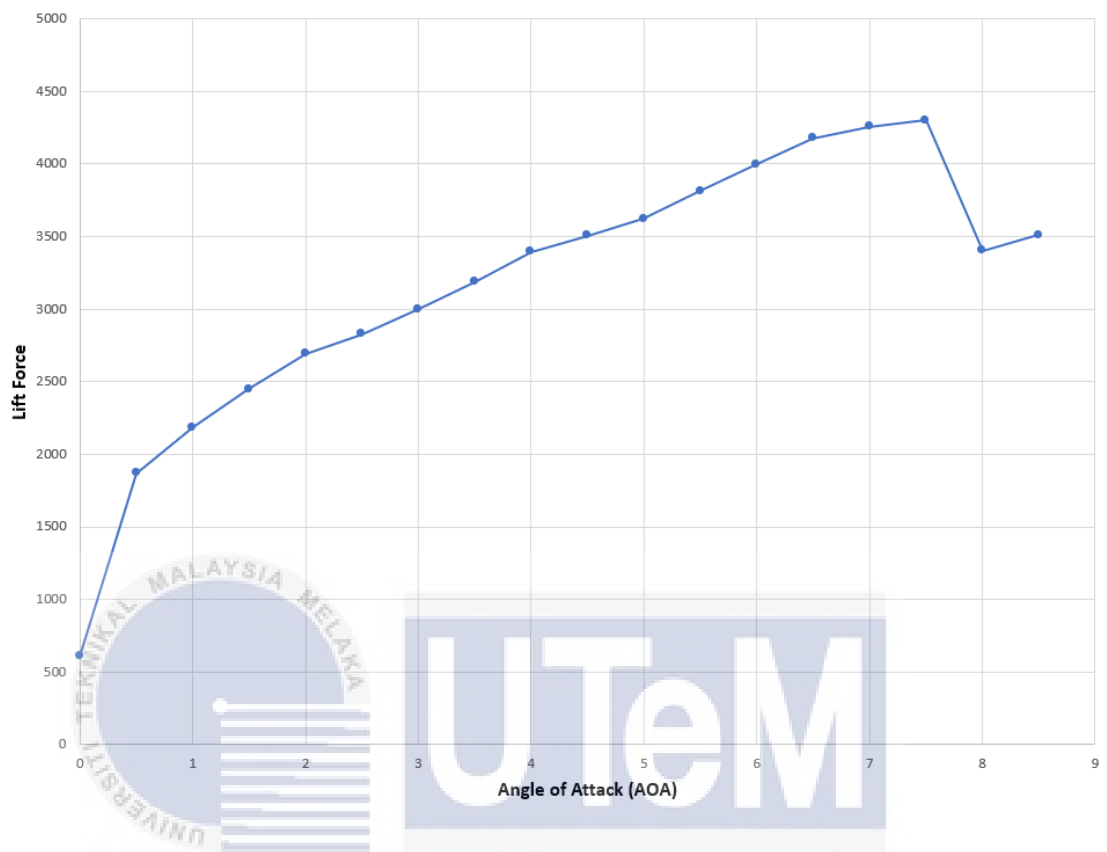


Figure 4.2.4-3: Graph 3: Lift force in varying angle of attack (AOA) for NACA 0015

### 4.3 Analysis of Naca 2414 Airfoil Design

#### 4.3.1 Process of Modelling and Meshing generation

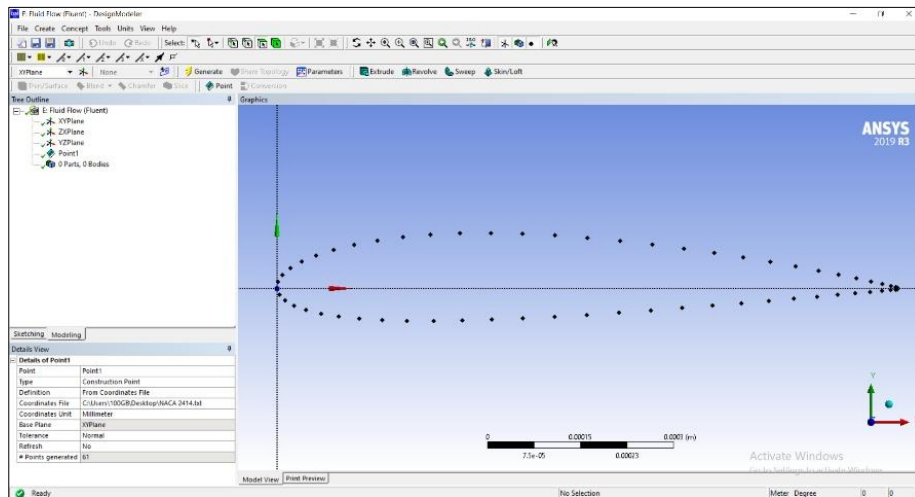


Figure 4.3.1-1: Coordinates of NACA 2414

As an example, this step shows a subsonic tunnel was used to simulate a NACA 2414 airfoil placed at varying angles of attack. Fluent is used to create a simulation environment for this experiment. A table of coordinates is compiled, from which the profile is drawn as in Figure 4.3.1-1 and Figure 4.3.1-2. To build the geometric shape that would be used in the simulation procedure, the NACA 2414 airfoil coordinates were input in this stage and converted. Figure 4.3.1-3 shows the geometry of the NACA 2414 airfoil section.

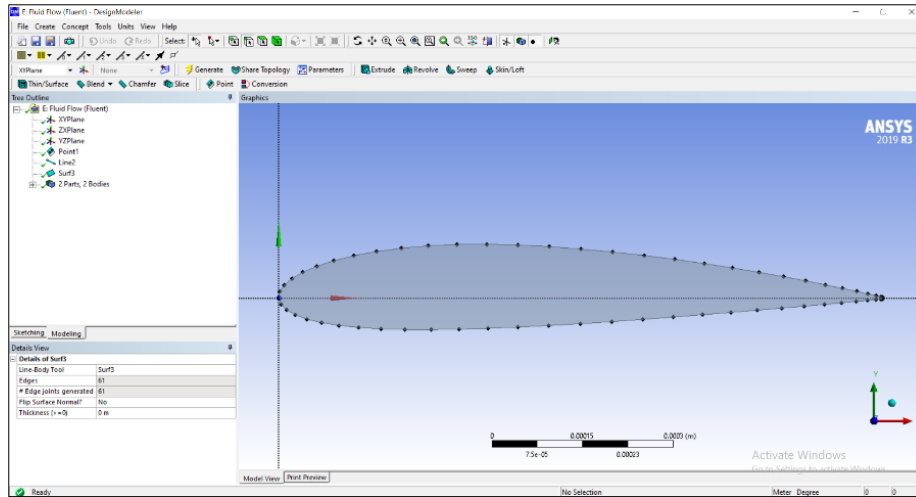


Figure 4.3.1-2: Grid generation of NACA 2414

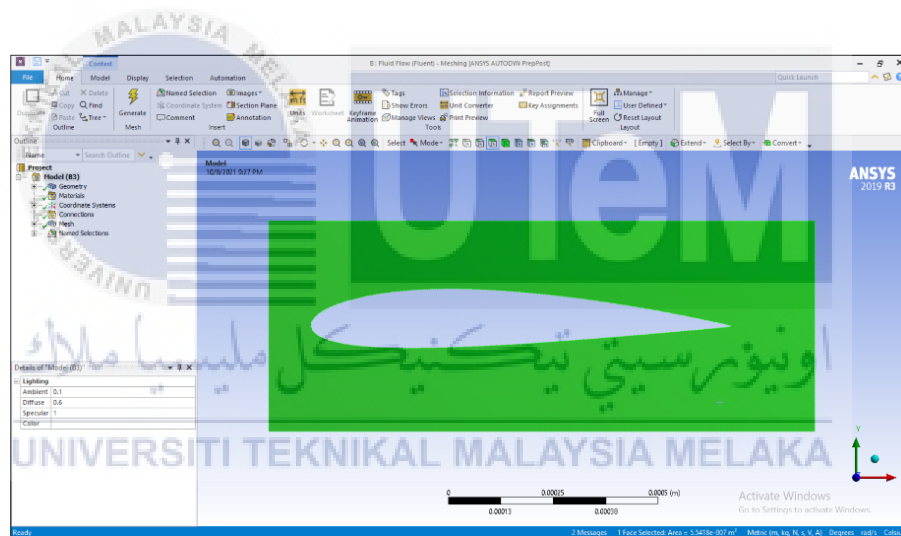


Figure 4.3.1-3: Geometry of the NACA 2414 airfoil section

To specify boundary conditions, the meshable surface must be created after the airfoil profile has been generated. The meshing procedure begins with the creation of a coordinate system at the tail of the airfoils. The flow domain must be divided into smaller subdomains in order to analyse the fluid flow. Figure 4.3.1-4 shows the meshing of air profile around the NACA 2414 airfoil. These are each mesh elements. As a result of mesh

analysis, it has total nodes are 3124 and total elements is 2859. Analyzed mesh based on the assumption that the relevance centre is fine and smoothing.

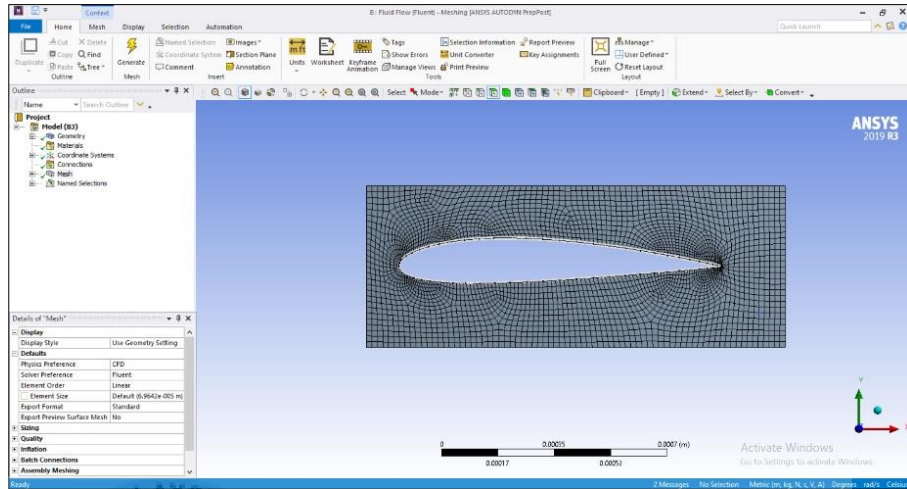


Figure 4.3.1-4: Meshing of air profile around the NACA 2414 airfoil

#### 4.3.2 Static pressure NACA 2414

Figure 4.3.2-1 shows the Static pressure contour distribution around the NACA 2414 at  $0^\circ$  Angle of attack (AOA). At zero angle of attack, it can be seen that the static pressure is little higher on the lower surface than on the upper surface. This generates a pressure gradient which causes a force on the total surface area of the airfoil.

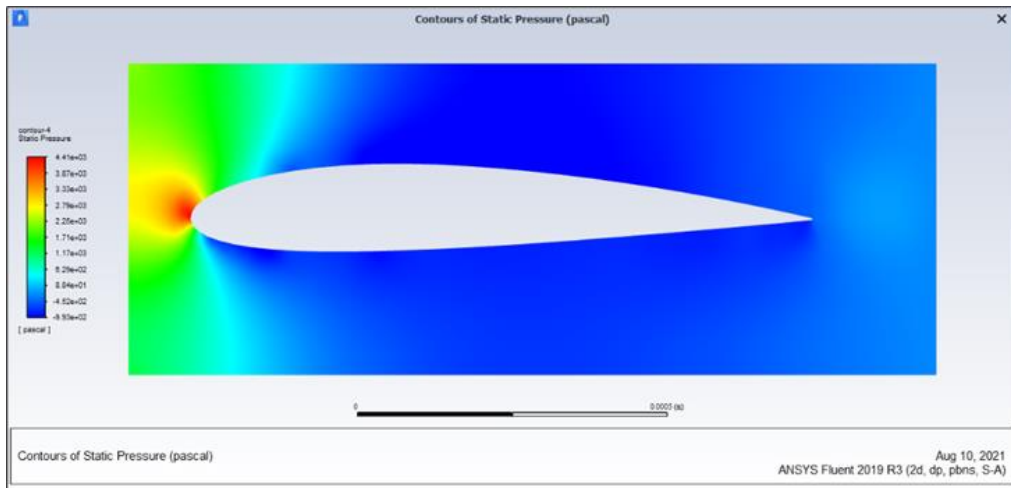


Figure 4.3.2-1: Static pressure contour distribution around the NACA 2414 at 0° Angle of attack (AOA)

Figure 4.3.2-2 shows the streamline of static pressure NACA 2414. As the angle of attack increases the pressure difference between the upper surface and the lower surface increases thus causing an increase in the force which causes increase in lift and drag coefficient.

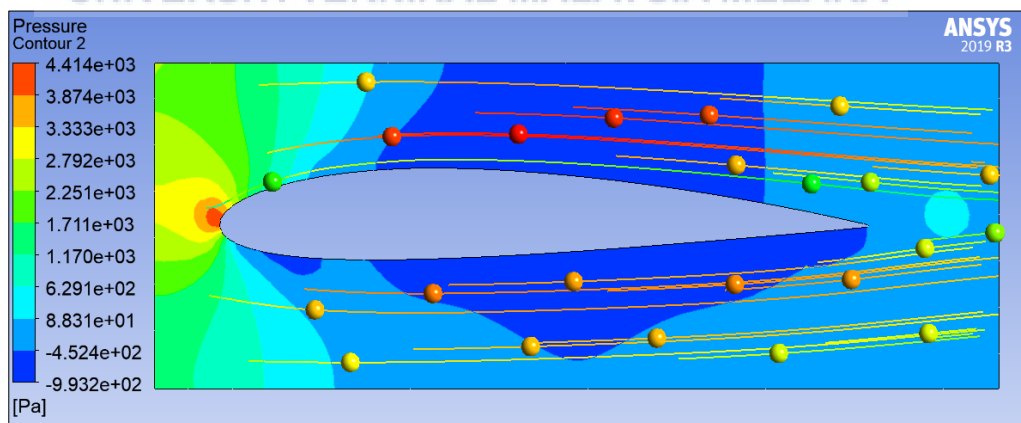


Figure 4.3.2-2: Streamline of static pressure NACA 2414

### 4.3.3 Velocity magnitude NACA 2414

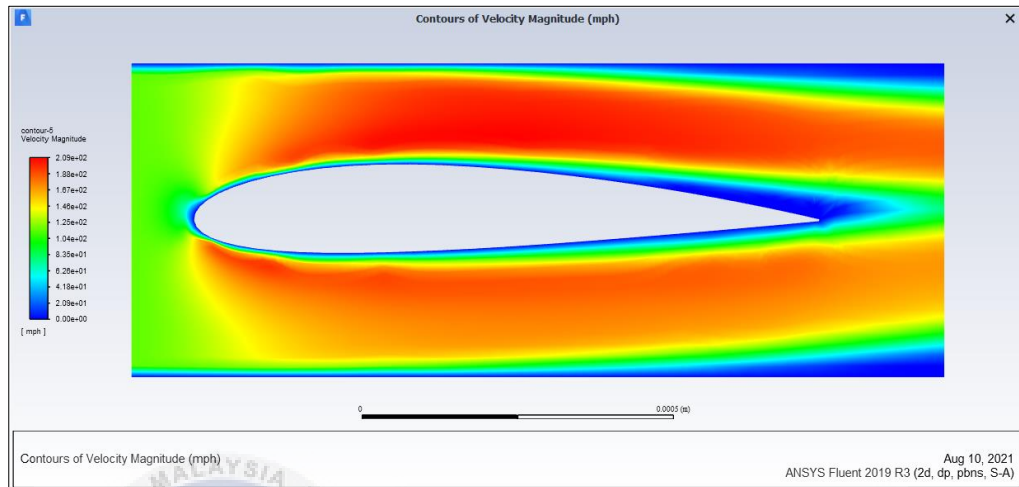


Figure 4.3.3-1: Contours of velocity magnitude in m/s of NACA 2414 at 0° Angle of attack (AOA)

From the Figure 4.3.3-1, the contours velocity magnitude of airfoil NACA 2414 at angle of attack 0°, degree is little higher on upper compare with lower layer of the airfoil. Velocity distribution at zero angle of attack can be seen different on both upper and lower layer of airfoils. Figure 4.3.3-2 shows the streamline of velocity magnitude NACA 2414, it can see which gives rise more on upper surface of airfoil. At higher angle of attack, the flow separates from upper layer of flow thus leading to increase in velocity at upper layer of flow and decrease in value of lift coefficient.



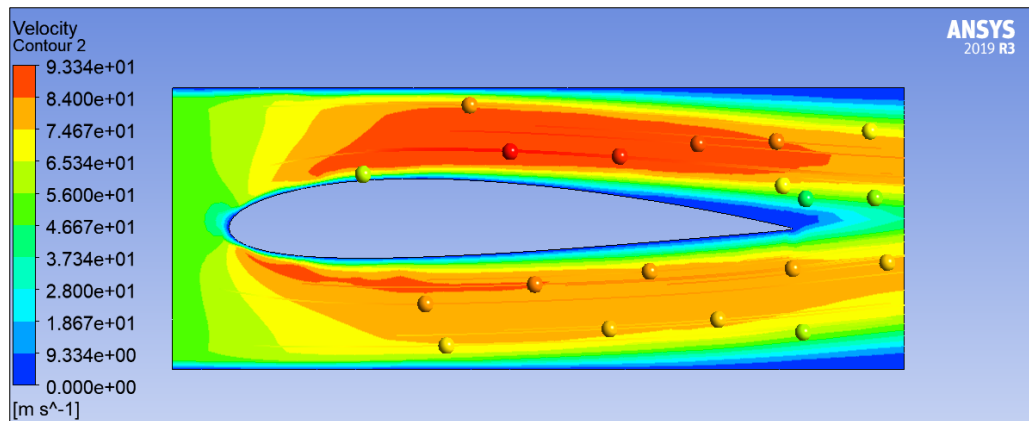


Figure 4.3.3-2: Streamline of velocity magnitude NACA 2414

#### 4.3.4 Variation of lift and drag coefficient with Angle of attack (AOA)

Next, from the simulation of static pressure and magnitude velocity of NACA 2414, the data coefficient of lift (LF), coefficient of drag (LD) and Lift Force (LF) of NACA 2414 were found for different angle of attack. Finally, the ratio of CL to CD was calculated. The Table 4.3.4-1 shown the data CL, CD and LF with different AOA.

Table 4.3.4-1: Result Coefficient of Lift (CL), Coefficient of Drag (CD) and Lift Force with different angle of attack for NACA 2414

Angle of Attack (AOA) *Parameter	Result		
	Coefficient of Lift (CL)	Coefficient of Drag (CD)	Lift Force
0	0.2152	0.02566	9938
0.5	0.3222	0.02594	19094.6
1	0.3971	0.02669	25223.4
1.5	0.4472	0.03119	27891.1
2	0.4875	0.03841	29618.7
2.5	0.5261	0.04452	32316.8
3	0.5564	0.04926	33952.8
3.5	0.5921	0.05442	34447.2
4	0.6328	0.06114	35295.8
4.5	0.6797	0.06701	35796.3
5	0.7216	0.07332	36449.5
5.5	0.7561	0.07932	37774.1
6	0.7864	0.08756	38195.4
6.5	0.8043	0.09028	35881.8
7	0.8135	0.09354	33745.2
7.5	0.8215	0.10698	29478.25

Next, the Coefficient of lift (LF) depends on angle of attack (AOA). The results obtained from the model airfoil NACA 2414 are plotted on graph. The Figure 4.3.4-1 shows that the lift coefficient increases with increasing angle of attack and this angle is called stall angle. It can be observed from the graph that lift coefficient increases and maximum (0.8215) at angle of attack 7.5°, degree. Therefore, Stall angle of attack in this graph at angle of attack 7.5°, degree.

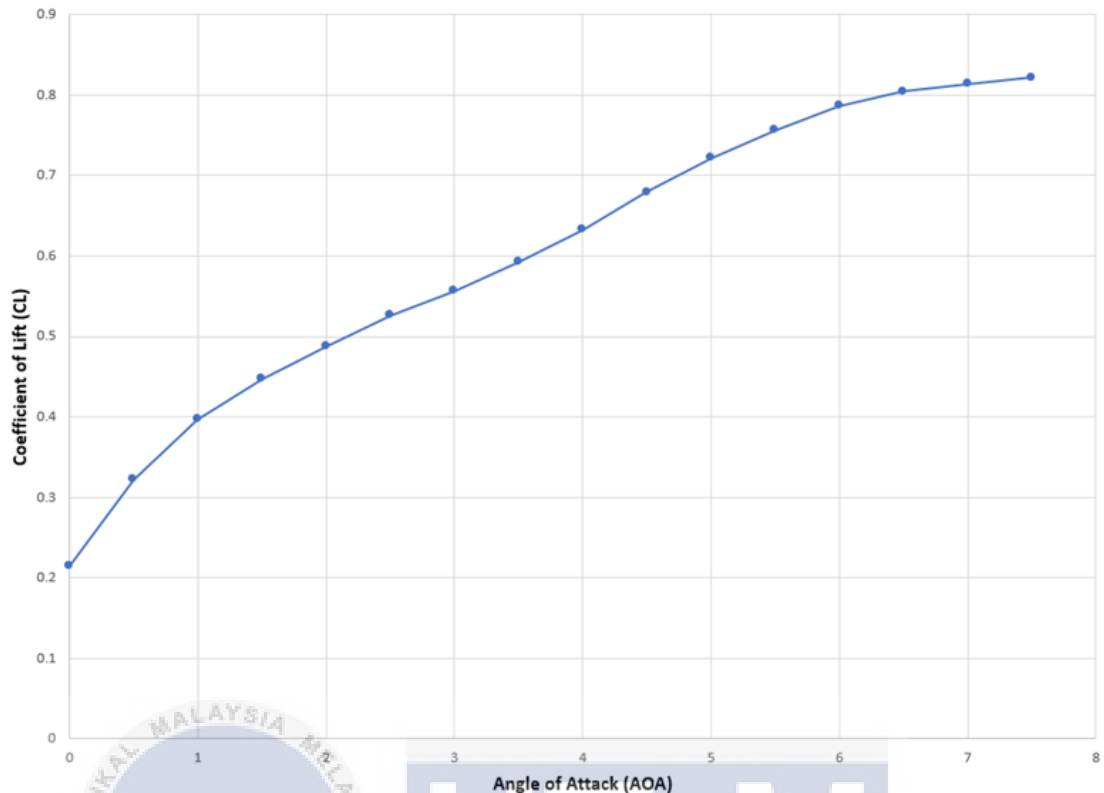


Figure 4.3.4-1: Graph 1: Coefficient of lift (CL) in varying angle of attack (AOA) for NACA 2414

Furthermore, Coefficient of drag (CD) also depends on angle of attack (AOA).

The results obtained from the model airfoil NACA 2414 are plotted on graph. From Figure 4.3.4-2 in the case of drag coefficient it can be seen that the drag coefficient increases ever so slightly till angle of attack at 1°, degree at the value 0.02669 but at the angle of attack 1.5° degree, (0.03119) the value of drag coefficient becomes highly increased. The value drag coefficient is increased as angle of attack is increased. Drag coefficient is maximum (0.10698) at angle of attack 7.5°, degree.

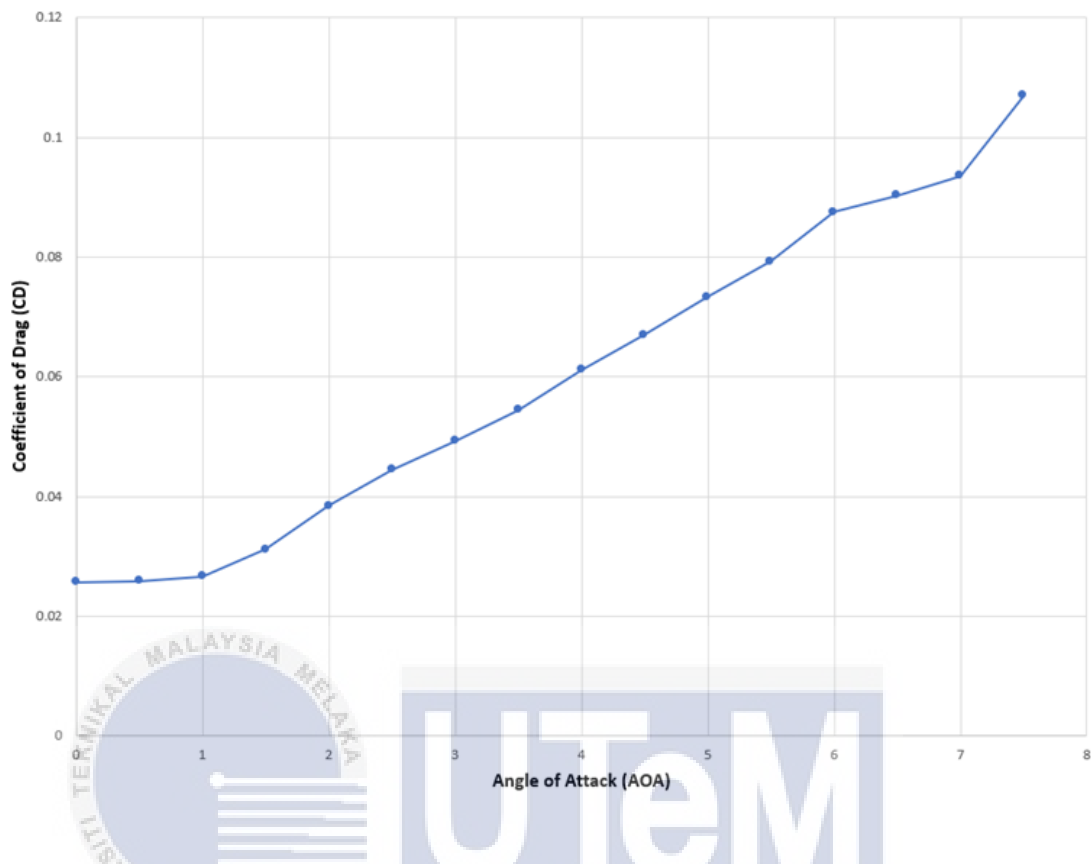


Figure 4.3.4-2: Graph 2: Coefficient of drag (CD) in varying angle of attack (AOA) for NACA 2414

Next, Lift force (LF) was calculated using the lift coefficient and plotted against the angle of attack. The speed was assumed as 10 m/s for the calculation of lift force. The analysis results obtained from the model airfoil NACA 2414 are plotted on graph. From figure 4.3.2-3 shows the lift force increases with increasing angle of attack and after a certain angle of attack it is decreased. It can be observed from the graph that lift force increases and maximum (38195.4) at angle of attack 6°, degree after which it begins to decrease (29478.25) at angle of attack 7.5°, degree.

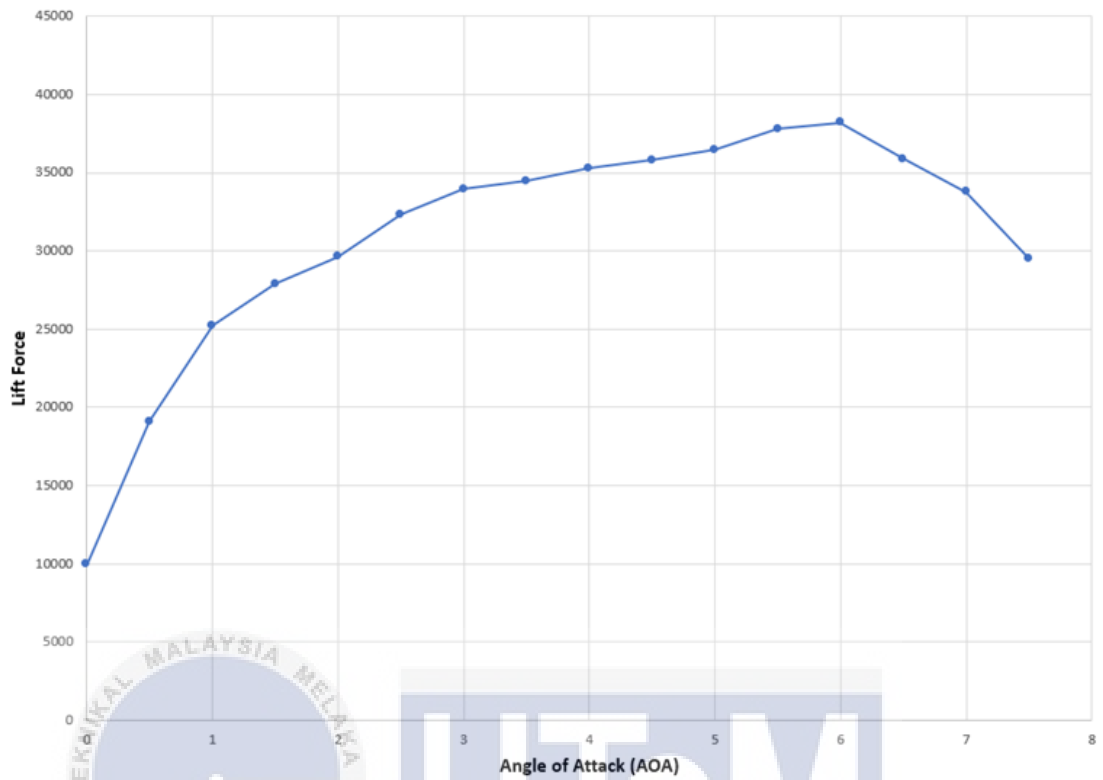


Figure 4.3.4-3: Graph 3: Lift force in varying angle of attack (AOA) for NACA 2414



#### 4.4 Analysis of Naca 4415 Airfoil Design

##### 4.4.1 Process of Modelling and Meshing generation

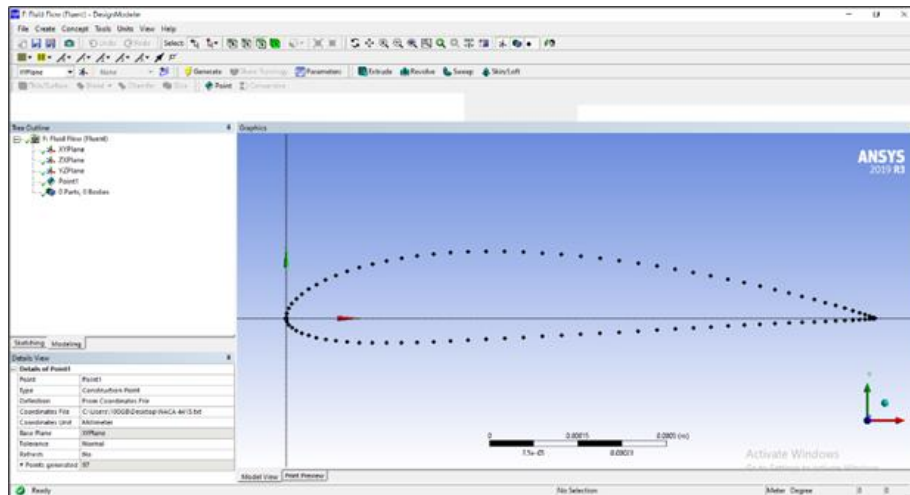


Figure 4.4.1-1: Coordinates of NACA 4415

As an example, this step shows a subsonic tunnel was used to simulate a NACA 4415 airfoil placed at varying angles of attack. Fluent is used to create a simulation environment for this experiment. A table of coordinates is compiled, from which the profile is drawn as in Figure 4.4.1-1 and Figure 4.4.1-2. To build the geometric shape that would be used in the simulation procedure, the NACA 2414 airfoil coordinates were input in this stage and converted. Figure 4.4.1-3 shows the geometry of the NACA 4415 airfoil section.

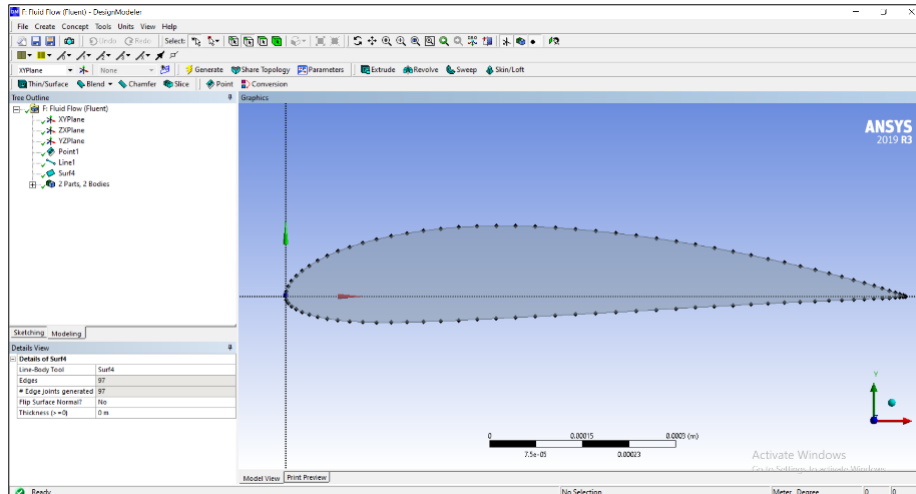


Figure 4.4.1-2: Grid generation of NACA 4415

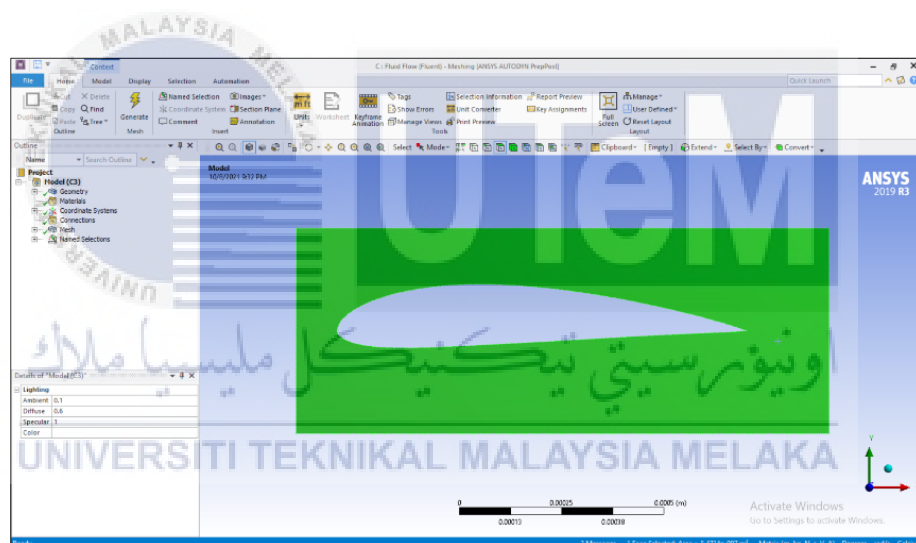


Figure 4.4.1-3: Geometry of the NACA 4415 airfoil section

To specify boundary conditions, the meshable surface must be created after the airfoil profile has been generated. The meshing procedure begins with the creation of a coordinate system at the tail of the airfoils. The flow domain must be divided into smaller subdomains in order to analyse the fluid flow. These are each mesh elements. The mesh

mode is shown in Figure 4.4.1-4. As a result of mesh analysis, it has total nodes are 4055 and total elements is 3735. Analyzed mesh based on the assumption that the relevance centre is fine and smoothing.

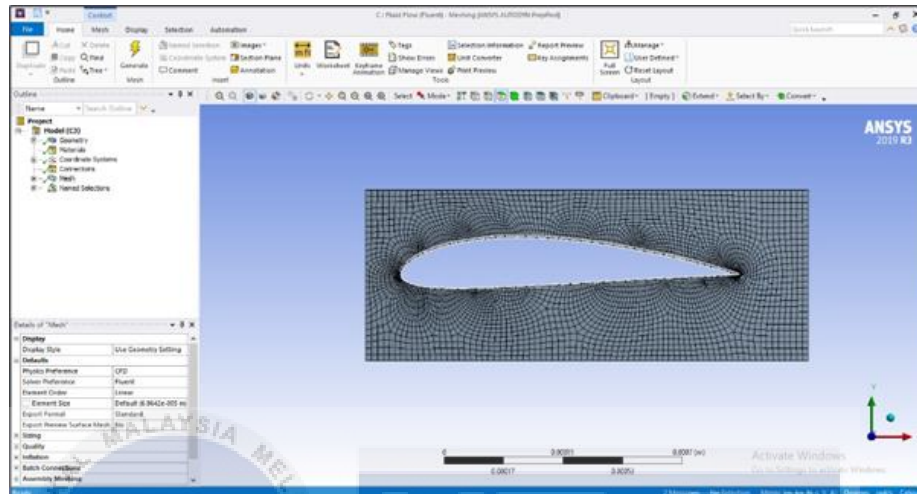


Figure 4.4.1-4: Meshing of air profile around the NACA 2414 airfoil

#### 4.4.2 Static pressure NACA 4415



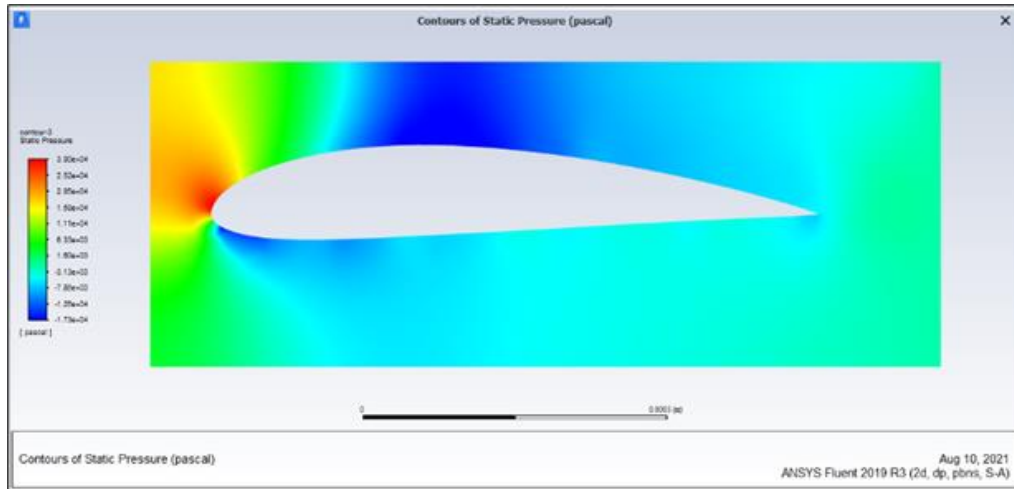


Figure 4.4.2-1: Static pressure contour distribution around the NACA 4415 at 0° Angle of attack (AOA)

Next, Figure 4.4.2-1 static pressure contour and velocity magnitude for NACA 4415 is close to NACA 2414. At zero angle of attack, it can be seen that the static pressure is little higher on the lower surface than on the upper surface. This generates a pressure gradient which causes a force on the total surface area of the airfoil. Figure 4.4.2-2 shows the streamline of static pressure NACA 4415.

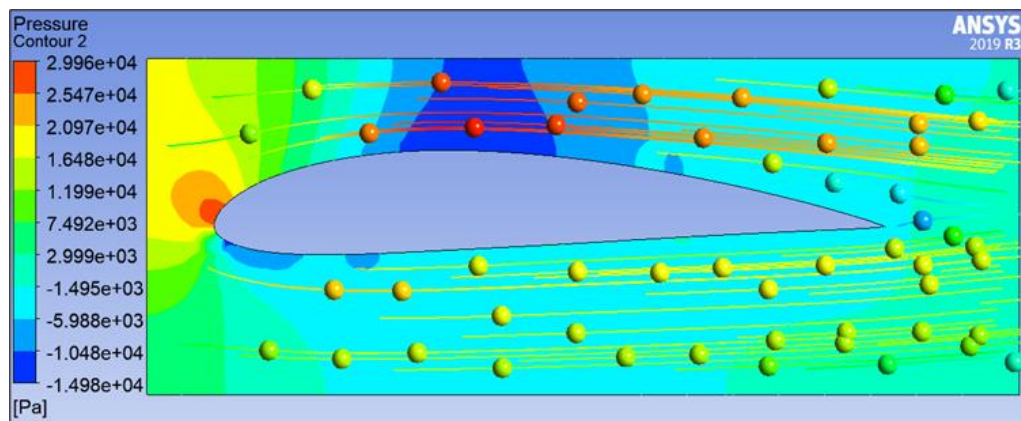


Figure 4.4.2-2: Streamline of static pressure NACA 4415

#### 4.4.3 Velocity magnitude NACA 4415

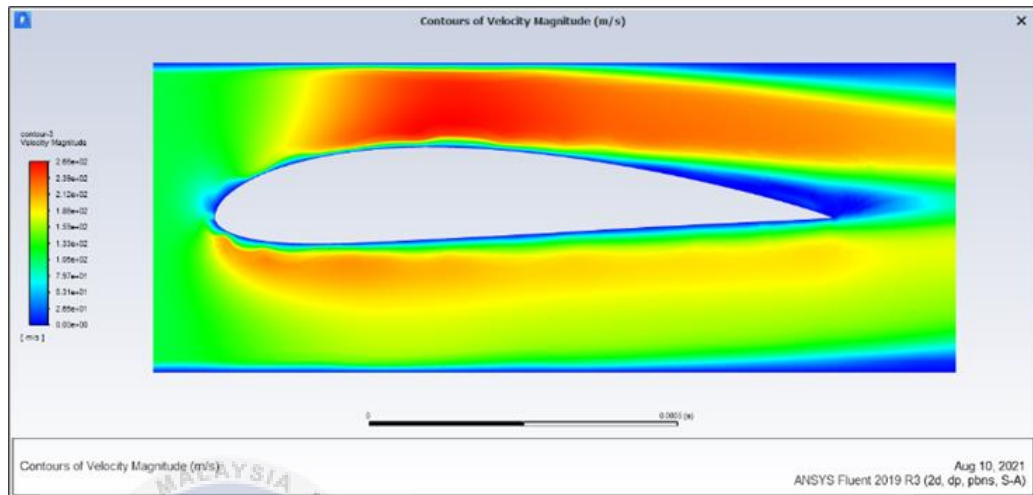


Figure 4.4.3-1: Contours of velocity magnitude in m/s of NACA 4415 at 0° Angle of attack (AOA)

From Figure 4.4.3-1, it can see the contours of velocity magnitude in m/s of NACA 4415 at 0° Angle of attack (AOA). As the angle of attack increases the velocity difference between the upper surface and the lower surface increases thus causing an increase in the force which causes increase in lift and drag coefficient. Figure 4.4.3-2 shows the streamline of velocity magnitude NACA 4415. Velocity magnitude of airfoil is little higher on the upper compare to the lower layer of the airfoil.

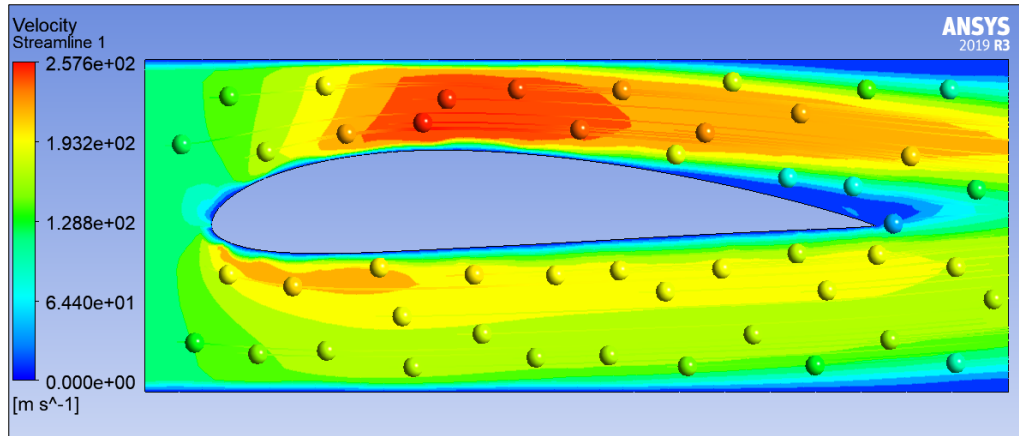


Figure 4.4.3-2: Streamline of velocity magnitude NACA 4415

#### 4.4.4 Variation of lift and drag coefficient with Angle of attack (AOA)

Furthermore, from the simulation of static pressure and magnitude velocity of NACA 4415, the data coefficient of lift (LF), coefficient of drag (LD) and Lift Force (LF) of NACA 4415 were found for different angle of attack. Finally, the ratio of CL to CD was calculated. The Table 4.4.4-1 shown the data CL, CD and LF with different AOA.

Table 4.4.4-1: Result Coefficient of Lift (CL), Coefficient of Drag (CD) and Lift Force with different angle of attack for NACA 4415

Angle of Attack (AOA) *Parameter	Result		
	Coefficient of Lift (CL)	Coefficient of Drag (CD)	Lift Force
0	0.2053	0.02816	3615.2
0.5	0.3019	0.02852	5316.3
1	0.3784	0.02911	6663.5
1.5	0.4351	0.03001	7661.8
2	0.4765	0.03112	8390.9
2.5	0.5138	0.03254	9047.7
3	0.5563	0.03391	9796.1
3.5	0.5691	0.03657	10021.5
4	0.6091	0.03811	10725.9
4.5	0.6101	0.04129	10743.5
5	0.6432	0.04326	11326.4
5.5	0.6378	0.04718	11231.3
6	0.6985	0.04927	12300.1
6.5	0.6472	0.05412	11396.8
7	0.7001	0.05542	12328.3
7.5	0.6757	0.05174	11898.7
8	0.7482	0.05982	13175.3
8.5	1.0102	0.03294	17788.9
9	0.9751	0.03351	17170.9
9.5	0.9432	0.03755	16609.2
10	0.9582	0.04218	16873.3
10.5	1.0265	0.04775	18076.1
11	1.0574	0.05421	18620.2
11.5	1.0472	0.06013	18440.5
12	1.0162	0.06668	17894.7
12.5	0.9732	0.07452	17137.5
13	0.9264	0.08465	16313.3
13.5	0.7885	0.11075	13884.9

Next, Coefficient of lift (LF) depends on angle of attack (AOA). The analysis results obtained from the model airfoil NACA 4415 are plotted on graph. The Figure 4.4.4-1 shows that the lift coefficient increases with increasing angle of attack and after a certain angle of attack it is decreased and this angle is called stall angle. It can be observed from the graph that lift coefficient increases and maximum (1.0102) at angle of attack 8.5°, degree after which it begins to decrease slowly (0.9432) at angle of attack 9.5°,

degree. Therefore, the graph increases ever so slightly till angle of attack at 11°, degree at the value 1.0574 and drop again till at the angle of attack 13.5° at the point 0.7885.

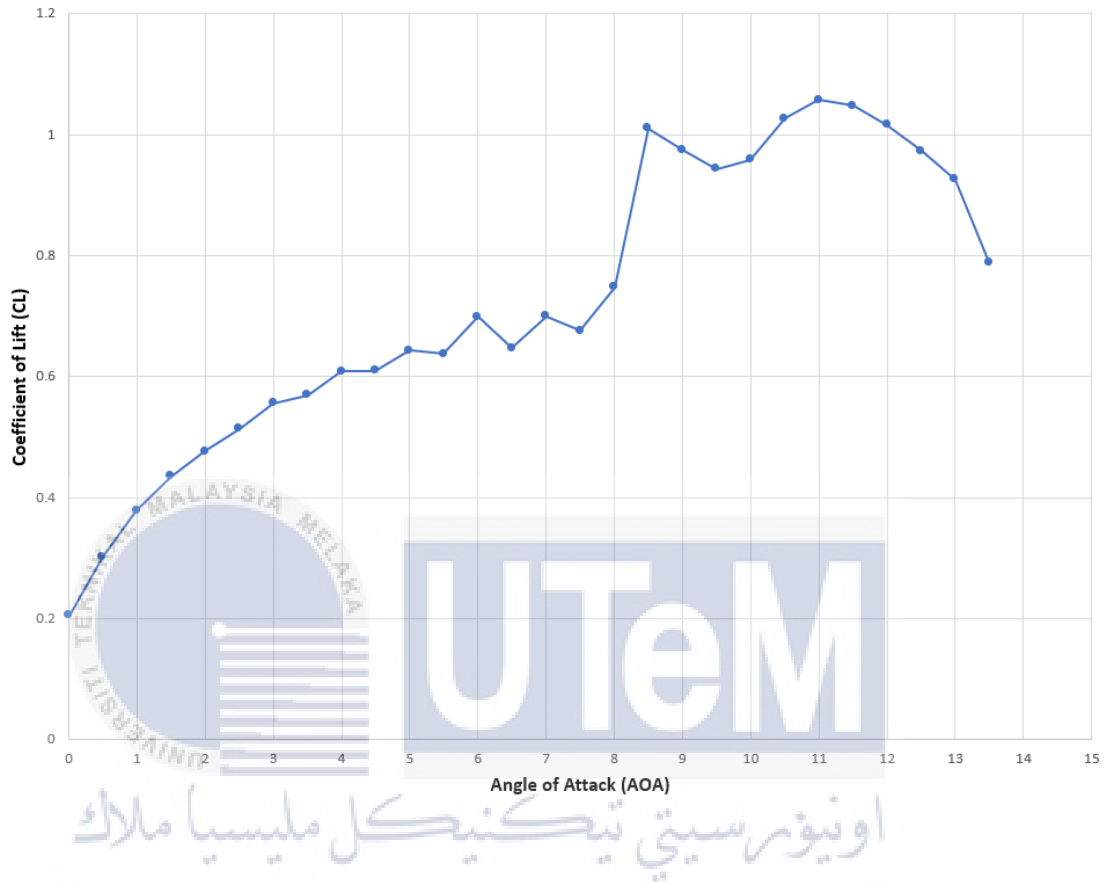


Figure 4.4.4-1: Graph 1: Coefficient of lift (CL) in varying angle of attack (AOA) for NACA 4415

Furthermore, Coefficient of drag (CD) also depends on angle of attack (AOA). The results obtained from the model airfoil NACA 4415 are plotted on graph. From Figure 4.4.4-2 in the case of drag coefficient it can see that the drag coefficient slowly increases till angle of attack at 8°, degree at the value 0.05982 but the graph suddenly dropped sharply at the angle of attack 8.5° degree with the value 0.03294. After that, the

value drag coefficient increases highly again till at the angle of attack  $13.5^\circ$ . Drag coefficient is maximum (0.11075) at angle of attack  $13.5^\circ$ , degree.

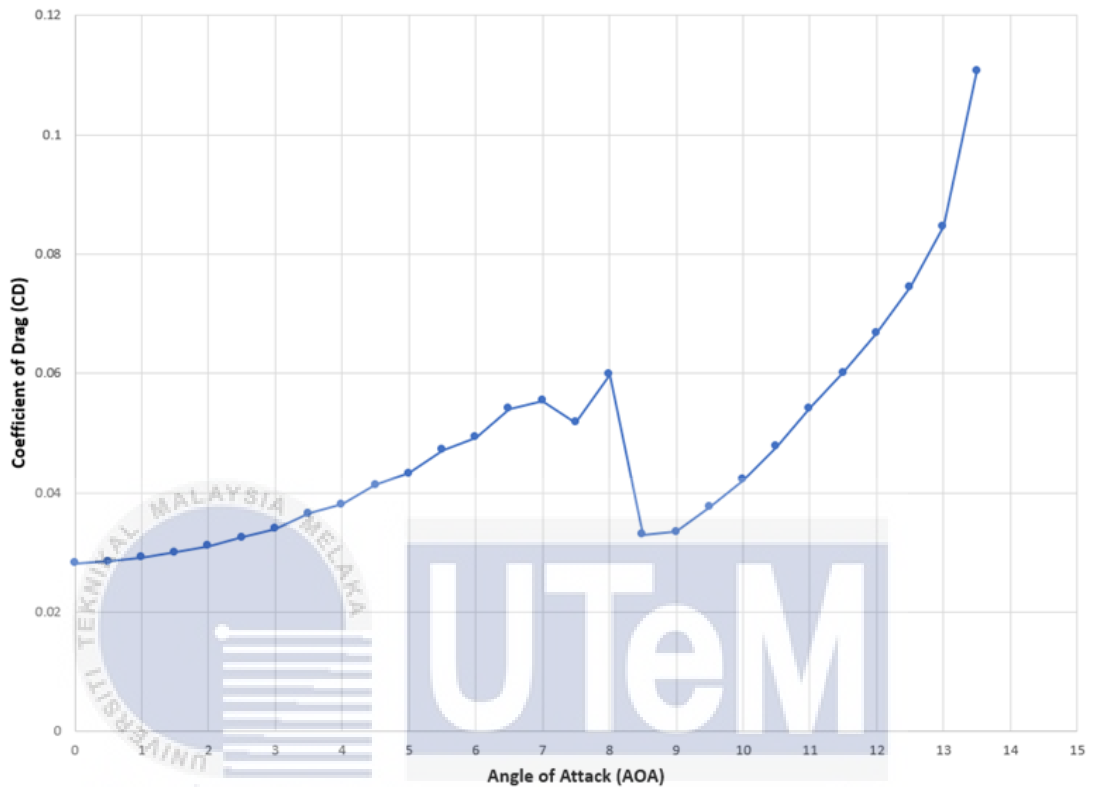


Figure 4.4.4-2: Graph 2: Coefficient of drag (CD) in varying angle of attack (AOA) for NACA 4415

Next, Lift force (LF) was calculated using the lift coefficient and plotted against the angle of attack. The speed was assumed as 10 m/s for the calculation of lift force. The analysis results obtained from the model airfoil NACA 4415 are plotted on graph. From Figure 4.4.4-3 shows the lift force increases with increasing angle of attack and after a certain angle of attack it is decreased. It can be observed from the graph that the lift force increases and maximum at angle of attack  $8.5^\circ$ , degree with the point 17788.9 after which

it begins to decrease slowly at angle of attack  $9.5^\circ$ , degree. Therefore, the graph increases ever so slightly till angle of attack at  $11^\circ$ , degree at the value 18620.2 and drop again till at the angle of attack  $13.5^\circ$  at the point 13884.9.

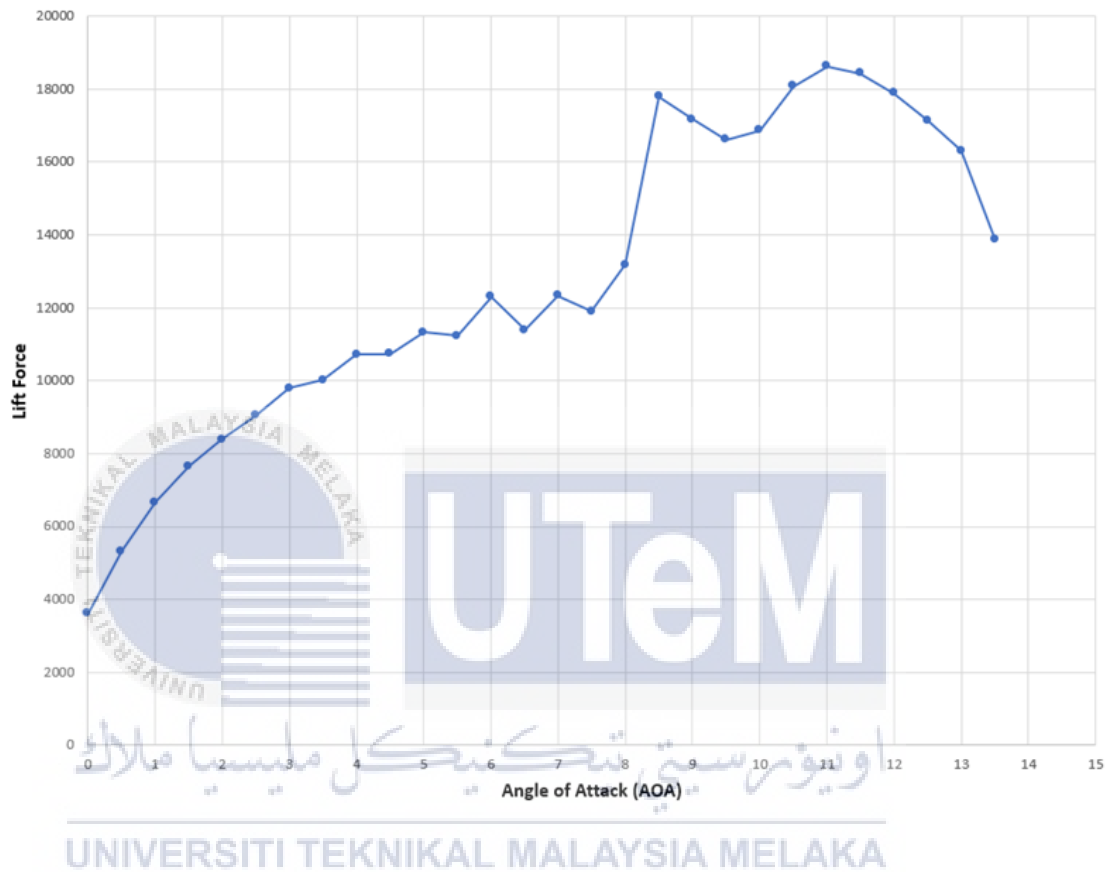


Figure 4.4.4-3: Graph 3: Lift force in varying angle of attack (AOA) for NACA 4415

#### 4.5 Comparison Result of NACA 0015, NACA 2414 and NACA 4415

#### 4.5.1 Comparison Result of NACA 0015, NACA 2414 and NACA 4415 Based on Coefficient of Lift (CL)

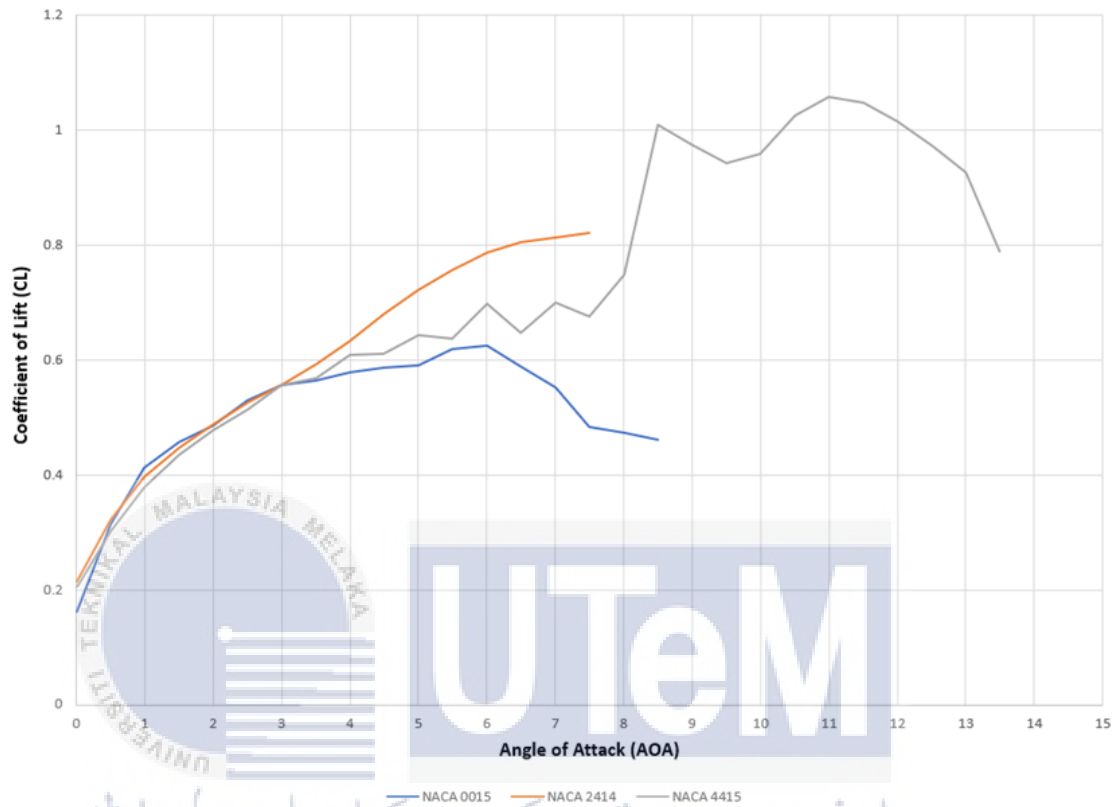


Figure 4.5.1-1: Graph 1: Coefficient of lift (CL) in varying angle of attack (AOA) with different type of airfoil

Figure 4.5.1-1 it can be seen that at the starting lift coefficient are nearly the same for all the three airfoil but with increase in angle of attack for NACA 2414 shows a higher lift coefficient at value 0.8215 at angle of attack 7.5°, degree compare with NACA 0015 and NACA 4415. While all the three airfoils NACA 0015, NACA 2414 AND NACA 4415 have nearly the same lift coefficient for smaller angle of attack but at the angle of attack 7.5°, degree the NACA 2414 shows the higher coefficient lift compared with the



other NACA. At angle of attack  $8.5^\circ$ , degree for NACA 4415 has higher lift coefficient compared with others NACA but the performance plotting the graph are not consistence for both graphs. So, it can be concluded that the NACA 2414 have the higher coefficient lift with good pattern plotting performance at the graph for the same angle of attack  $7.5^\circ$ , degree compared with NACA 0015 and NACA 4415.

#### 4.5.2 Comparison Result of NACA 0015, NACA 2414 and NACA 4415 Based on Coefficient of Drag (CD)

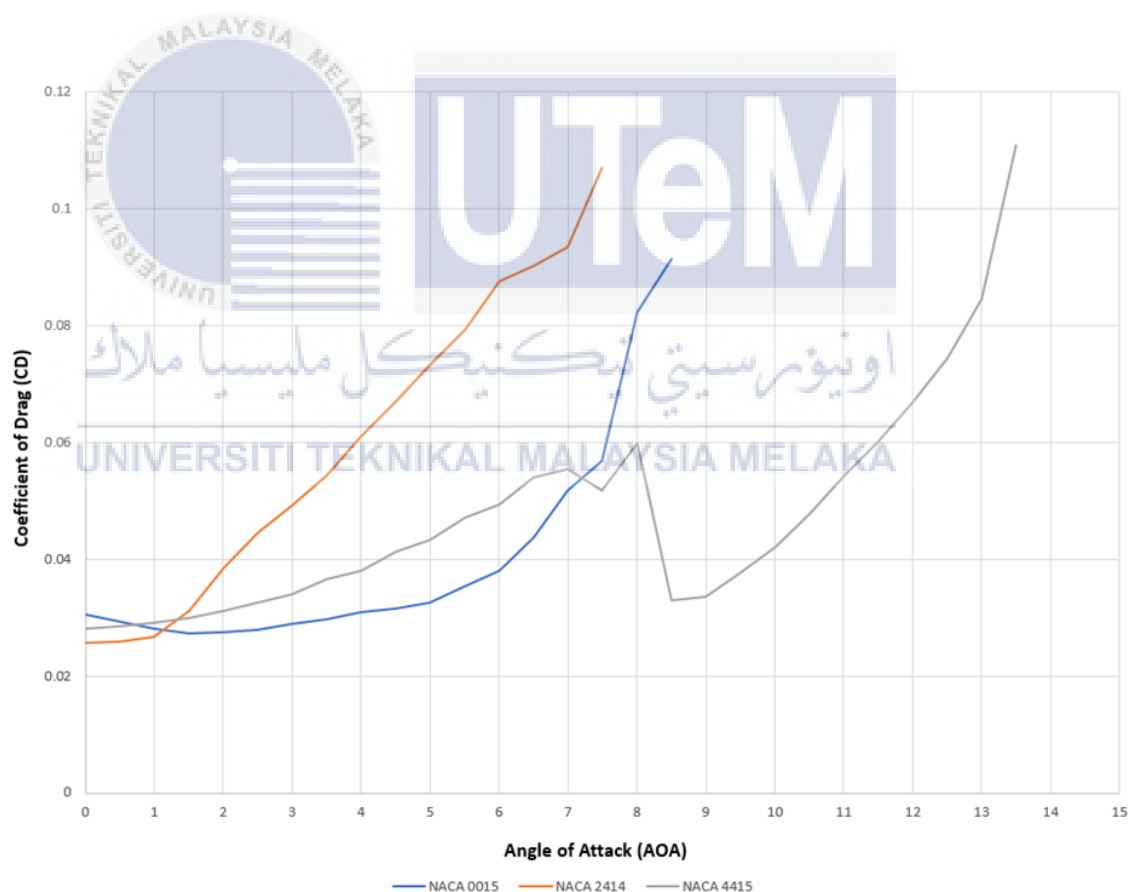


Figure 4.5.2-1: Graph 2: Coefficient of drag (CD) in varying angle of attack (AOA) with different type of airfoil

Figure 4.5.2-1 it is clearly that NACA 2414 has a higher initial value of drag coefficient at value 0.10698 at angle of attack  $7.5^\circ$ , degree compare with NACA 0015 and NACA 4415. While, the NACA 4415 takes over due to its wide range of angle of attack at  $13.5^\circ$ , degree. At the starting of the graph for the three NACA, it has nearly same drag coefficient at angle of attack  $1^\circ$ , degree. While, the pattern for the graph NACA 2414 increases constantly in good condition compared with the others two NACA. So, it can be concluded with the NACA 2414 have the higher coefficient drag with good pattern plotting performance at the graph for the same angle of attack  $7.5^\circ$ , degree compared with NACA 0015 and NACA 4415.

#### 4.5.3 Comparison Result of NACA 0015, NACA 2414 and NACA 4415 Based on Lift Force



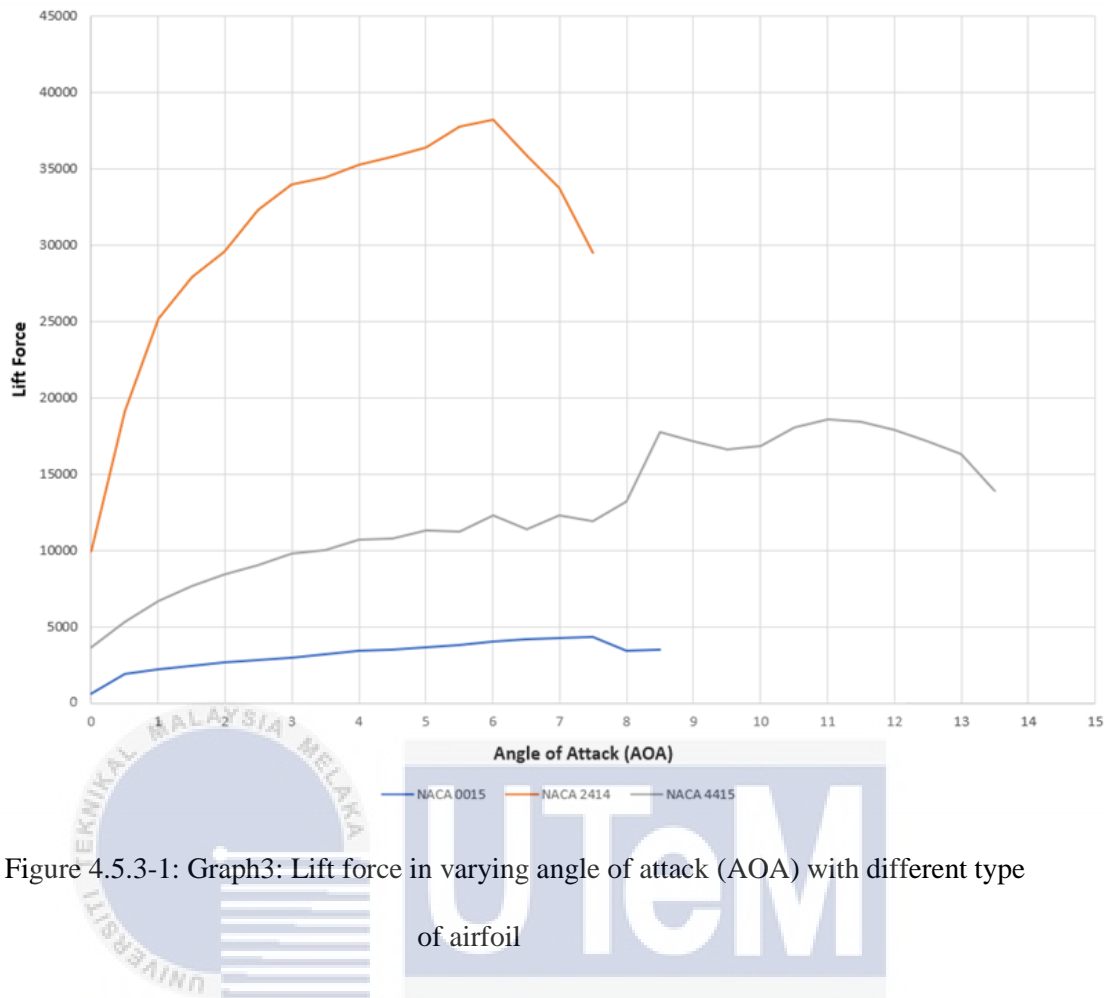


Figure 4.5.3-1: Graph3: Lift force in varying angle of attack (AOA) with different type of airfoil

Figure 4.5.3-1 it can see that NACA 2414 can generate very high amount of lift force at value of 38195.4 at angle of attack at 6°, degrees as compared to NACA 0015 and NACA 4415. A big difference shown of NACA 2414 plotting when the pattern increases highly from the NACA 0015 and NACA 4415. However, during 6°, degree angle of attack for NACA 2414, it is shown a drop of lift force till 7°, degree while the NACA 0015 and NACA 4415 does not shown any differences. So, it can be concluded with the NACA 2414 have the higher lift force with good pattern plotting performance at the graph for the same angle of attack 6°, degree compared with NACA 0015 and NACA 4415.

## CHAPTER 5

### CONCLUSION & RECOMMENDATION

#### 5.1 Introduction

This chapter detailed the overall topic that has been done while this project has been operating were discussed. In this chapter, the topics that have been discussed previously are also concluded. This project was a success because the objectives were achieved and the results of the analysis were acceptable. In this chapter, the recommendation for this project has been discussed for the purposes of improvement.

#### 5.2 Conclusion

This report was completed on time and according to the project's schedule within the problem statements, objective, scope and limitations that belongs to this project. The main target of this project is to investigate different type of aerofoil design that can be

apply to paddle fin drive. The type of aerofoil for the paddle fin drive has been determined during literature review and in order to collect the data, some analysis has been done. The data then being used in ANSYS software method to get the good airfoil to improve design of the paddle fin drive. Next, the design of fin with different type of airfoil was constructed by using Solidwork software. A series of objectives has been identified and needed to archive before the accomplishment of this project. The objectives need to be identified in order to know the process that need to be done. All the objectives that have been identified in this project has been achieved successfully according to project flow.

The first objective that has been achieved is investigate different type of aerofoil design that can be apply to paddle fin drive. Some different type of airfoil needed to being analyse before proceed into the next step. Selection on different types of aerofoil design with the focus on NACA 0015 (symmetrical), NACA 2414 (semi symmetrical) and NACA 4415 (chambered). This process was done to make sure selection of airfoil that needed in order to make a good design for paddle fin. Research in literature review has been done and used to knowing what has been done. By doing literature review, the knowledge about the type of airfoil can be known and this information gained can help in solving the problem.

The second objective that has been identified is to develop viable prototype of paddle fin drive that integrates with different type of aerofoils. This objective was done to build the design of fin with different types of aerofoil design that focus on NACA 0015 (symmetrical), NACA 2414 (semi symmetrical) and NACA 4415 (chambered). The design of fin was being done through the Solidwork software. This modelling software was used because it easier to design and adjusting the design. The selection of airfoil was done through the literature review.

The third objective that has been identified is to validate the type of aerofoil with an optimum forward thrust for fishing kayak. After finish generate the fin design with different type of airfoil in Solidwork software, the design of fin was imported to ANSYS software to continue the analysis in this project. In this process, the modelling, meshing generation, static pressure, velocity magnitude, Coefficient of lift (CL), Coefficient of drag (CD) and Lift force have been collected. The comparisons of data have been done for NACA 0015 (symmetrical), NACA 2414 (semi symmetrical) and NACA 4415 (chambered). According to the result, the airfoil design that have good performance is the NACA 2414 (semi symmetrical) compared with other two airfoil. It is because the NACA 2414 have good performance in Coefficient of lift (CL), Coefficient of drag (CD) and Lift force.



### 5.3 Recommendation

The project has been done completely. There are some points that can be applied on future to improve the performance and design of paddle fin. Firstly, added more type of airfoil in this project to get more data and result. Next, for design the paddle fin, trying to change or improve the shape of the design. Another recommendation is using another software in order to achieve the main objective of this project.

## 5.4 Sustainable Design and Development

In this project, the design of fin was generated with the sustainability aspects of reducing environmental impacts for future as the prototypes were designed simple by using as few materials as possible. Next, the design of fin with different of airfoil was generated in simple design that has least number of parts in which good to save material usage. So that, this project is considered sustainable due to low impact on the environment.

## 5.5 Complexity

In this project, the first complexity parts were to design the fin with the different type of airfoil in Solidwork software. The difficult parts are when to import the database of airfoil and applied it to the fin for creating the modelling. the Next, complexity in this project is to generate the model in ANSYS software for getting the data and result. Many steps and procedure are required which is to generate the airfoil modelling in this software. In this project, generate the airfoil model needs a lot of focus and consideration that needs to be taken and to ensure the collecting data is correct.

## 5.6 Life Long Learning

During this project, there have a lot of learning phase that happened in order to finishing this project. Using the Solidwork software to create and generate the model of fin with different type of airfoil. Next, using the ANSYS software to simulate and generate the model of fin for getting





## REFERENCE

- Albrecht, T., del Campo, V., Weier, T., & Gerbeth, G. (2012). Comparison of PIV-Based Methods for Airfoil Loads Evaluation. *Symposium on Applications of Laser Techniques to Fluid Mechanics*.
- Buscher, A. J., Rozsa, J. D., & Yechout, T. R. (2013). Aerodynamic evaluation of non-flush field repair patches on the a-10 horizontal stabilizer. *51st AIAA Aerospace Sciences Meeting Including the New Horizons Forum and Aerospace Exposition 2013*. <https://doi.org/10.2514/6.2013-964>
- Carswell, D., & Lavery, N. (2006). 3D solid fin model construction from 2D shapes using non-uniform rational B-spline surfaces. *Advances in Engineering Software*. <https://doi.org/10.1016/j.advengsoft.2006.01.002>
- Chu, D., Liu, X., & Zhang, M. (2007). Research on turtle hydrofoil motion principle and bionics. *Proceedings of the IEEE International Conference on Automation and Logistics, ICAL 2007*. <https://doi.org/10.1109/ICAL.2007.4338974>
- Gately, R. D., Beirne, S., Latimer, G., Shirlaw, M., Kosasih, B., Warren, A., Steele, J. R., & In Het Panhuis, M. (2017). Additive Manufacturing, Modeling and Performance Evaluation of 3D Printed Fins for Surfboards. *MRS Advances*. <https://doi.org/10.1557/adv.2017.107>
- Gordnier, R. E. (2009). High fidelity computational simulation of a membrane wing airfoil. *Journal of Fluids and Structures*. <https://doi.org/10.1016/j.jfluidstructs.2009.03.004>
- Hossain, A., Rahman, A., Hossen, J., Iqbal, P., Shaari, N., & Sivaraj, G. K. (2011). Drag

reduction in a wing model using a bird feather like winglet. *Jordan Journal of Mechanical and Industrial Engineering*.

Huang, S., Hu, Y., & Wang, Y. (2021). Research on aerodynamic performance of a novel dolphin head-shaped bionic airfoil. *Energy*.  
<https://doi.org/10.1016/j.energy.2020.118179>

Industrial Designers Society of America. (2003). *Design Secrets: Products 50 Real-Life Projects Uncovered*.

Kandwal, S., & Singh, S. (2012). Computational Fluid Dynamics Study Of Fluid Flow And Aerodynamic Forces On An Airfoil. *International Journal of Engineering Research & Technology (IJERT)*.

Kostas, K. V., Ginnis, A. I., Politis, C. G., & Kaklis, P. D. (2017). Shape-optimization of 2D hydrofoils using an Isogeometric BEM solver. *CAD Computer Aided Design*.  
<https://doi.org/10.1016/j.cad.2016.07.002>

Kumar, A. (2014). *INVESTIGATION OF AIRFOIL DESIGN*.

Madnia, C. K. (2010). Review of “Fundamentals of Aerodynamics.” *AIAA Journal*.  
<https://doi.org/10.2514/1.52157>

Mohammed, M. A., Tarfaoui, M., Laurens, J. M., & Moyne, S. (2015). Design of composite ducted horizontal axis tidal turbine. *MARINE 2015 - Computational Methods in Marine Engineering VI*.

Novak, J. I. (2020). A parametric method to customize surfboard and stand up paddle board fins for additive manufacturing. *Computer-Aided Design and Applications*.  
<https://doi.org/10.14733/cadaps.2021.297-308>

Paudel, S. (2016). Aerodynamic and Stability Analysis of Blended Wing Body Aircraft. *International Journal of Mechanical Engineering and Applications*.  
<https://doi.org/10.11648/j.ijmea.20160404.12>

- Pavlov, V. V., Wilson, R. P., & Lucke, K. (2007). A new approach to tag design in dolphin telemetry: Computer simulations to minimise deleterious effects. *Deep-Sea Research Part II: Topical Studies in Oceanography*.  
<https://doi.org/10.1016/j.dsr2.2006.11.010>
- Pinkerton, R. M. (1936). Report No. 563: Calculated and Measured Pressure Distributions Over THE Distributions Over the Midspan Section of the NACA Airfoil. In *National Advisory Committee For Aeronautics*.
- Prandtl's Essentials of Fluid Mechanics. (2004). In *Prandtl's Essentials of Fluid Mechanics*. <https://doi.org/10.1007/b97538>
- Selk, E. E. (2005). Book Review: Darwin and Design: Does Evolution Have a Purpose? *Theological Studies*. <https://doi.org/10.1177/004056390506600135>
- Shoele, K., & Zhu, Q. (2015). Drafting mechanisms between a dolphin mother and calf. *Journal of Theoretical Biology*. <https://doi.org/10.1016/j.jtbi.2015.07.017>
- Torenbeek, E. (2013). Advanced Aircraft Design: Conceptual Design, Analysis and Optimization of Subsonic Civil Airplanes. In *Advanced Aircraft Design: Conceptual Design, Analysis and Optimization of Subsonic Civil Airplanes*.  
<https://doi.org/10.1002/9781118568101>
- Tuncay Kamas. (2009). 2D and 3D Assessment of Cambered and Symmetric Airfoils: A *Computational Fluid Dynamics Study*.
- Vishnu Chavan, S., & Suresh Pawar, S. (2018). The modified design of aeroplane fuselage to overcome drag resistance acting due to flow of air. *Materials Today: Proceedings*. <https://doi.org/10.1016/j.matpr.2018.02.331>
- Wakayama, S., & Kroo, I. (1995). Subsonic wing planform design using multidisciplinary optimization. *Journal of Aircraft*. <https://doi.org/10.2514/3.46786>
- Watson, K. P., & Granger, R. A. (1998). Hydrodynamic effect of a satellite transmitter

on a juvenile green turtle (*Chelonia mydas*). *Journal of Experimental Biology*.

Wyneken, J. (2001). The anatomy of sea turtles. *U.S. Department of Commerce NOAA*

*Technical*

*Memorandum*

*NMFS-SEFSC*.

[https://doi.org/10.1007/SpringerReference\\_87356](https://doi.org/10.1007/SpringerReference_87356)

Yan, J., Augier, B., Korobenko, A., Czarnowski, J., Ketterman, G., & Bazilevs, Y. (2016).

FSI modeling of a propulsion system based on compliant hydrofoils in a tandem

configuration.

*Computers*

*and*

*Fluids*.

<https://doi.org/10.1016/j.compfluid.2015.07.013>

Zhang, C., Duan, L., & Choudhari, M. M. (2018). Direct numerical simulation database

for supersonic and hypersonic turbulent boundary layers. *AIAA Journal*.

<https://doi.org/10.2514/1.J057296>



# APPENDIX

## APPENDIX 1: GANTT CHART PSM 1

<b>Gantt Chart for PSM 1</b>															
No.	Activity	Week													
		1	2	3	4	5	6	7	8	9	10	11	12	13	14
1	Title approval from supervisor														
2	Planning and make appointment with supervisor														
3	Draft content of Chapter 1,2 and 3														
4	Chapter 1 (Introduction) • Problem Statement • Objective • Scope of project														
5	Chapter 2 (Literature Review) • Introduction • NACA 0015, NACA 2414, NACA 4415														
6	Chapter 3 (Methodology) • Process flow of project • Data collection														
7	Full draft report for Chapter 1,2 and 3														
8	Edit Chapter 1,2 and 3														
9	Update and Recheck report														
10	Preparation slide presentation														
11	Presentation for PSM 1														
12	Submit full report to panel and supervisor														

## APPENDIX 1: GANTT CHART PSM 1